NOVEL INHIBITORS OF GLUTAMATE AND NUCLEOSIDE TRANSPORTERS

by

Cody Guan-Nan Wu

A thesis submitted in partial fulfillment of the requirements for the degree of

Master of Science

Department of Physiology
University of Alberta

Abstract

Membrane transporters play integral roles in the functioning of cells by controlling movement of molecules across the phospholipid bilayer. In this thesis, utilization of radioisotope uptake assays permitted examination of intentional and unintentional inhibition of three membrane transporter families: the excitatory amino acid transporter family (hEAATs), the concentrative nucleoside transporter family (hCNTs), and the equilibrative nucleoside transporter family (hENTs).

hEAATs, while being the topic of intensive neurophysiological research as well as attractive pharmacological targets for treatment of glutamate related-diseases, suffer from lack of availability of isoform-specific inhibitors. In collaboration with Dr. S.A. Baldwin and colleagues at the University of Leeds (UK), a series of glutamate analogues were synthesized as potential glutamate transport inhibitors. By varying the concentration of inhibitors, we were able to determine the concentration of each compound required to cause 50% inhibition of L-glutamate uptake (IC_{50} value) for each of the four human EAAT family members produced in *Xenopus laevis* oocytes. Of eight compounds tested, seven showed high specificity for the hEAAT2 isoform. Of these seven hEAAT2-specific inhibitors, two showed high-potency ($IC_{50} \sim 5$ μM). With further testing, these compounds may prove useful in hEAAT research and pharmaceutical development.

The design of new and novel classes of inhibitors for research and pharmaceutical purposes requires care and awareness to prevent, or at least minimize, spillover inhibition of other proteins. This was not the case with mitogen-activated protein kinase kinase (MEK) inhibitors, a class of small-molecule kinase inhibitors designed to inhibit proteins within the mitogen activated protein kinase (MAPK) pathway. This pathway plays an

integral role in the transduction of cell growth and proliferation signals from receptors on the cell surface to the nucleus through a complex multi-protein intracellular phosphorylation cascade. Deregulation of this pathway and its protein mediators can result in abnormal, uncontrolled cell growth and the development of cancer. Due to the high prevalence of MAPK pathway deregulation in cancer patients (roughly 30%), development of inhibitory compounds that target its various protein mediators has received intense attention in recent years. Inhibitors such as binimetinib, trametinib, and selumetinib targeting MEK1/2 have demonstrated unexpectedly poor clinical performance when used in combined therapy with nucleoside analogue anticancer drugs. Since these nucleoside analogues require human nucleoside transporter (hNT) proteins to enter the cell at pharmacologically effective concentrations, we hypothesized that the purine and pyridopyrimidine-like structures found within these inhibitors allowed for binding to and inhibition of hNTs. Radioisotope uptake assays using radiolabelled uridine and adenosine in *Xenopus laevis* oocytes producing individual hNTs from both the hCNT and hENT transporter families (hCNT1-3 and hENT1-4, respectively) have revealed high-potency binimetinib, trametinib, and selumetinib inhibition of hENT3 (average IC_{50} values in the range 2.7 - 5.1 μM), more moderate inhibition of hENT4 (average IC_{50} values in the range 57.1 - 274 μM), and low-potency inhibition of other hNTs. Some adverse effects of MEK administration may be attributable to spillover inhibition of hENT3/4.

Acknowledgements

First and foremost, I would like to thank my supervisor Dr. James Young for his continued support throughout my entire experience in academia. From my summer research project to my undergraduate honors thesis and finally to completion of this Master's thesis, he has showed me endless kindness, patience, respect, and most importantly, a healthy dose of reality when I needed to toe the line.

I would also like to thank Dr. Sylvia Yao who spent many hours providing advice and patiently bringing up my experimental skills to the required standard. Her availability and willingness to help when issues arose helped make the laboratory feel more like a second home. Many thanks also to Dr. Kyla Smith, who was always a friendly face to talk to and bounce ideas off of, in addition to being a valuable wealth of knowledge.

To my other colleagues that shared the laboratory with me, both in my undergraduate and graduate research, thank you for your advice, company, and support.

To my parents, I am most grateful for their faith and trust in my path despite its rather lengthy and roundabout nature.

And lastly, my gratitude to the late Dr. Edward Karpinski for his company and mentorship throughout the years. He is missed.

Contributions

Preliminary screening data for the glutamate transport inhibitor project was undertaken by Dr. Sylvia Yao. Dose-dependence experiments for that project were completed by both Dr. Sylvia Yao and myself. All of the MEK inhibitor data are my own.

Table of Contents

List of Tables

List of Figures

List of Nomenclature and Abbreviations

AMPA	α-amino-3-hydroxy-5-methyl-4-isoxazolepropionic acid
AQ1	aquaporin 1
AZT	azidothymidine
BCSFB	blood-cerebrospinal fluid barrier
BLAST	basic local alignment search tool
CFTR	cystic fibrosis transmembrane conductance regulator
cib	concentrative, NBMPR-insensitive, broadly selective; hCNT3
cif	concentrative, NBMPR-insensitive, formycin B-transporting; hCNT2
cit	concentrative, NBMPR-insensitive, thymidine-transporting; hCNT1
CME	cystoid macular edema
DOS	diversity oriented synthesis
ei	equilibrative, NBMPR-insensitive; hENT2
ERK	extracellular signal-regulated kinase
es	equilibrative, NBMPR-sensitive; hENT1
EST	expressed sequence tag
Glt_{Ph}	*Pyrococcus horikoshii* glutamate transporter
hAA	hENT3-mutant with a dialanine mutation replacing the dileucine targeting motif allowing for cell surface expression

hCNT	human concentrative nucleoside transporter
hEAAT	human excitatory amino acid transporter
HEK 293	human embryonic kidney 293 cells
hENT	human equilibrative nucleoside transporter
hNT	human nucleoside transporter
iGluR	ionotropic glutamate receptor
MAPK	mitogen activated protein kinase
MCT	monocarboxylate transporter
MD	molecular dynamics
MEK	MAPK/ERK kinase; mitogen activated protein kinase kinase
mGluR	metabotropic glutamate receptor
MPP$^+$	1-methyl-4-phenylpyridinium
NBMPR	nitrobenzylmercaptoopurine ribonucleoside
nd	not determined
NMDA	N-methyl-D-aspartate
Ns	nosyl
NSCLC	non-small cell lung cancer
PMAT	plasma membrane monoamine transporter; hENT4
RAF	rapidly accelerated fibrosarcoma
RPE	retinal pigment epithelium
TBOA	DL-threo-beta-benzyloxyaspartate
TEVC	two microelectrode voltage clamp
TFB TBOA	(2S,3S)-3-[3-[4-

(trifluoromethyl)benzoylamino]benzyloxy]aspartate

TFEB	transcription factor EB
TKI	tyrosine kinase inhibitor
TKR	tyrosine kinase receptor
VGLUT	vesicular glutamate transporter
β-THA	β-*threo*-hydroxyaspartate

Chapter 1:

General Introduction

Membrane Transport

The maintenance of homeostasis is fundamental to the survival of the cell, and is aided by the presence of an outer phospholipid bilayer, which isolates the internal controlled environment from external perturbations. The exchange of nutrients and waste products across this selectively permeable membrane requires mediation by the integral membrane transport proteins present within this bilayer.

Traditionally, these membrane transport proteins were thought to fall under one of two distinct categories (channels and transporters), but more recent evidence suggests that they may in fact comprise a spectrum of structures and functionalities (Lin *et al.*, 1998; Ryan & Mindell, 2007; Jih *et al.*, 2012). Despite this, the classical classifications of channel and transporter proteins remains useful in the discussion of the majority of membrane transport proteins for the purposes of simplification and organization. Transporters can, in turn, be additionally broken down into active and passive transporters.   Active transporters utilize either energy derived directly from ATP hydrolysis (primary active transporters) or from ion gradients (secondary active transporters) to concentrate permeants across the phospholipid bilayer. Passive transporters on the other hand facilitate diffusion of permeants down its concentration gradients.

This thesis investigates inhibitors of transporters involved in the passage of glutamate and nucleosides across cell membranes.

Glutamate

Glutamate is a non-essential amino acid which requires *de novo* synthesis within the body due to intestinal metabolism (Brosnan & Brosnan, 2013). Its low pKa of 4.1 is due to the presence of a γ-carbon carboxylic acid functional group which, at physiological pH, is deprotonated. Due to this negative charge, glutamate cannot easily be translocated across the cell membrane without the aid of transporters. Physiologically, glutamate has several functions: in protein synthesis, as a metabolic intermediate, as a tastant, and as the primary neurotransmitter of the central nervous system (CNS) (Brosnan & Brosnan, 2013). Due to the electronegative oxygen on its functional group, glutamate can be involved in both electrostatic interactions with other amino acid side chains, in addition to being a hydrogen bond acceptor, making glutamate integral to both the function and structure of proteins.

Beyond its function as a proteinogenic amino acid, glutamate's role in signaling is three-fold. As a primary tastant, glutamate activates various receptors thereby eliciting the taste umami or savory (Brosnan & Brosnan, 2013). Recent evidence also demonstrates that glutamate in high concentrations is additionally involved in allosteric modulation of the sweet and salty response (Shim *et al.*, 2015). Within the visual system, glutamate release by photoreceptors activates interneurons to transduce information from the retina to the visual centers of the brain (Szmajda & DeVries, 2011). Although glutamate and the regulation of its release within the retina is vital to the proper functioning of the visual system, glutamate's arguably most important signaling role is that within the brain.

While the role of glutamate in the central nervous system as an excitatory neurotransmitter has been known for well over 50 years, the specifics of is function and transport remained elusive (Meldrum, 2000). The role of glutamate as an endogenous

excitatory neurotransmitter necessitates the presence of a rapid transporter-mediated removal system to prevent excitotoxic neuronal death (Bridges & Esslinger, 2005).

Excitatory Amino Acid Transporters

There are five known excitatory amino acid transporters in humans (hEAAT1, hEAAT2, hEAAT3, hEAAT4, and hEAAT5), each differing in kinetics, function, and localization. Human EAAT1-5 share several evolutionary conserved domains and are 50-60% identical in amino acid sequence (Shigeri *et al.*, 2004). Mechanistically, the import of one glutamate molecule across the cell membrane is coupled to the import of three sodium ions and one proton in addition to the export of one potassium ion. Utilization of multiple ion gradients to power transport allows for the concentration of glutamate up to 10^5-fold across the membrane (Bridges & Esslinger, 2005).

hEAAT1 (SLC1A3)

Human EAAT1 is a high-affinity glutamate and aspartate transporter found in glial membranes, and is encoded by the gene SLC1A3 located at 5p13 in the human genome. The rat homologue known as GLAST was initially isolated by Storck *et al.* in 1992 as a 66 kDa hydrophobic glycoprotein purified from rat brain extract (Storck *et al.*, 1992). Subsequent partial sequencing using Edman degradation allowed for the construction of a degenerative probe for screening a rat cDNA library. The resulting isolated 3 kb clone encoded a 543 aa protein which, when produced in *Xenopus laevis* oocytes, conferred the ability to take up

glutamate and aspartate. The human homologue (hEAAT1) was isolated and cloned soon thereafter by Arriza *et al.* from human motor cortex, alongside hEAAT2 and hEAAT3 (Arriza *et al.*, 1994).

hEAAT1 plays major roles within both the cerebellum as well as the retina. Knockout GLAST (hEAAT1 mouse isoform) mice were observed to be more susceptible to motor discoordination, and there is reduced signaling between photoreceptors and bipolar cells (Kanai & Hediger, 2004). Recently, it has been demonstrated that hEAAT1 may also function in clearance of glutamate across the blood-retinal barrier (Sakurai *et al.*, 2015).

hEAAT2 (SLC1A2)

hEAAT2 is a high-affinity glutamate and aspartate transporter found in glial and presynaptic membranes encoded by the SLC1A2 gene located at 5p13 in the human genome. hEAAT2 handles the bulk of glutamate reuptake at the synaptic cleft. The rat homologue GLT-1 was first isolated by Pines *et al.* (Shigeri *et al.*, 2004; Bridges & Esslinger, 2005) by immunoscreening a rat brain λ_{ZAP} cDNA library using an antibody against the purified protein (Pines *et al.*, 1992). The resulting cDNA was then used to screen a secondary rat brain 4 kb λ_{ZAP} cDNA library. The cDNA (pT7-GLT-1) that was identified conferred sodium-dependent L-glutamate transport following transfection into HeLa cells. The human homologue (hEAAT2) was isolated and cloned soon thereafter by Arriza *et al.* from human motor cortex, alongside hEAAT1 and hEAAT3 (Arriza *et al.*, 1994).

Consistent with hEAAT2 playing a major role in the removal of glutamate from the synapse, EAAT2-knockout mice succumb to lethal seizures (Kanai & Hediger, 2004).

hEAAT3 (SLC1A1)

hEAAT3 is also a high-affinity glutamate and aspartate transporter found in postsynaptic membranes, and is encoded by the gene SLC1A1 located at 9p24 in the human genome. The rat homologue GLAST was accidentally co-purified by *Storck et al.* alongside UDP-galactose:ceramide galactosyltransferase as a 66 kDa protein from rat brain (Storck *et al.*, 1992). Edman degradation and construction of a degenerate oligonucleotide probe permitted successful screening of a rat brain cDNA library. The resulting 3 kb cDNA encoded a 543 aa protein that, when produced in *Xenopus laevis* oocytes, conferred the ability to transport glutamate. The human homologue (hEAAT3) was isolated and cloned soon thereafter by Arriza *et al.* from human motor cortex, alongside hEAAT1 and hEAAT2 (Arriza *et al.*, 1994).

hEAAT3 has roles in neurotransmission within the brain as well as in solute transport within the kidney (Kanai & Hediger, 2004). In the brain, it is primarily localized to cell bodies and dendrites, thereby playing an important role in clearance of extra-synaptic glutamate (Amara & Fontana, 2002).

hEAAT4 (SLC1A6)

hEAAT4 is a high-affinity glutamate and aspartate transporter found in postsynaptic membranes primarily in the cerebellum, and is encoded by the gene SLC1A6 located at 19p13.12 in the human genome. While the discovery of hEAAT1-3 happened rather

serendipitously, hEAAT4 was identified as the result of a targeted search: it was realized that hEAAT1-3 were unable to account for all the glutamate flux in cerebellar neurons and, therefore, an additional transport isoform was predicted (Fairman *et al.*, 1995). Utilizing a probe constructed from conserved sections of hEAAT1-3, Fairman *et al.* screened a cerebellar cDNA library. The resulting cDNA encoded a transporter similar in sequence to hEAAT1-3, but with different kinetic properties. When produced in *Xenopus laevis* oocytes, the protein conferred the ability to take up glutamate in a sodium-dependent, saturable manner, and with an apparent permeant affinity higher than hEAAT1-3.

hEAAT4 is predominately expressed in the cerebellum, and more specifically on the dendrites of Purkinje cells (Fairman *et al.*, 1995; Zhou & Danbolt, 2013). hEAAT4 has the highest affinity for glutamate of all hEAATs, and therefore may play a role in uptake during low glutamate release (Dehnes *et al.*, 1998).

hEAAT4 has been demonstrated to coexist alongside hEAAT5 in the inner ear, specifically on type I and type II hair cells in addition to calyx endings (Dalet *et al.*, 2012) where they may combine to facilitate glutamate removal. While all hEAATs have a thermodynamically uncoupled chloride current, hEAAT4 and hEAAT5 have the largest chloride fluxes of the family, suggesting potential roles as inhibitory transporters (Zhou & Danbolt, 2013).

hEAAT5 (SLC1A7)

hEAAT5 is a high-affinity glutamate and aspartate transporter found primarily in retinal presynaptic membranes, and is encoded by the gene SLC1A7 located at 1p32.3 in

the human genome. Cloning and characterization of hEAAT5 was the result of examination of glutamate fluxes in the salamander retina, where *Arriza et al.* noted the existence of a previously unknown glutamate flux with an unusually large chloride conductance (Arriza *et al.*, 1997). Creation of a probe utilizing the corresponding salamander cDNA as a template yielded a cDNA from a human retina cDNA library that encoded a 560 aa protein. Production in *Xenopus laevis* oocytes conferred the ability to take up glutamate in a sodium-dependent manner.

While hEAAT5 was originally thought to be expressed specifically in the retina, it has recently been demonstrated to be present alongside hEAAT4 in the inner ear, specifically on type I and type II hair cells in addition to calyx endings (Dalet *et al.*, 2012). Much like hEAAT4, hEAAT5 also has a large uncoupled chloride current that may be involved in inhibitory roles (Zhou & Danbolt, 2013).

Glutamate Binding Proteins

Due to the importance of glutamate in the synapse, there are numerous proteins that bind it. Following the synthesis and import of glutamate into the presynaptic cell, it is transported into synaptic vesicles through vesicular glutamate transporters (VGLUTs) (Shigeri *et al.*, 2004). Action potentials control the docking and subsequent release of these vesicles into the synaptic cleft where they activate postsynaptic glutamate receptors. Postsynaptic membranes contain variable combinations of different glutamate receptors (Bridges & Esslinger, 2005). Metabotropic glutamate receptors (mGluRs) potentiate the action potential via secondary messengers (Niswender & Conn, 2010), whereas ionotropic

glutamate receptors (iGluRs) directly control the influx and efflux of ions to propagate the action potential. Aptly named after the compounds that activate them, the two iGluRs are: the α-amino-3-hydroxy-5-methyl-4-isoxazolepropionic acid (AMPA) receptor and the N-methyl-D-aspartate (NMDA) receptor (Karakas *et al.*, 2015).

Bacterial Glt$_{Ph}$

Glt$_{Ph}$ is a human glutamate transporter homologue from *Pyrococcus horikoshii* that shares a relatively high level of amino acid sequence identity (36-37%) with hEAATs, despite being a prokaryotic transporter (Yernool *et al.*, 2004; Boudker *et al.*, 2007). Transport is powered by the import of either sodium ions or protons, but unlike hEAATs, lacks the counter-transported potassium ion or the uncoupled chloride conductance (Yernool *et al.*, 2004). Because of the relatively high sequence homology specifically in areas of functional and structural importance, crystallization of Glt$_{Ph}$ and resolving of the structure to a resolution of 3.2 Å by Yernool *et al.* greatly increased our understanding of human glutamate transporter structure and function.

Structural Insights

Crystallographic data demonstrates that Glt$_{Ph}$ exists as a homotrimer facilitated by inter-monomeric interactions between TM2, TM4, and TM5 (Yernool *et al.*, 2004). The resulting quaternary structure is not unique to Glt$_{Ph,}$ as it has been demonstrated that hEAATs also exhibit this feature (Leary *et al.*, 2011). This configuration forms a basin

embedded deep within the membrane with a diameter of 80 Å (Yernool *et al.*, 2004), allowing for the putative permeant binding sites (one per monomer) to be located approximately halfway into the membrane on all 3 subunits. Unexpectedly low rates of inhibitor reversal seen in electrophysiological experiments utilizing the competitive inhibitor β-2-fluorenyl-aspartylamide (2-FAA) in *Xenopus laevis* oocytes suggests that the resulting aqueous basin formed by the trimeric structure plays a vital role in transporter function by likely conferring the ability to restrict retrograde ligand diffusion, and thus maintaining glutamate in close proximity to all three subunits for re-association (Leary *et al.*, 2011). This in turn negates the necessity for a highly stable permeant bound state, which would prevent permeant dissociation and reduce transport turnover. Above and below the permeant binding site are two helical hairpins (HP1 and HP2), which are hypothesized to act as intracellular and extracellular gates, respectively (Yernool *et al.*, 2004). Based upon the structure obtained when crystalized with bound glutamate, the evolutionarily conserved NMDGT motif present on TM7, in addition to the two hairpins and a section of TM8, form this binding site.

Functional Insights

Structural data in addition to molecular dynamic (MD) simulations based upon the Glt$_{Ph}$ crystal structure have given rise to a new transport model (Shrivastava *et al.*, 2008; Heinzelmann *et al.*, 2011). The prediction by Yernool *et al.* that HP1 and HP2 act as intracellular and extracellular gates was mirrored by the findings of MD simulations undertaken by Shrivastava *et al.*, that permeant recognition within the basin is facilitated

by Gly-354 on the tip of HP2 which is capable of making large movements (Shrivastava *et al.*, 2008). The interaction is strengthened and the permeant drawn closer into the amino acid-binding pocket with the aid of a second glycine residue (Gly-357) also found in this hairpin. The binding pocket, comprised of the triple serine motif on HP1, the NMDGT motif on TM7, and Arg-397-Thr-398 on TM8, draws the permeant deeper into the binding site, reducing the likelihood of dissociation back into the aqueous basin.

Binding of permeant to the transporter also requires the cooperative binding of sodium ions in a manner indicative of involving large conformational changes. Mutagenesis studies on hEAAT1 in conjunction with structural and functional data obtained from the GLT$_{Ph}$ crystal structure also propose a potential mechanism for the thermodynamically uncoupled chloride conductance observed during transport (Cater *et al.*, 2014). Cater *et al.* hypothesize that there exists a phase in transport in which several key anion coordinating residues align between the transport and trimerization domains, allowing for the movement of anions across the membrane. Additionally, since these residues lie within areas of high conservation amongst isoforms, Cater *et al.* propose that this anion conducting state is applicable across all hEAATs.

<u>Control and Regulation of hEAATs</u>

Expression Regulation

hEAAT expression is modulated by a variety of different endogenous and exogenous compounds including its permeant glutamate. Studies suggest that each subtype has varying mechanisms of control, likely a byproduct of their varying physiological roles. A

recent study demonstrated that hEAAT1 expression is modulated by the expression of monocarboxylate transporter 4 (MCT4) via a currently unknown mechanism during hypoxic conditions (Gao *et al.*, 2015). hEAAT2 expression in astrocytes is induced by the presence of neurons in culture through an unknown neuronal soluble factor (Gegelashvili *et al.*, 2000). A recent study suggests that tumor necrosis factor-α (TNF-α) could potentially play a role in this, since expression of hEAAT2 in astrocytes was increased in hypoxic conditions with TNF-α application (Ding *et al.*, 2014).

Membrane Localization

hEAAT modulation through membrane localization is a relatively new topic of glutamate-related research. Murphy-Royal *et al.*, utilizing antibodies bound to nanoparticles, were able to demonstrate that hEAAT2 has a high degree of mobility within the membrane (Edwards, 2015), which might aid in rapid clearance of glutamate from the synaptic cleft by replacing saturated transporters with unbound transporters from the periphery. Cross-linking using antibodies to restrict mobilization without affecting the activities of individual transporters significantly decreased glutamate fluxes across the membrane. This novel finding suggests the potential importance of transporter mobility within the plane of the membrane in the clearance of glutamate at the synapse.

On the other hand, while glutamate transporters are dispersed throughout astrocyte membranes, live cell imaging has revealed low diffusion rates of glutamate transporters at synaptic junctions, suggesting that processes are in place to anchor transporters in areas of glutamate release.

Inhibitory Compounds

Current Landscape of Inhibitors

Because of their critical role in neurotransmission and the pathogenesis of numerous neurological disorders, hEAATs have been subject to extensive research in the years following their discovery. The current lack of subtype-specific inhibitors for use as research tools and as potential therapeutic agents has, however, been a notable limitation (Dunlop, 2006). The most important small molecule glutamate transport inhibitors discovered to date are β-hydroxy-substituted aspartate molecules.

β-Hydroxy-substituted aspartates are aspartate derivatives that introduce different functional groups onto the β-carbon of aspartatic acid (Shigeri *et al.*, 2004; Bridges & Esslinger, 2005). The two most notable β-hydroxy-substituted aspartates are β-threo-hydroxyaspartate (β-THA) and β-threo-benzyloxyaspartate (TBOA). β-THA was one of the first aspartate analogues synthesized that had inhibitory effects on glutamate transport. Its usefulness as an inhibitor is compromised because it is a transported permeant for hEAAT1-4 (Lebrun *et al.*, 1997). Addition of a bulky methyl-benzyl group to β-THA to form TBOA prevented transport, and thus generated the most potent EAAT inhibitor currently available. Recent crystallography findings with Glt_{Ph} show that TBOA binds to the permeant-binding pocket as predicted, but that the bulky phenyl group interacts with residues on HP2 (extracellular gate). These interactions prevent closure/transport and stabilize HP2, restricting it from making large movements within the trimer basin (Boudker *et al.*, 2007; Shrivastava *et al.*, 2008).

Synthesis Methodology and Rationale

Since TBOA is a potent broadly acting non-permeant EAAT inhibitor, further chemical modifications of the TBOA structure may exploit corresponding differences in molecular structure between different hEAAT subtypes, and lead to the creation of isoform-specific transport inhibitors.

Diversity Oriented Synthesis

Diversity oriented synthesis (DOS) is a technique aimed at generating a large skeletally diverse compound library from one or a small group of starter compounds. This is accomplished through multiple series of reactions applied and reapplied to the previous iteration's products (Connor *et al.*, 2012).

Since the goal was to generate glutamate-mimetics, a small number of starting compounds with aspartate backbones were selected. These compounds were then subjected to synthetic reactions to append various simple unsaturated caps to their structures. The addition of an unsaturated bond made the new compounds prime substrates for metathesis reactions which, following their completion, resulted in the generation of hydroxyaspartate analogues with diverse backbones. These new compounds were then screened for inhibitory activity utilizing a radioisotope glutamate uptake assay (10 μM inhibitor, 30 μM L-Glutamate (50 μL 300 μM L-Glutamate supplemented with 0.075

μL L-[3,4-^{3}H]-Glutamate), 15 minute incubation) in HEK 293 cells producing hEAAT1, hEAAT2, or hEAAT3.

From the lead compounds that demonstrated significant transport inhibition, further modifications were then undertaken. By systematically moving various functional groups into different positions on the compounds, the three-dimensional space around the EAAT amino acid binding pocket was chemically probed in the hope of producing compounds that exploited the likely small differences in structure between transporter subtypes. The resulting compounds were to sent our laboratory for detailed screening and functional characterization (**Table 1.1**).

Project I Hypothesis and Goals

It is hypothesized that the new and novel series of compounds described above include isoform-specific glutamate transport inhibitors. To test this hypothesis, recombinant hEAATs were produced individually in *Xenopus laevis* oocytes and sensitivity to inhibition by these compounds were evaluated with the ultimate goal of identifying and characterizing each inhibitor's isoform selectivity.

Nucleosides

Nucleosides consist of a nucleobase linked to a pentose sugar, many of which are biologically active metabolites involved in numerous processes within the body. Since their biosynthesis is energy intensive, they are often salvaged and repurposed as precursors for nucleotide synthesis, linking them intimately to the body's genetic and metabolic processes

(Parkinson *et al.*, 2011). Nucleosides are categorized into two major groups according to the structure of the nucleobase. Pyrimidine nucleosides are comprised of a heterocyclic aromatic benzene-like ring with nitrogen substitutions on the first and third positions. The second group, purine nucleosides, contains a heterocyclic ring comprised of fused pyrimidine and imidazole rings. Purine nucleosides, particularly adenosine, have an additional role as paracrine-signaling molecules. Acting through purinergic G-protein coupled receptors (GPCRs) (A_1, A_{2A}, A_{2B}, A_3), adenosine signaling cascades are involved in multiple regulatory processes in the central nervous system, cardiovascular system, and immune system, typically in responses to ischemia or cellular damage (Parkinson *et al.*, 2011). Nucleosides are hydrophilic in nature, and therefore require specific transporter proteins (nucleoside transporters) to facilitate their cellular import and export across the phospholipid bilayer membrane (Young *et al.*, 2013).

Nucleoside Transport

Human nucleoside transporters (hNTs) are comprised of two structurally and evolutionarily unrelated protein families, each with members that have varying permeant selectivites: the human concentrative nucleoside transporter (hCNT) family and the human equilibrative nucleoside transporter (hENT) family (Young *et al.*, 2013). These proteins are variously located within the body, and are present in both plasma and organellar membranes. Although some members have distinctive localizations, multiple transporter subtypes can be found co-expressed in the same cell. In certain situations, such as in polarized cells of intestinal and kidney epithelia, the two families function together on

opposite membranes to facilitate trans-cellular transport (Young *et al.*, 2013). In other cases, there is co-expression of multiple transporter subtypes with overlapping functionalities in the same membrane. While the exact reasons for this are not fully understood, one hypothesis is that it allows for redundancy in situations where nucleoside transport is vital.

Concentrative Nucleoside Transporters

The human concentrative nucleoside transporter family (SLC28) is a family of secondary active transporters with predominantly plasma membrane localizations involved in the cellular uptake of endogenous nucleosides in addition to various anti-cancer and anti-viral nucleoside analogues. hCNT1, hCNT2, and hCNT3 were initially termed *cit*, *cif*, and *cib*, respectively, due to their <u>c</u>oncentrative nature, NBMPR-<u>i</u>nsensitivity, and permeant selectivities (<u>t</u>hymidine, <u>f</u>ormycin, and <u>b</u>road-selectivity, respectively) (Smith *et al.*, 2005).

hCNT1 (SLC28A1)

Located at 15q25.3 in the human genome, hCNT1 is a concentrative nucleoside transporter with a cation coupling ratio of 1 sodium to 1 nucleoside. With the exception of adenosine, hCNT1 is pyrimidine nucleoside-selective. The cDNA encoding rCNT1, the rat homologue of hCNT1, was initially cloned by our laboratory using expression screening of a rat jejunum epithelium cDNA library, following demonstration that injection of poly-A RNA from rat jejunum into *Xenopus laevis* oocytes conferred the ability to transport nucleosides

in a sodium-dependent manner (Huang *et al.*, 1994). This cDNA encoded a 648 aa protein, which mediated pyrimidine-selective transport corresponding to the previously described *cit* system. Additionally, rCNT1 conferred the ability to transport the AIDS drug azidothymidine (AZT), thereby providing a mechanism for its previously unknown mechanism of cellular uptake. The anticancer nucleoside analogue gemcitabine was also transported, implicating this new class of membrane transporter proteins in the uptake of both antiviral and anticancer compounds (Mackey *et al.*, 1999).

hCNT2 (SLC28A2)

Located at 15q15 in the human genome, hCNT2 is a concentrative nucleoside transporter with a cation coupling ratio of 1 sodium to 1 nucleoside. With the exception of uridine, hCNT2 is purine nucleoside-selective (Young *et al.*, 2013) and corresponds to the previously known system *cif* (Parkinson *et al.*, 2011). Identified by our laboratory utilizing a combined PCR/hybridization strategy based upon the previously isolated/identified rat homolog rCNT1 sequence (Ritzel *et al.*, 1998), hCNT2 is predominantly plasma membrane localized, and expressed in a variety of tissues including the polarized cells of the kidney and intestine, where it is involved in the transcellular movement of nucleosides (Young *et al.*, 2013).

hCNT3 (SLC28A3)

Located at 9q22.2 in the human genome, hCNT3 is a concentrative nucleoside transporter with a cation coupling ratio of 2 sodium to 1 nucleoside or 1 proton to 1 nucleoside. hCNT3 is broadly selective, being able to transport both purine and pyrimidine nucleosides.

Initially found by our laboratory through BLAST searches of human ESTs from mammary gland and colon adenocarcinoma, the initially identified partial overlapping sequences indicated existence of a transporter homologous to, but distinct from the previously identified hCNT1 and hCNT2, and therefore potentially corresponding to system *cib*. RACE utilizing the partial EST cDNA sequence in HL-60 cells, known to contain the *cib* system, resulted in isolation of a 691 bp sequence which encoded a transport protein, hCNT3, which mediated both purine and pyrimidine transport activity when produced in *Xenopus laevis* oocytes (Ritzel *et al.*, 2001).

Equilibrative Nucleoside Transporters

The human equilibrative nucleoside transporter family (SLC29) is a group of structurally-related proteins that facilitate the movement of endogenous nucleosides and anticancer and antiviral nucleoside-analogues down their concentration gradients. hENT1 and hENT2 were initially termed *es* and *ei*, respectively, due to the e̲quilibrative nature of transport and their s̲ensitivity or i̲nsensitivity to the inhibitor nitrobenzylmercaptoopurine ribonucleoside (NBMPR), and were the first two members of this family to be cloned and characterized (Baldwin *et al.*, 2004). Unlike the hCNTs, the hENTs typically have broader

permeant selectivities with varying abilities to transport nucleobases and monoamines in addition to physiological nucleosides (Young *et al.*, 2013).

hENT1 (SLC29A1)

Located at 6p21.1 in the human genome (Young *et al.*, 2013), hENT1 is an equilibrative nucleoside transporter with ubiquitous expression in human cells and tissues (Baldwin *et al.*, 2004). Functioning predominantly in plasma membranes, hENT1 was initially termed *es* due to its high sensitivity to inhibition by NBMPR, which contributed to its identification and purification prior to cloning (Kwong *et al.*, 1988). Purification allowed for N-terminal amino acid sequencing which was used to screen a human placental cDNA library by PCR, yielding a 456 residue protein which conferred NBMPR-sensitive purine and pyrimidine nucleosides transport activity when produced in *Xenopus laevis* oocytes (Griffiths *et al.*, 1997). In addition to transporting all physiological nucleosides and nucleobases (except cytosine), hENT1 is responsible for the transport of several anticancer and antiviral nucleoside drugs (Yao *et al.*, 2011).

As well as mediating cellular uptake or release of nucleosides (and nucleobases) from non-polarized cells, co-expression of hENT1 alongside other nucleoside transporters in polarized cells such as intestinal epithelia, hepatocytes, and endothelial cells of the blood-brain barrier (BBB) and blood-CSF barrier (BCSFB) indicates a functional role in the transcellular flow of physiological nucleosides and nucleobases (Young *et al.*, 2013).

hENT2 (SLC29A2)

Located at 11q13 in the human genome, hENT2 is an equilibrative nucleoside transporter with a predominantly plasma membrane localization and ubiquitous expression in human cells and tissues (Young *et al.*, 2013). hENT2 was initially termed *ei* due to its relative insensitivity to inhibition by NBMPR, in contrast to hENT1 which is inhibited by nanomolar concentrations of NBMPR (Parkinson *et al.*, 2011). Cloning of hENT2 using touchdown PCR in a human placental cDNA library was the result of an observation that the previously cloned hENT1's C-terminal domain shared high sequence similarity to the human and mouse HNP36 proteins. It was additionally noted that the open reading frame upstream of the human HNP36 cDNA encoded additional sequence that shared 49% amino acid sequence identity with the N-terminal region of hENT1. It was therefore hypothesized that the full open reading frame of human HNP36 cDNA encoded a functional transporter related to hENT1 (Griffiths *et al.*, 1997).

hENT2 has the broadest selectivity of all nucleoside transporters with the ability to transport physiological nucleosides and nucleobases in addition to various anticancer and antiviral drugs (Yao *et al.*, 2002; Parkinson *et al.*, 2011; Young *et al.*, 2013). In particular, hENT2 has a greater capacity to transport nucleobases than hENT1.

hENT3 (SLC29A3)

Located at 10q22.1 in the human genome, hENT3 is a pH-sensitive equilibrative nucleoside transporter localized to lysosomal membranes (Young *et al.*, 2013). Its discovery and cloning was the result of a targeted BLAST search of GeneBank™ sequence

databases which revealed a 419 bp EST sequence from a mouse kidney cDNA clone that shared sequence homology with the two previously cloned and characterized equilibrative nucleoside transporters: hENT1 and hENT2 (Hyde *et al.*, 2001). Subsequent sequencing identified a 1425 bp open reading frame that encoded a 474 aa protein which was termed mENT3, in addition to also revealing a truncated sequence in a human placental cDNA library. Genomic sequence database searches revealed a human chromosome 10 clone that encoded the full 475 aa protein, including the missing N-terminal residues. Due to its lysosomal localization, expression is expected to be ubiquitous, as suggested by testing of multiple tissue RNA arrays (Baldwin *et al.*, 2004). Able to transport all physiological nucleosides in addition to the nucleobase adenine (Baldwin *et al.*, 2004; Young *et al.*, 2013), hENT3 is likely involved in the recovery and salvaging of lysosomal nucleic acid degradation products. Its pH-sensitivity (activated at low pH) suggests the possibility that transport may be proton-coupled (Baldwin *et al.*, 2005).

Mutation of an N-terminal dileucine targeting motif to a double alanine (mutant termed hAA or hENT3AA) allows for targeting of a fully functional hENT3 to the plasma membrane for whole-cell transport studies in *Xenopus laevis* oocytes (Baldwin *et al.*, 2005).

hENT4 (SLC29A4)

Located at 7p22.1 in the human genome, hENT4 is a pH-sensitive equilibrative nucleoside/polyspecific organic cation transporter that is the most evolutionarily divergent member of the hENT family of proteins (Young *et al.*, 2013). The transporter was identified through targeted genomic database searches for putative ENTs in non-

mammalian taxa (Acimovic & Coe, 2002). The resulting sequences were then used to reverse screen mammalian genome databases for potential novel ENTs. This resulted in the identification of a novel putative mouse ENT (mENT4) which was subsequently used to identify its human homologue: hENT4. Also referred to as the plasma membrane monoamine transporter (PMAT), hENT4 is the only nucleoside transporter (hENTs and hCNTs) that lacks the ability to transport uridine but, rather, selectively transports adenosine under acidic conditions in addition to various structurally unrelated permeants such as serotonin and 1-methyl-4-phenylpyridinium (MPP^+), the transport of which appears to be pH-insensitive (Young *et al.*, 2008). Multiple tissue RNA arrays (Baldwin *et al.*, 2004) indicate predominant expression in brain and cardiac tissues, indicating a potential role in adenosine homeostasis during acidotic ischemic conditions (Young *et al.*, 2008; Parkinson *et al.*, 2011). Like hENT3, adenosine transport by hENT4 may be proton-coupled.

The MAPK Pathway

The MAPK pathway is a signaling cascade comprised of numerous protein constituents that mediate cell growth and differentiation signals (Santarpia *et al.*, 2012). As such, aberrant uncontrolled signaling within this pathway can result in malignancy. The large number of protein mediators attests to the importance of this pathway, but complicates the cancer treatment process. To reduce therapeutic spillover side effects, inhibitors designed to target the major steps in the pathway need to be specific.

The MAPK pathway acts to transduce cell surface signals to the nucleus where mitogenic effects can be initiated (Santarpia *et al.*, 2012). The signaling cascade is initiated by the binding of a signaling molecule to tyrosine kinase receptors (TKRs). These receptors, upon activation, dimerize and phosphorylate each other's cytoplasmic domains, initiating recruitment of adapter proteins (Christensen, 2007).

The physiological importance of this pathway in regulating cell growth and proliferation can be seen from the large number of cancer types that exhibit mutations in members of the pathway. Rapidly accelerated fibrosarcoma (RAF) kinases, for example, are a family of proteins within the MAPK pathway upstream of mitogen-activated protein kinase kinase (MEK), consisting of three members (A-RAF, B-RAF and C-RAF). Sequencing results identify the presence of a B-RAF mutation in approximately 8% of all human cancers and 66% of melanomas (Davies *et al.*, 2002). Furthermore, 90% of these B-RAF mutations are the result of a single valine to glutamic acid point mutation at position 600 (V600E) resulting in a constitutively active B-RAF protein (Zhang, 2015).

MEK Inhibitors

The binding of allosteric MEK inhibitors to MEK1/2 exploits a unique inhibitor binding site adjacent to the ATP binding site in the interlobal cleft of the protein (Sebolt-Leopold & Bridges, 2009). The absence of such a binding site in other kinases allows for a high level of selectivity of inhibition, which greatly increases the therapeutic potential of drugs that target this site. Binding of the MEK inhibitor to its binding site does not prevent the binding of ATP in the adjacent pocket. Rather, crystal structures co-crystallized in the

presence of several MEK inhibitors suggest that interactions between the hydroxamate tail of the inhibitor and the γ-phosphate of ATP actually enhances ATP binding stability. The inhibitor mechanism is due to minor conformational changes within the catalytic domains thereby transforming the protein into a catalytically inactive state. This is accomplished by disrupting the extracellular signal-regulated kinase (ERK) binding site, in addition to disruption of the critical Lys97-Glu114 salt-bridge, locking the protein into an inactive conformation (Roskoski, 2012).

Compounds

Many of the initial MEK inhibitors were developed without access to MEK protein structural data. As a guide for the synthesis of novel MEK inhibitors, researchers have constructed a MEK pharmacophore model based upon data from the pre-existing compounds (Sebolt-Leopold & Bridges, 2009).

Binimetinib (MEK162, ARRY-162)

Binimetinib (**Figure 1.1A**) is an allosteric inhibitor of MEK1/2 currently in phase 3 clinical trials for low-grade serous ovarian cancer (ClinicalTrials.gov number NCT01849874) and B-RAF/NRAS-mutant melanoma (ClinicalTrials.gov number NCT01909453 and NCT01763164). Results of the phase 2 clinical trials for binimetinib demonstrated improvements in tumor shrinkage, making it the first targeted therapy drug

to exhibit effective results in NRAS-mutant melanoma (Sebolt-Leopold & Bridges, 2009). Common adverse side effects include acneiform dermatitis, rash, edema, and diarrhea.

Trametinib (Mekinist™, GSK1120212)

Trametinib (**Figure 1.1B**) is an orally available allosteric inhibitor of MEK1/2 currently FDA approved for treatment of metastatic or unresectable melanoma either by itself or in combined therapy with dabrafinib (B-RAF inhibitor) (Marzuka *et al.*, 2015). Results from a phase 1 dose escalation trial showed two complete and ten partial responses to trametinib in B-RAF-mutant melanoma (Falchook *et al.*, 2012). Common adverse side effects include rash, fatigue, and diarrhea, all three of which are frequently associated adverse effects of other MEK1/2 inhibitors (Lugowska *et al.*, 2015).

Clinical trials performed in combined therapy with the nucleoside analogue drug gemcitabine demonstrated no improvement when compared to gemcitabine alone (ClinicalTrial.gov Numbers: NCT01428427 and NCT01231581) (Infante *et al.*, 2013).

Selumetinib (AZD6244, ARRY-142886)

Selumetinib (**Figure 1.1C**) is an allosteric inhibitor of MEK1/2 currently in phase 3 clinical trials for KRAS mutant non-small cell lung cancer (NSCLC) (ClinicalTrial.gov number NCT01933932), thyroid cancer (ClinicalTrial.gov number NCT01843062), and uveal melanoma (in conjunction with the alkylating agent dacarbazine) (Carvajal *et al.*, 2015) (ClinicalTrial.gov number NCT01974752). Common side effects of selumetinib

observed in clinical trials include rash, edema, diarrhea, and fatigue (Ciombor & Bekaii-Saab, 2014).

Project II Rationale, Hypothesis and Goals

Our clinical collaborator at the Cross Cancer Institute, Dr. Michael Sawyer, noted that failed clinical trials with MEK inhibitors in combined therapy with nucleoside-analogue drugs demonstrated unexpected low in-trial efficacy (M. Sawyer, personal communication). Examination of the chemical structures of these MEK inhibitors revealed the presence of analogous internal structures also present in nucleosides.

Because of these similarities, it was hypothesized that these compounds may be able to bind to nucleoside transporters, the uptake route for cellular entry for nucleoside-analogue drugs, and thereby block drug entry into the cell. It was also hypothesized that these compounds may elicit side effects through disruption of nucleoside transporter-mediated adenosine reuptake. To investigate these hypotheses, recombinant hENTs and hCNTs were produced individually in *Xenopus laevis* oocytes and tested for sensitivity to MEK inhibitors with the goal of identifying the molecular mechanism responsible for the adverse effects associated with MEK inhibitor therapy.

References

Acimovic Y & Coe IR (2002). Molecular evolution of the equilibrative nucleoside transporter family: identification of novel family members in prokaryotes and eukaryotes. *Mol Biol Evol* **19,** 2199–2210.

Amara SG & Fontana ACK (2002). Excitatory amino acid transporters: keeping up with glutamate. *Neurochemistry International* **41,** 313–318.

Arriza JL, Eliasof S, Kavanaugh MP & Amara SG (1997). Excitatory amino acid transporter 5, a retinal glutamate transporter coupled to a chloride conductance. *Proc Natl Acad Sci U S A* **94,** 4155–4160.

Arriza JL, Fairman WA, Wadiche JI, Murdoch GH, Kavanaugh MP & Amara SG (1994). Functional comparisons of three glutamate transporter subtypes cloned from human motor cortex. *J Neurosci* **14,** 5559–5569.

Baldwin SA, Beal PR, Yao SYM, King AE, Cass CE & Young JD (2004). The equilibrative nucleoside transporter family, SLC29. *Pflugers Arch* **447,** 735–743.

Baldwin SA, Yao SYM, Hyde RJ, Ng AML, Foppolo S, Barnes K, Ritzel MWL, Cass CE & Young JD (2005). Functional characterization of novel human and mouse equilibrative nucleoside transporters (hENT3 and mENT3) located in intracellular membranes. *J Biol Chem* **280,** 15880–15887.

Boudker O, Ryan RM, Yernool D, Shimamoto K & Gouaux E (2007). Coupling substrate and ion binding to extracellular gate of a sodium-dependent aspartate transporter. *Nature* **445,** 387–393.

Bridges RJ & Esslinger CS (2005). The excitatory amino acid transporters: pharmacological insights on substrate and inhibitor specificity of the EAAT subtypes. *Pharmacol Ther* **107,** 271–285.

Brosnan JT & Brosnan ME (2013). Glutamate: a truly functional amino acid. *Amino Acids* **45,** 413–418.

Carvajal RD, Schwartz GK, Mann H, Smith I & Nathan PD (2015). Study design and rationale for a randomised, placebo-controlled, double-blind study to assess the efficacy of selumetinib (AZD6244; ARRY-142886) in combination with dacarbazine in patients with metastatic uveal melanoma (SUMIT). *BMC Cancer* **15,** 467.

Cater RJ, Vandenberg RJ & Ryan RM (2014). The domain interface of the human glutamate transporter EAAT1 mediates chloride permeation. *Biophys J* **107,** 621–629.

Christensen JG (2007). A preclinical review of sunitinib, a multitargeted receptor tyrosine kinase inhibitor with anti-angiogenic and antitumour activities. *Ann Oncol* **18 Suppl 10,** x3–x10.

Ciombor KK & Bekaii-Saab T (2014). Selumetinib for the treatment of cancer. *Expert Opin Investig Drugs* **24,** 111–123.

Connor CJO, Beckmann HSG & Spring DR (2012). Diversity-oriented synthesis: producing chemical tools for dissecting biology. *Chem Soc Rev* **41,** 4444–4456.

Dalet A, Bonsacquet J, Gaboyard-Niay S, Calin-Jageman I, Chidavaenzi RL, Venteo S, Desmadryl G, Goldberg JM, Lysakowski A & Chabbert C (2012). Glutamate transporters EAAT4 and EAAT5 are expressed in vestibular hair cells and calyx endings. *PLoS ONE* **7,** e46261.

Davies H et al. (2002). Mutations of the BRAF gene in human cancer. *Nature* **417,** 949–954.

Dehnes Y, Chaudhry FA, Ullensvang K, Lehre KP, Storm-Mathisen J & Danbolt NC (1998). The Glutamate Transporter EAAT4 in Rat Cerebellar Purkinje Cells: A Glutamate-Gated Chloride Channel Concentrated near the Synapse in Parts of the Dendritic Membrane Facing Astroglia. *J Neurosci* **18,** 3606–3619.

Ding Y, Zhang K, Liu S, Zhang Q, Ma C, Bruce IC & Zhang X (2014). Tumor necrosis factor-α promotes the expression of excitatory amino-acid transporter 2 in astrocytes: Optimal concentration and incubation time. *Exp Ther Med* **8,** 1909–1913.

Dunlop J (2006). Glutamate-based therapeutic approaches: targeting the glutamate transport system. *Curr Opin Pharmacol* **6,** 103–107.

Edwards RH (2015). Mobile binding sites regulate glutamate clearance. *Nat Neurosci* **18,** 166–168.

Fairman WA, Vandenberg RJ, Arriza JL, Kavanaugh MP & Amara SG (1995). An excitatory amino-acid transporter with properties of a ligand-gated chloride channel. *Nature* **375,** 599–603.

Falchook GS et al. (2012). Activity of the oral MEK inhibitor trametinib in patients with advanced melanoma: a phase 1 dose-escalation trial. *The Lancet Oncology* **13,** 782–789.

Gao C, Zhu W, Tian L, Zhang J & Li Z (2015). MCT4-mediated expression of EAAT1 is involved in the resistance to hypoxia injury in astrocyte-neuron co-cultures. *Neurochem Res* **40,** 818–828.

Gegelashvili G, Dehnes Y, Danbolt NC & Schousboe A (2000). The high-affinity glutamate transporters GLT1, GLAST, and EAAT4 are regulated via different signalling mechanisms. *Neurochemistry International* **37,** 163–170.

Griffiths M, Beaumont N, Yao SY, Sundaram M, Boumah CE, Davies A, Kwong FY, Coe I, Cass CE, Young JD & Baldwin SA (1997). Cloning of a human nucleoside transporter implicated in the cellular uptake of adenosine and chemotherapeutic drugs. *Nat Med* **3,** 89–93.

Heinzelmann G, Baştuğ T & Kuyucak S (2011). Free energy simulations of ligand binding to the aspartate transporter Glt(Ph). *Biophys J* **101,** 2380–2388.

Huang QQ, Yao SY, Ritzel MW, Paterson AR, Cass CE & Young JD (1994). Cloning and functional expression of a complementary DNA encoding a mammalian nucleoside transport protein. *J Biol Chem* **269,** 17757–17760.

Hyde RJ, Cass CE, Young JD & Baldwin JDSA (2001). The ENT family of eukaryote nucleoside and nucleobase transporters: recent advances in the investigation of structure/function relationships and the identification of novel isoforms. *Molecular Membrane Biology* **18,** 53–63.

Infante JR, Papadopoulos KP, Bendell JC, Patnaik A, Burris HA, Rasco D, Jones SF, Smith L, Cox DS, Durante M, Bellew KM, Park JJ, Le NT & Tolcher AW (2013). A phase 1b study of trametinib, an oral Mitogen-activated protein kinase kinase (MEK) inhibitor, in combination with gemcitabine in advanced solid tumours. *Eur J Cancer* **49,** 2077–2085.

Jih K-Y, Sohma Y & Hwang T-C (2012). Nonintegral stoichiometry in CFTR gating revealed by a pore-lining mutation. *J Gen Physiol* **140,** 347–359.

Kanai Y & Hediger MA (2004). The glutamate/neutral amino acid transporter family SLC1: molecular, physiological and pharmacological aspects. *Pflugers Arch* **447,** 469–479.

Karakas E, Regan MC & Furukawa H (2015). Emerging structural insights into the function of ionotropic glutamate receptors. *Trends in Biochemical Sciences* **40,** 328–337.

Kwong FY, Davies A, Tse CM, Young JD, Henderson PJ & Baldwin SA (1988). Purification of the human erythrocyte nucleoside transporter by immunoaffinity chromatography. *Biochem J* **255,** 243–249.

Leary GP, Holley DC, Stone EF, Lyda BR, Kalachev LV & Kavanaugh MP (2011). The central cavity in trimeric glutamate transporters restricts ligand diffusion. *Proc Natl Acad Sci USA* **108,** 14980–14985.

Lebrun B, Sakaitani M, Shimamoto K, Yasuda-Kamatani Y & Nakajima T (1997). New β-Hydroxyaspartate Derivatives Are Competitive Blockers for the Bovine Glutamate/Aspartate Transporter. *J Biol Chem* **272,** 20336–20339.

Lin C-LG, Tzingounis AV, Jin L, Furuta A, Kavanaugh MP & Rothstein JD (1998). Molecular cloning and expression of the rat EAAT4 glutamate transporter subtype1. *Molecular Brain Research* **63,** 174–179.
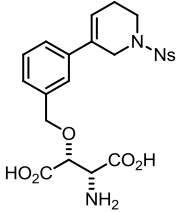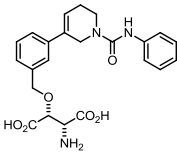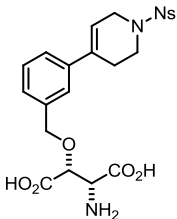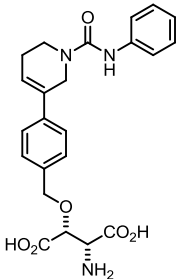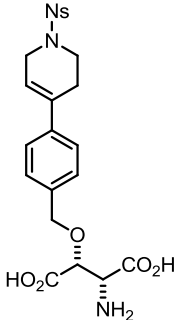
Lugowska I, Koseła-Paterczyk H, Kozak K & Rutkowski P (2015). Trametinib: a MEK inhibitor for management of metastatic melanoma. *Onco Targets Ther* **8,** 2251–2259.

Mackey JR, Yao SYM, Smith KM, Karpinski E, Baldwin SA, Cass CE & Young JD (1999). Gemcitabine Transport in Xenopus Oocytes Expressing Recombinant Plasma Membrane Mammalian Nucleoside Transporters. *JNCI J Natl Cancer Inst* **91,** 1876–1881.

Marzuka A, Huang L, Theodosakis N & Bosenberg M (2015). Melanoma Treatments: Advances and Mechanisms. *J Cell Physiol* n/a – n/a.

Meldrum BS (2000). Glutamate as a Neurotransmitter in the Brain: Review of Physiology and Pathology. *J Nutr* **130,** 1007–1007.

Niswender CM & Conn PJ (2010). Metabotropic glutamate receptors: physiology, pharmacology, and disease. *Annu Rev Pharmacol Toxicol* **50,** 295–322.

Parkinson FE, Damaraju VL, Graham K, Yao SYM, Baldwin SA, Cass CE & Young JD (2011). Molecular biology of nucleoside transporters and their distributions and functions in the brain. *Curr Top Med Chem* **11,** 948–972.

Pines G, Danbolt NC, Bjørås M, Zhang Y, Bendahan A, Eide L, Koepsell H, Storm-Mathisen J, Seeberg E & Kanner BI (1992). Cloning and expression of a rat brain L-glutamate transporter. *Nature* **360,** 464–467.

Ritzel MW, Ng AM, Yao SY, Graham K, Loewen SK, Smith KM, Ritzel RG, Mowles DA, Carpenter P, Chen XZ, Karpinski E, Hyde RJ, Baldwin SA, Cass CE & Young JD (2001). Molecular identification and characterization of novel human and mouse concentrative Na+-nucleoside cotransporter proteins (hCNT3 and mCNT3) broadly selective for purine and pyrimidine nucleosides (system cib). *J Biol Chem* **276,** 2914–2927.

Ritzel MW, Yao SY, Ng AM, Mackey JR, Cass CE & Young JD (1998). Molecular cloning, functional expression and chromosomal localization of a cDNA encoding a human Na+/nucleoside cotransporter (hCNT2) selective for purine nucleosides and uridine. *Mol Membr Biol* **15,** 203–211.

Roskoski R (2012). MEK1/2 dual-specificity protein kinases: structure and regulation. *Biochem Biophys Res Commun* **417,** 5–10.

Ryan RM & Mindell JA (2007). The uncoupled chloride conductance of a bacterial glutamate transporter homolog. *Nat Struct Mol Biol* **14,** 365–371.

Sakurai T, Akanuma S, Usui T, Kubo Y, Tachikawa M & Hosoya K (2015). Excitatory Amino Acid Transporter 1-Mediated L-Glutamate Transport at the Inner Blood-Retinal

Barrier: Possible Role in L-Glutamate Elimination from the Retina. *Biol Pharm Bull* **38,** 1087–1091.

Santarpia L, Lippman SM & El-Naggar AK (2012). Targeting the MAPK–RAS–RAF signaling pathway in cancer therapy. *Expert Opinion on Therapeutic Targets* **16,** 103–119.

Sebolt-Leopold JS & Bridges AJ (2009). Road to PD0325901 and beyond: The MEK Inhibitor Quest. In *Kinase Inhibitor Drugs*, ed. Li R & Stafford JA, pp. 203–227. John Wiley & Sons, Inc. Available at: http://onlinelibrary.wiley.com/doi/10.1002/9780470524961.ch8/summary [Accessed May 11, 2015].

Shigeri Y, Seal RP & Shimamoto K (2004). Molecular pharmacology of glutamate transporters, EAATs and VGLUTs. *Brain Res Brain Res Rev* **45,** 250–265.

Shim J, Son HJ, Kim Y, Kim KH, Kim JT, Moon H, Kim MJ, Misaka T & Rhyu M-R (2015). Modulation of Sweet Taste by Umami Compounds via Sweet Taste Receptor Subunit hT1R2. *PLoS One*; DOI: 10.1371/journal.pone.0124030.

Shrivastava IH, Jiang J, Amara SG & Bahar I (2008). Time-resolved mechanism of extracellular gate opening and substrate binding in a glutamate transporter. *J Biol Chem* **283,** 28680–28690.

Smith KM, Slugoski MD, Loewen SK, Ng AML, Yao SYM, Chen X-Z, Karpinski E, Cass CE, Baldwin SA & Young JD (2005). The broadly selective human Na+/nucleoside cotransporter (hCNT3) exhibits novel cation-coupled nucleoside transport characteristics. *J Biol Chem* **280,** 25436–25449.

Storck T, Schulte S, Hofmann K & Stoffel W (1992). Structure, expression, and functional analysis of a Na(+)-dependent glutamate/aspartate transporter from rat brain. *Proc Natl Acad Sci U S A* **89,** 10955–10959.

Szmajda BA & DeVries SH (2011). Glutamate Spillover between Mammalian Cone Photoreceptors. *J Neurosci* **31,** 13431–13441.

Yao SYM, Ng AML, Cass CE, Baldwin SA & Young JD (2011). Nucleobase transport by human equilibrative nucleoside transporter 1 (hENT1). *J Biol Chem* **286,** 32552–32562.

Yao SYM, Ng AML, Vickers MF, Sundaram M, Cass CE, Baldwin SA & Young JD (2002). Functional and molecular characterization of nucleobase transport by recombinant human and rat equilibrative nucleoside transporters 1 and 2. Chimeric constructs reveal a role for the ENT2 helix 5-6 region in nucleobase translocation. *J Biol Chem* **277,** 24938–24948.

Yernool D, Boudker O, Jin Y & Gouaux E (2004). Structure of a glutamate transporter homologue from Pyrococcus horikoshii. *Nature* **431,** 811–818.

Young JD, Yao SYM, Baldwin JM, Cass CE & Baldwin SA (2013). The human concentrative and equilibrative nucleoside transporter families, SLC28 and SLC29. *Mol Aspects Med* **34,** 529–547.

Young JD, Yao SYM, Sun L, Cass CE & Baldwin SA (2008). Human equilibrative nucleoside transporter (ENT) family of nucleoside and nucleobase transporter proteins. *Xenobiotica* **38,** 995–1021.

Zhang W (2015). BRAF inhibitors: the current and the future. *Current Opinion in Pharmacology* **23,** 68–73.

Zhou Y & Danbolt NC (2013). GABA and Glutamate Transporters in Brain. *Front Endocrinol (Lausanne)* **4,** 165.

Table 1.1: Glutamate transport inhibitors.

Compound Name	Structure	R-Group	Organic Nomenclature
AF314		Ns	(2R*, 3R*)-2-Amino-3-(3-(1-(2-nitrophenylsulfonyl)-1,2,5,6-tetrahydropyridin-3-yl)benzyloxy)succinic acid
AF327		CONHPh	(2R*, 3R*)-2-Amino-3-(3-(1-(phenylcarbamoyl)-1,2,5,6-tetrahydropyridin-3-yl)benzyloxy)succinic acid
AF340		Ns	(2R*, 3R*)-2-Amino-3-(3-(1-(2-nitrophenylsulfonyl)-1,2,3,6-tetrahydropyridin-4-yl)benzyloxy)succinic acid
AF375		CONHPh	(2R*, 3R*)-2-Amino-3-(4-(1-(phenylcarbamoyl)-1,2,5,6-tetrahydropyridin-3-yl)benzyloxy)succinic acid
AF380		Ns	(2R*, 3R*)-2-Amino-3-(4-(1-(2-nitrophenylsulfonyl)-1,2,3,6-tetrahydropyridin-4-yl)benzyloxy)succinic acid
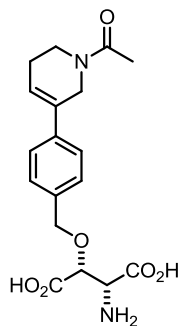
AF383		COMe	(2R*, 3R*)-2-(4-(1-Acetyl-1,2,5,6-tetrahydropyridin-3-yl)benzyloxy)-3-aminosuccinic acid
AF403		CONHPh	(2R*, 3R*)-2-Amino-3-(4-(1-(phenylcarbamoyl)-1,2,3,6-tetrahydropyridin-4-yl)benzyloxy)succinic acid
AF451		CONHPh	(2R*, 3R*, 6'R) and (2R*, 3R*, 6'S)-2-Amino-3-(3-(6'-methyl-1'-(phenylcarbamoyl)-1',2',3',6'-tetrahydropyridin-4'-yl)benzyloxy)succinic acid
AF452		SO$_2$Ph	(2R*, 3R*, 6'R) and (2R*, 3R*, 6'S)-2-Amino-3-(3-(6'-methyl-1'-(phenylsulfonyl)-1',2',3',6'-tetrahydropyridin-4'-yl)benzyloxy)succinic acid
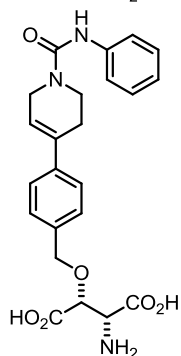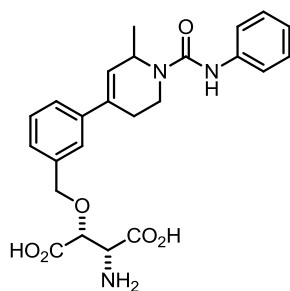
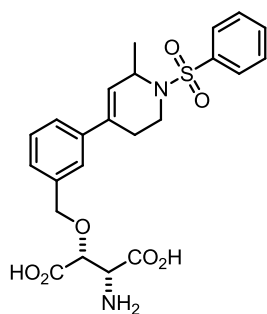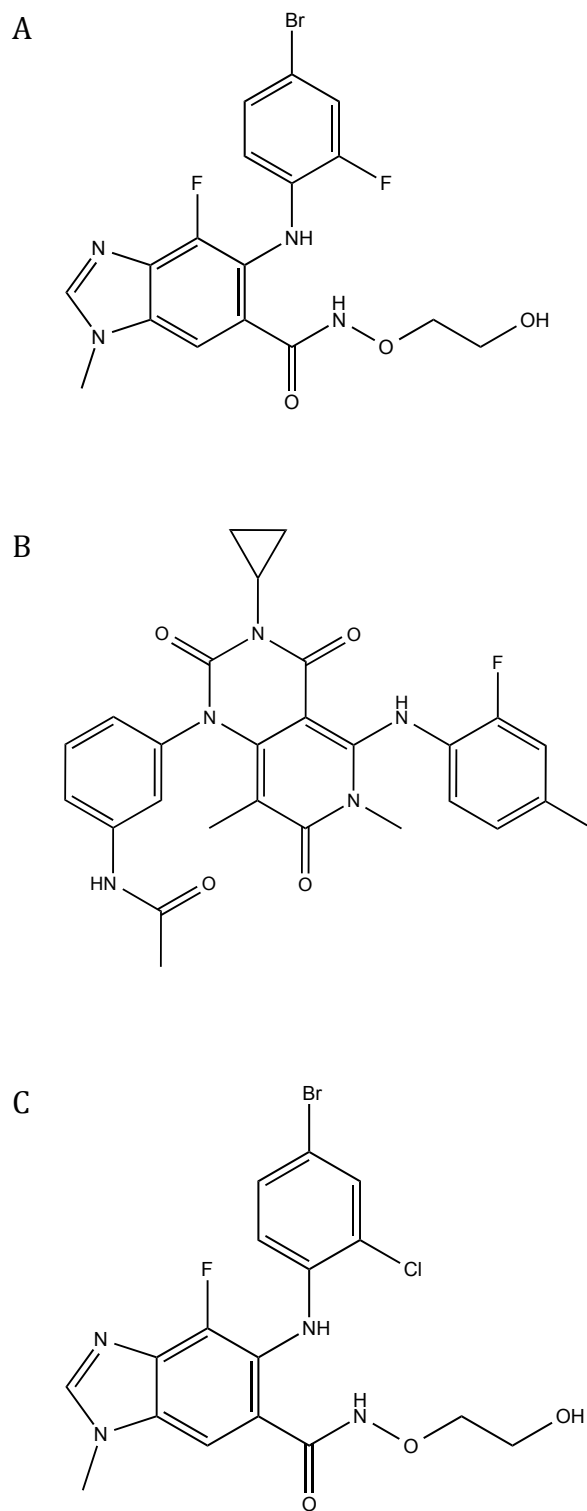**Figure 1.1**: Chemical structure of MEK inhibitors (A) binimetinib, (B) trametinib, and (C) selumetinib.

Chapter 2:

Materials and Methods

Xenopus laevis Oocyte Heterologous Expression System

Introduction

The *Xenopus laevis* oocyte heterologous expression system is a powerful model system for the study of membrane transport proteins. Approximately 1-1.2 mm in diameter, these spherical oocytes consist of a dark brown-colored animal pole, beneath which lies the nucleus, and a light beige-colored vegetal pole (Yao *et al.*, 2000). The oocyte is surrounded by a permeable vitelline membrane consisting of cross-linked protein fibers that maintain the oocyte's spherical structure, in addition to an impermeable follicle layer that lies above it (Theodoulou & Miller, 1995; Vo *et al.*, 2003).

A typical female frog will have anywhere between a few hundred to a few thousand viable unfertilized eggs in various stages of development (Theodoulou & Miller, 1995). Class V and class VI oocytes, which are optimal for heterologous expression experiments, are identifiable by their relatively larger size and a clear differentiation between their brown- and beige-colored poles. Class VI oocytes are further distinguishable from class V oocytes due to the presence of a sharp white band along the equator between these poles (Dumont, 1972). Fully matured oocytes prior to fertilization are arrested in metaphase II (Philpott & Yew, 2008) and house all the necessary cellular machinery and materials for heterologous protein expression. Due to their large size (allowing easy manipulation and microinjection) and low expression of endogenous membrane transport proteins, *Xenopus laevis* oocytes are an ideal model for the study of heterologous transporters by either radioisotope uptake assays or electrophysiology (Yao *et al.*, 2000).

The innate ability for these cells to produce and post-transcriptionally modify foreign transporter transcripts from vertebrate and non-vertebrate species has made this heterologous expression system the primary model system of study for many laboratories, including our own. Since the nucleus is consistently located under the animal pole, DNA injection is possible (Yao *et al.*, 2000). This, however, is more technically challenging than RNA injection into the cytoplasm, and the latter results in a higher survival rate due to decreased risk of cellular damage and activation of apoptotic pathways. With sterile incubation and frequent solution changes, oocytes can typically survive for 1-2 weeks post-injection, allowing sufficient time for production of slow-expressing proteins.

While *Xenopus laevis* oocytes represent an extremely robust expression system, they are subject to limitations. Size and production level vary between eggs and frogs, and this is exacerbated by seasonal variation when oocyte quality drops during the hotter summer months. The latter issue can be controlled for the most part with proper husbandry and housing (Delpire *et al.*, 2011).

Oocyte Preparation

Mature female *Xenopus laevis* (Biological Sciences Vivarium, University of Alberta) were anesthetized by immersion in a solution of 0.3 % (w/v) tricaine methanesulphonate (pH 7.4). The ovarian lobes were then removed using sterile scissors and forceps and immersed into a petri dish containing Modified Barth's Medium (MBM, 88 mM NaCl, 1 mM KCl, 0.33 mM $Ca(NO3)_2$, 0.41 mM $CaCl_2$, 0.82 mM $MgSO_4$, 2.4 mM $NaHCO_3$, 10 mM Hepes, 2.5 mM sodium pyruvate, 0.05 mg/ml penicillin, and 0.1 mg/ml gentamycin sulfate, pH 7.5)

as described by Yao *et al.*, 2000. The frogs were then humanely euthanized in accordance with Canadian Council on Animal Care guidelines.

Ovarian tissue was separated into small, approximately 10 oocyte clusters, in a glass vial and incubated at room temperature on a shaker for 2 hours with 2 mg/ml collagenase I (Worthington Biochemical Corp., USA). Following enzymatic digestion, oocytes were allowed to recover at 18°C after washing 5 times with MBM. Under a dissection microscope, oocytes were then sorted by selecting for undamaged class V and class VI oocytes of similar size.

Removal of the follicle layer was undertaken manually using watchmaker forceps following a 20-min incubation in hypotonic 100 mM K_2PO_4, after which cells were rinsed 5 times with MBM, and allowed to recover for at least 20 min in the same medium.

Oocytes were then injected with 10 ng of capped *in vitro* transcribed RNA dissolved in filtered double distilled H_2O at a concentration of 1 μg/μl or, for control oocytes, an equivalent volume of water alone, using a manual pneumatic injector (Inject+Matic, Switzerland) with borosilicate glass micropipette (Drummond Scientific, USA) made using a micropipette puller (Inject+Matic, Switzerland). Subsequent incubation of oocytes at 18 °C was for 1-4 days depending on the protein of interest to provide time for optimal expression, maturation, and trafficking to the plasma membrane.

Experimental Materials

Transport Media

A variety of transport media were used for the different transporters examined. Except for experiments requiring acidic incubation conditions at pH 5.5 (hENT3/hAA and hENT4), oocytes were pre-incubated for 1 hour in the appropriate transport medium (with added inhibitor as necessary) at room temperature prior to experimentation. Standard sodium-containing (NaCl) transport medium contained 100 mM NaCl, 2 mM KCl, 1 mM $CaCl_2$, 1 mM $MgCl_2$, and 10 mM HEPES (pH 7.5) in addition to a varying concentrations of inhibitor. Standard sodium-free (ChCl) transport medium contained 100 mM choline chloride, 2 mM KCl, 1 mM $CaCl_2$, 1 mM $MgCl_2$, and 10 mM HEPES (pH 7.5) in addition to varying concentrations of inhibitor. For hENT3/hAA and hENT4 transport assays performed in NaCl transport medium at pH 5.5 (with MOPS in place of HEPES as buffer), oocytes were pre-incubated with or without inhibitor for 1 hour in standard NaCl transport medium at pH 7.5 instead of pH 5.5 to prevent acidic overload prior to flux measurement.

Experiments with hENT4 required the addition of 1 μM deoxycoformycin to the incubation medium to prevent metabolism of radiolabelled adenosine by adenosine deaminase.

Inhibitors

Glutamate transport inhibitors were obtained from our collaborators Drs. Fowkes, Baldwin, and Nelson at the University of Leeds where they were synthesized (Fowkes, 2010). Powdered purified inhibitor compounds were dissolved in dimethyl sulfoxide (DMSO) at a concentration of 100 mM and stored at -20°C, while more dilute inhibitor solutions in NaCl transport medium at pH 7.5 were stored at 4°C prior to use.

MEK inhibitors were obtained from ActiveBiochem (USA) and also dissolved in DMSO at a concentration of 5 mM and stored at -80°C due to their reduced chemical stability, in accordance with manufacturer's storage instructions. Diluted inhibitor solutions were made up fresh prior to experimentation.

High-Performance Liquid Chromatography (HPLC) Analysis

To ensure purity and stability during storage, MEK inhibitors were individually analyzed upon receipt and during use in concentration dependence experiments using HPLC (Agilent Technologies, USA) with a 5 μm C18 column (Agilent Eclipse Plus, Agilent Technologies, USA). The mobile phase was composed of water (A) and acetonitrile (B) at a constant flow rate of 0.8 ml/min and at a temperature of 22°C with the following gradient program: 0-15 min, linear gradient 0-30% B; 15-25 min, linear gradient 30-50 % B; 25-35 min, linear gradient 50-75 % B; 35-40 min, linear gradient 75-95 % B; 45-54 min, isocratic 95 % B; 45-54 min, linear gradient 95-1 % B. The variable wavelength detector was set at 254 nm. No contaminants or degradation over time was detected for any of the compounds.

Flux Assays

Flux assays were performed as described previously (Yao *et al.*, 2000). Groups of 12 oocytes producing the recombinant transporter of interest were pre-incubated in individual vials with gentle shaking for 1 hour prior to measurement of uptake, these vials containing a predetermined concentration of inhibitor compound in an incubation volume of 0.2 ml. To aid in solubility of some compounds at higher concentrations, addition of DMSO to a maximum concentration of 5 (v/v) % was required. Testing of oocytes in the

presence or absence of 5 (v/v) % DMSO found no significant difference in uptake for any of the permeants/transporters tested.

At the end of the pre-incubation period, medium was aspirated, and fluxes initiated by the addition of media plus inhibitor also containing radioactive permeant (1 μCi/ml for [^{14}C]glutamate, 1 μCi/ml for [^{14}C]uridine, 1 μCi/ml for [^{14}C]adenosine and 2.5 μCi/ml for [^{3}H]uridine; Moravek Biochemicals, USA). The glutamate concentration (radioactive + non-radioactive) was 10 μM for hEAATs and the uridine or adenosine concentration (radioactive + non-radioactive) was 20 μM for hNTs. The incubation volume was 0.2 ml.

Following incubation at room temperature for a preset period of time to measure initial rates of transport, oocytes were rapidly washed 5 times with ice-cold ChCl (pH 7.5) transport medium to arrest transport and remove extracellular radioactivity. Oocytes were then separated into individual scintillation vials, lysed by the addition of 200 μl of 0.5 (w/v) % SDS and counted for radioactivity in a liquid scintillation counter (Beckman Coulter Inc., USA) following addition of 2.5 ml of Scintisafe Econo 2 linear alkylbenzene liquid scintillator (Fisher Scientific, USA).

Data Analysis

Flux values from experiments are presented as means ± SEM and, with the exception of some experiments in Chapter 3, were corrected for the low basal uptake in control water-injected oocytes. Kinetic parameters ± SE (V_{max} and K_M) were obtained by non-linear regression analysis using Sigmaplot (Sigmaplot Software, USA) software. IC_{50} values were obtained by non-linear regression analysis using Prism (Graphpad Software,

USA) software. Experiments in Chapters 3 and 4 were undertaken once. Experiments in Chapter 5 were undertaken twice.

V_{max}

V_{max} is the maximum rate of transport when the transporter is fully saturated with permeant.

K_M

K_M is the Michaelis Constant and is defined as the concentration of permeant required for ½ of V_{max}.

IC_{50}

IC_{50} is defined as the concentration of inhibitor that results in 50% reduction in transport activity. For the purposes of this thesis, and unless noted otherwise, all reported IC_{50} values represent absolute IC_{50} values calculated on the assumption that the inhibitor was capable of causing complete inhibition of transport when applied at an appropriately high concentration.

Hill Coefficient

As described in Chapter 1, hEAATs and hCNTs are predicted to be homotrimers. Additionally, there is evidence that at least one hENT (hENT1) may be a homodimer (Jarvis *et al.*, 1980; Cravetchi *et al.*, 2015). The Hill coefficient is a quantification of cooperative binding of a ligand to a protein. A Hill coefficient with an absolute value of less than one

indicates negative cooperativity where binding of inhibitor to one transporter protomer reduces the binding affinities of the other protomers to inhibitor. Conversely, a Hill coefficient with an absolute value greater than one indicates positive cooperativity where binding of inhibitor to one transporter protomer increases the binding affinities of the other protomers to inhibitor. A Hill coefficient with an absolute value equal to one indicates non-cooperativity.

References

Cravetchi X, Vilas G & Hammond J (2015). Oligomerization of Equilibrative Nucleoside Transporter 1. *FASEB J* **29,** 939.8.

Delpire E, Gagnon KB, Ledford JJ & Wallace JM (2011). Housing and husbandry of Xenopus laevis affect the quality of oocytes for heterologous expression studies. *J Am Assoc Lab Anim Sci* **50,** 46–53.

Dumont JN (1972). Oogenesis in Xenopus laevis (Daudin). I. Stages of oocyte development in laboratory maintained animals. *J Morphol* **136,** 153–179.

Fowkes A (2010). *Synthesis and Evaluation of Skeletally Diverse Inhibitors of Excitatory Amino Acid Transporters* (thesis). University of Leeds, Leeds, England.

Jarvis SM, Young JD & Ellory JC (1980). Nucleoside transport in human erythrocytes. Apparent molecular weight of the nitrobenzylthioinosine-binding complex estimated by radiation-inactivation analysis. *Biochem J* **190,** 373–376.

Philpott A & Yew PR (2008). The Xenopus cell cycle: an overview. *Mol Biotechnol* **39,** 9–19.

Theodoulou FL & Miller AJ (1995). Xenopus oocytes as a heterologous expression system. *Methods Mol Biol* **49,** 317–340.

Vo LH, Yen TY, Macher BA & Hedrick JL (2003). Identification of the ZPC oligosaccharide ligand involved in sperm binding and the glycan structures of Xenopus laevis vitelline envelope glycoproteins. *Biology of Reproduction*.

Yao SY, Cass CE & Young JD (2000). The Xenopus oocyte expression system for the cDNA cloning and characterization of plasma membrane transport proteins. In *Membrane Transport: A Practical Approach*, ed. Baldwin SA, Practical Approach Series, p. 342. Oxford University Press, Oxford.

Chapter 3:

Kinetic Characterization of Glutamate Transporters Produced in Oocytes of *Xenopus laevis*

Introduction

Chapter 1 reviewed the physiological importance of glutamate and its transport within the human body and highlighted the need to develop specific inhibitors for different glutamate transporter isoforms for the purposes of research and therapy. The utilization of DOS by our collaborators at the University of Leeds was successful in generating a skeletally diverse panel of compounds which showed promise in preliminary screening to assess inhibitory activity.

Low endogenous glutamate uptake (Steffgen *et al.*, 1991) and robust heterologous expression capability (Yao *et al.*, 2000) make *Xenopus laevis* oocytes an ideal model system for the purposes of quantitative analysis of inhibitory potencies against different glutamate transporter isoforms. To do this, and as described in this Chapter, it was first necessary to (i) undertake radiotracer time-course experiments to determine conditions for measurements of initial rates of transport (influx) and (ii) undertake concentration-dependence studies to determine the kinetic properties for influx of glutamate by the different transporters produced in *Xenopus* oocytes.

<u>**Results**</u>

Human excitatory amino acid transporters 1-3 (hEAAT1-3), investigated for their role in the synaptic cleft, were characterized in the *Xenopus laevis* oocyte heterologous expression system. Time course experiments (**Figures 3.1-3.3**) determined that uptake of 10 μM glutamate was approximately linear with respect to time during the first 5 minutes of incubation for all three transporters. Using this incubation period to estimate initial rates of transport at different external glutamate concentrations, concentration-dependence experiments (**Figures 3.4-3.6**) were undertaken to quantify apparent K_M and V_{max} values for each of the three hEAATs. Values obtained are summarized in **Table 3.1**.

Time Course Experiments

Time-course of glutamate uptake by hEAAT1 – A plot of mediated [^{3}H]glutamate influx (10 μM) as a function of time in *Xenopus laevis* oocytes producing hEAAT1 is shown in **Figure 3.1**. Uptake within the first 5 minutes was approximately linear with time.

Time-course of glutamate uptake by hEAAT2 – A plot of mediated [^{3}H]glutamate influx (10 μM) as a function of time in *Xenopus laevis* oocytes producing hEAAT2 is shown in **Figure 3.2**. Uptake within the first 5 minutes was approximately linear with time.

Time-course of glutamate uptake by hEAAT3 – A plot of mediated [³H]glutamate influx (10 μM) as a function of time in *Xenopus laevis* oocytes producing hEAAT3 is shown in **Figure 3.3**. Uptake within the first 5 minutes was approximately linear with time.

Concentration-Dependence Experiments

Concentration-dependent influx of glutamate by hEAAT1 – A plot of mediated [³H]glutamate influx in *Xenopus laevis* oocytes producing hEAAT1 as a function of increasing [³H]glutamate concentration (0.01 – 1000 μM) is shown in **Figure 3.4**, giving an apparent K_M value of 82 ± 18 μM and a V_{max} of 173 ± 9 pmol/oocyte.5 min^{-1} (**Table 3.1**).

Concentration-dependent influx of glutamate by hEAAT2 – A plot of mediated [³H]glutamate influx in *Xenopus laevis* oocytes producing hEAAT2 as a function of increasing [³H]glutamate concentration (0.01 – 1000 μM) is shown in **Figure 3.5**, giving an apparent K_M value of 102 ± 15 μM and a V_{max} of 62 ± 2 pmol/oocyte.5 min^{-1} (**Table 3.1**).

Concentration-dependent influx of glutamate by hEAAT1 – A plot of mediated [³H]glutamate influx in *Xenopus laevis* oocytes producing hEAAT3 as a function of increasing [³H]glutamate concentration (0.01 – 1000 μM) is shown in **Figure 3.6**, giving an apparent K_M value of 111 ± 15 μM and a V_{max} of 112 ± 4 pmol/oocyte.5 min^{-1} (**Table 3.1**).

Discussion

While *Xenopus laevis* oocytes exhibit low endogenous glutamate uptake, they have been documented to express several endogenous glutamate transporters which potentially might affect the experimental results presented in this thesis (Sobczak *et al.*, 2010). As such, glutamate fluxes in control water-injected oocytes were examined. As shown in **Figures 3.1-3.3**, time-course studies revealed minimal uptake of glutamate in water-injected oocytes under the conditions used in this study. All values were nevertheless corrected for this minor component of uptake except where explicitly labelled (**Figures 3.1-3.3**), such that data reflect fluxes mediated by the heterologously produced transporter.

Time-course experiments were used to determine the duration for which all hEAATs transported glutamate under approximate initial rate conditions. This uptake interval (5-min) was used subsequently in this Chapter to determine apparent K_M and V_{max} values for glutamate influx and, in the next Chapter, for inhibition experiments.

In each case, the concentration dependence of hEAAT1-, hEAAT2-, and hEAAT3 mediated glutamate influx conformed to Michaelis-Menten kinetics (**Figures 3.4-3.6**), and apparent K_M and V_{max} values for the transporters calculated using non-linear regression analysis (Sigmaplot Systat Software Inc., USA) are presented in **Table 3.1** for each transporter. K_M and V_{max} values were in the range 80 – 110 μM and 62 – 173 pmol/oocyte.5 min^{-1}, respectively.

While hEAAT2 is responsible for the majority of glutamate reuptake in the synaptic cleft, its kinetics did not differ greatly from those of hEAAT1 and hEAAT3. This supports

the hypothesis that trafficking, localization, and regulation play a larger role in the function

of hEAAT2 than its kinetic properties (Murphy-Royal *et al.*, 2015).

References

Murphy-Royal C, Dupuis JP, Varela JA, Panatier A, Pinson B, Baufreton J, Groc L & Oliet SHR (2015). Surface diffusion of astrocytic glutamate transporters shapes synaptic transmission. *Nat Neurosci* **18,** 219–226.

Sobczak K, Bangel-Ruland N, Leier G & Weber W-M (2010). Endogenous transport systems in the Xenopus laevis oocyte plasma membrane. *Methods* **51,** 183–189.

Steffgen J, Koepsell H & Schwarz W (1991). Endogenous L-glutamate transport in oocytes of Xenopus laevis. *Biochim Biophys Acta* **1066,** 14–20.

Yao SY, Cass CE & Young JD (2000). The Xenopus oocyte expression system for the cDNA cloning and characterization of plasma membrane transport proteins. In *Membrane Transport: A Practical Approach*, ed. Baldwin SA, Practical Approach Series, p. 342. Oxford University Press, Oxford.
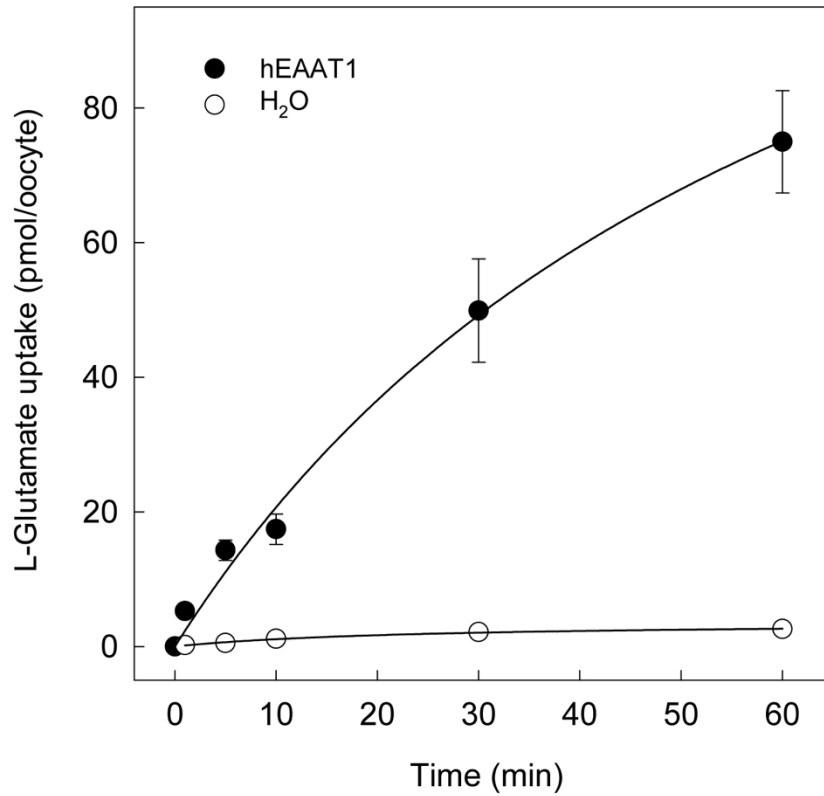
Figure 3.1: Time-courses of glutamate uptake in hEAAT1- and control water-injected oocytes. Values for [³H]glutamate uptake (10 µM) in this experiment are means ± SEM of 10-12 oocytes (closed circles, hEAAT1-producing oocytes; open circles, control H$_2$O-injected oocytes).
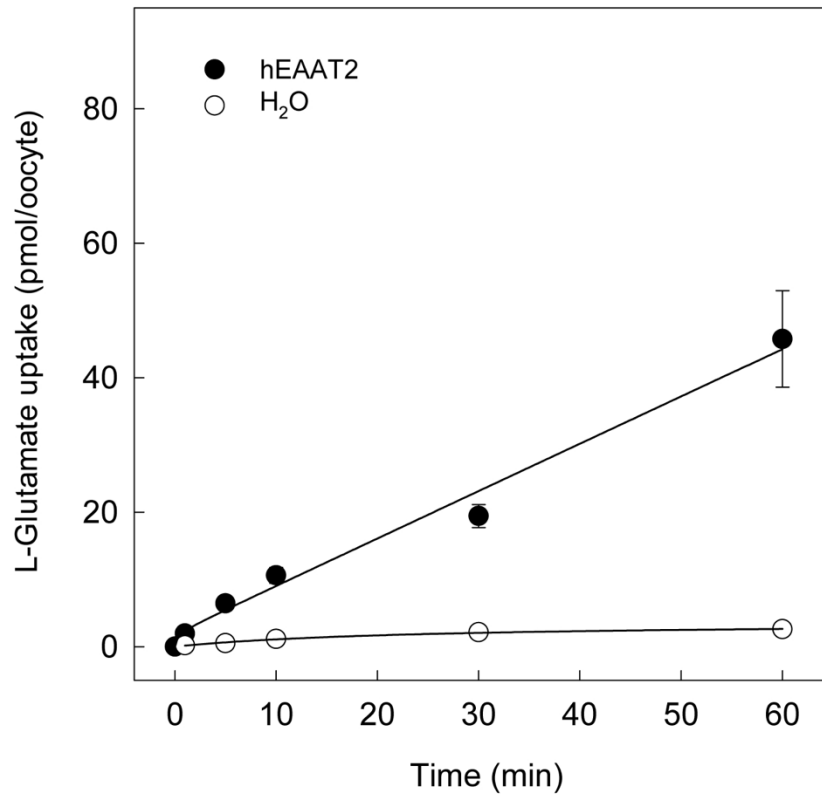
Figure 3.2: Time-courses of glutamate uptake in hEAAT2- and control water-injected oocytes. Values for [³H]glutamate uptake (10 μM) in this experiment are means ± SEM of 10-12 oocytes (closed circles, hEAAT1-producing oocytes; open circles, control H₂O-injected oocytes).
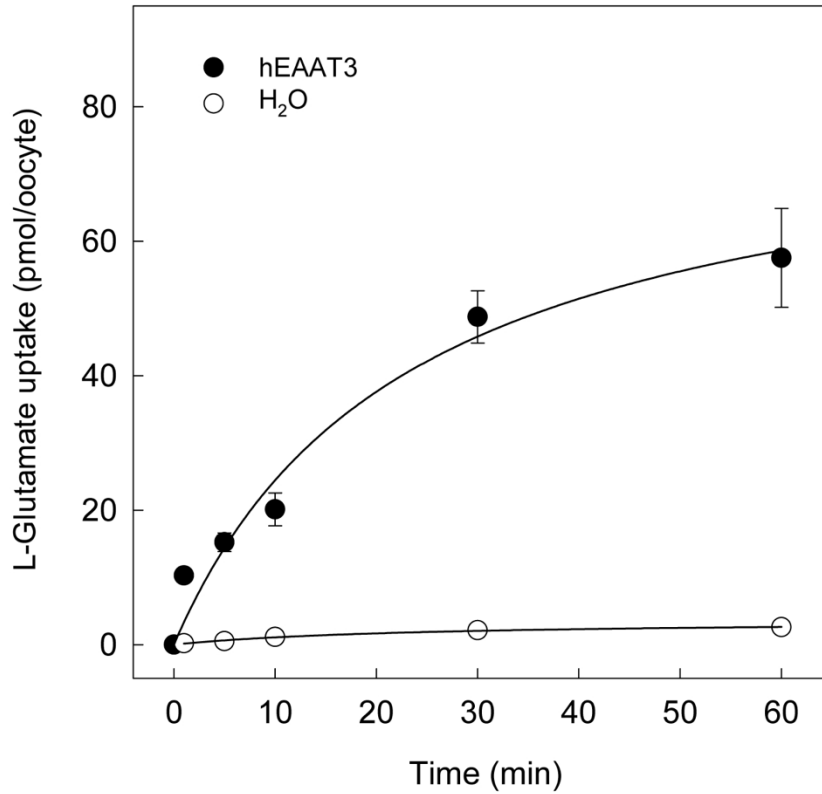
Figure 3.3: Time-courses of glutamate uptake in hEAAT3- and control water-injected oocytes. Values for [3H]glutamate uptake (10 µM) in this experiment are means ± SEM of 10-12 oocytes (closed circles, hEAAT1-producing oocytes; open circles, control H_2O-injected oocytes).
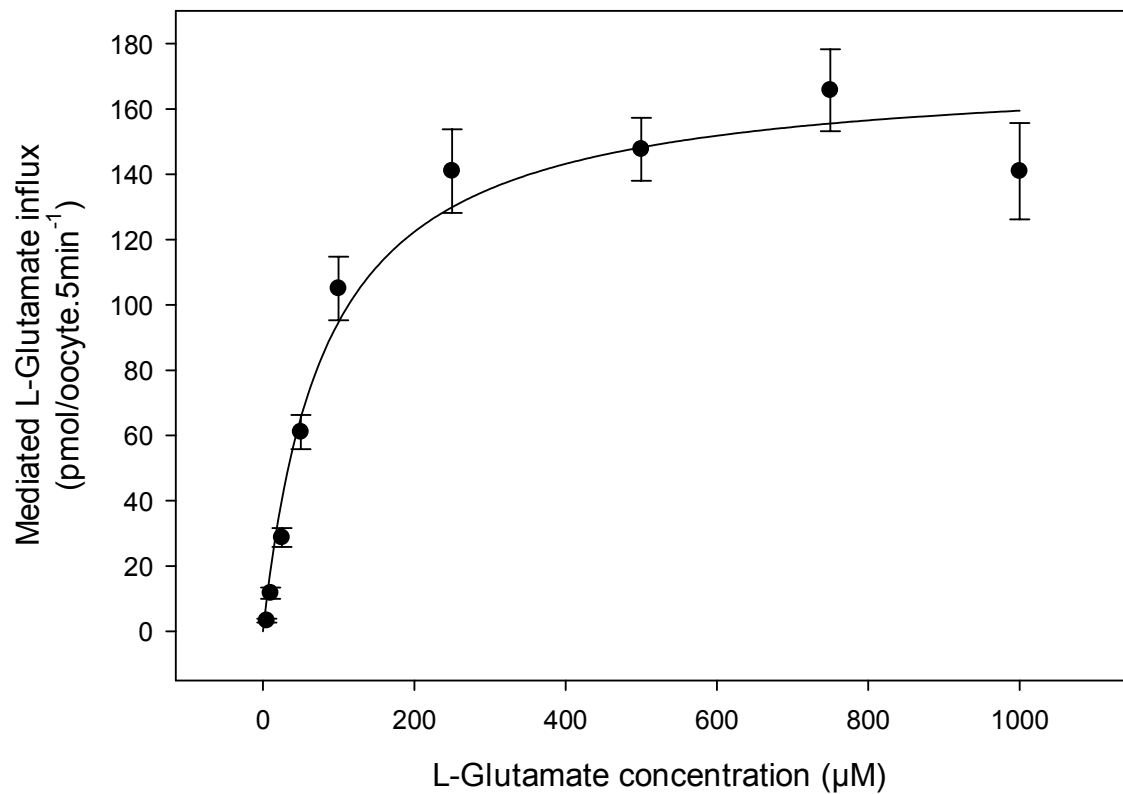
Figure 3.4: Concentration-dependence of hEAAT1-mediated glutamate influx. Values for $[^3H]$glutamate influx (5-min uptake interval) as a function of external glutamate concentration in this experiment are means $\pm$ SEM of 10-12 oocytes and are corrected for the low linear concentration dependence of glutamate uptake in control water-injected oocytes. The apparent K_M and V_{max} values were determined by non-linear regression analysis (Sigmaplot, Systat Software Inc., USA, software) and are presented in **Table 3.1**.
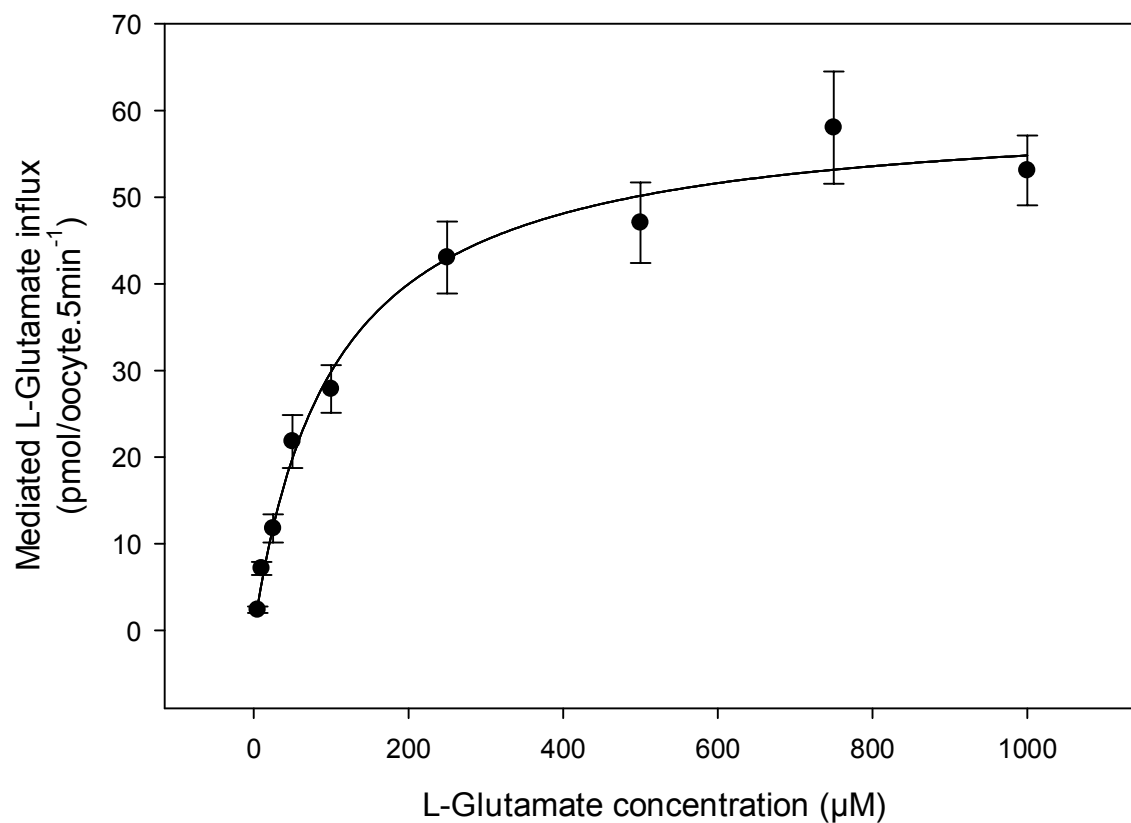
Figure 3.5: Concentration-dependence of hEAAT2-mediated glutamate influx. Values for [3H]glutamate influx (5-min uptake interval) as a function of external glutamate concentration in this experiment are means ± SEM of 10-12 oocytes and are corrected for the low linear concentration dependence of glutamate uptake in control water-injected oocytes. The apparent K_M and V_{max} values were determined by non-linear regression analysis (Sigmaplot, Systat Software Inc., USA, software) and are presented in **Table 3.1**.
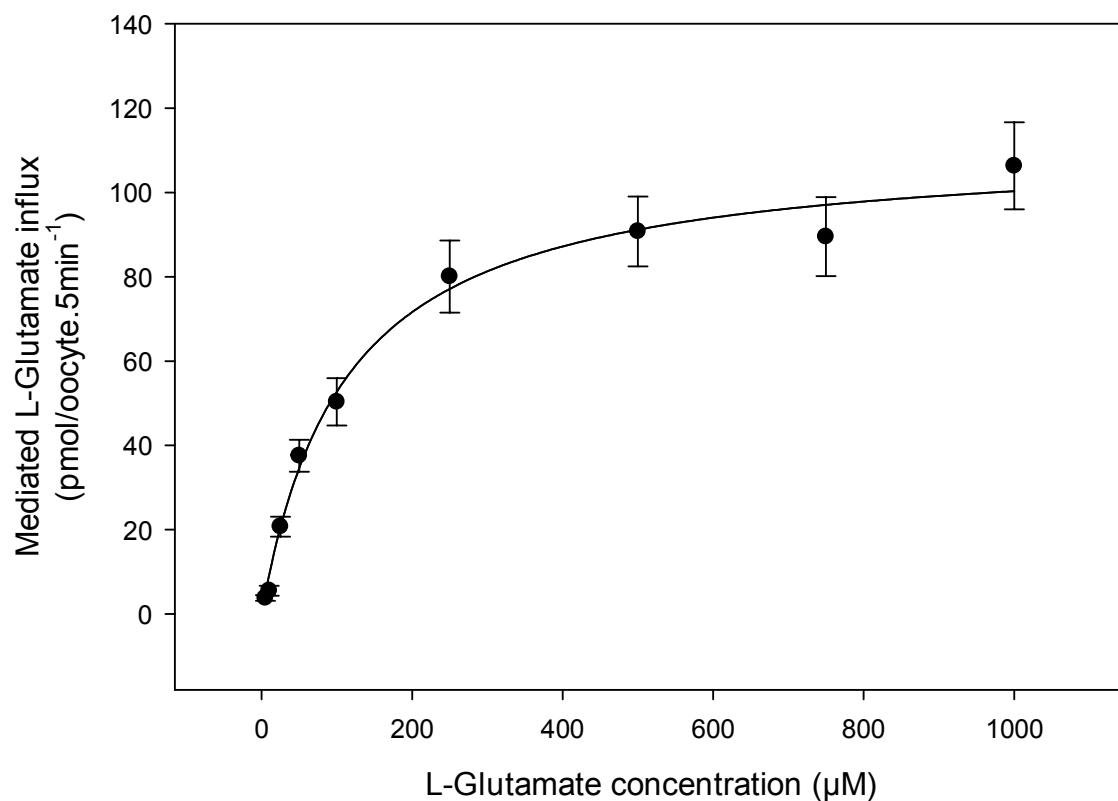
Figure 3.6: Concentration-dependence of hEAAT3-mediated glutamate influx. Values for [3H]glutamate influx (5-min uptake interval) as a function of external glutamate concentration in this experiment are means ± SEM of 10-12 oocytes and are corrected for the low linear concentration dependence of glutamate uptake in control water-injected oocytes. The apparent K_M and V_{max} values were determined by non-linear regression analysis (Sigmaplot, Systat Software Inc., USA, software) and are presented in **Table 3.1**.

Table 3.1: Apparent K_M and V_{max} values for hEAAT1-3 produced in *Xenopus laevis* oocytes. *

Transporter	K_M (μM)	V_{max} (pmol/oocyte.5 min^{-1})
hEAAT1	82 ± 18	173 ± 9
hEAAT2	102 ± 15	62 ± 2
hEAAT3	111 ± 15	112 ± 4

*Apparent K_M and V_{max} values from the concentration-dependence curves (5-1000 μM [3H]glutamate concentration range) shown in **Figures 3.4-3.6** and were determined by non-linear regression analysis using Sigmaplot (Systat Software Inc., USA).

Chapter 4:

Glutamate Transport Inhibition of Human Excitatory Amino Acid Transporters hEAAT1, hEAAT2, and hEAAT3

Introduction

Chapter 3 describes the kinetic characterization of hEAATs using the *Xenopus laevis* oocyte heterologous expression system. This enabled determination of conditions for measurements of initial rates of transport and provided K_M and V_{max} values for influx of glutamate by the different transporters.

Initial screening studies performed by our collaborators at the University of Leeds identified several novel potential glutamate transport inhibitors (Fowkes, 2010). Since these compounds were designed and synthesized in a systematic fashion utilizing compounds with the aspartate backbone, their chemical structures in relation to their inhibition profiles for different hEAATs will provide insight into isoform-specific differences in the permeant binding pockets. Mechanistically, the bulky substituents present on these compounds while, in some cases, allowing for competitive binding to the transporter permeant binding site, were anticipated to prevent the proper transport cycle conformational changes required for compound translocation across the cell membrane.

As described in Chapter 1 of this thesis, identification of novel high-affinity isoform-specific EAAT inhibitors has applications in both research and therapeutics.

Eight compounds were initially tested for inhibition of hEAAT1, hEAAT2 and hEAAT3 at a concentration of 1000 µM (**Figure 4.1**). Subsequent concentration-response inhibition experiments identified five compounds with high selectivity for the hEAAT2 isoform (AF314, AF327, AF340, AF403, and AF452) and one compound that was broadly inhibitory for all three isoforms (AF451). Inhibition curves for compounds showing measurable IC_{50} values are presented in **Figures 4.2, 4.3, 4.5-4.7, 4.9-4.12, and 4.14,** below. Also shown for comparison are curves for hEAAT1 and hEAAT3 for compounds that, in contrast to their effects on hEAAT2, were either without effect or only mildly inhibitory (**Figures 4.4, 4.8, 4.13, and 4.15).** IC_{50} values and Hill coefficient values are given in **Tables 4.1** and **4.2,** respectively.

hEAAT Inhibitor 1 mM Screen

Initial Screen – A plot of $[^3H]$glutamate (10 µM) influx for hEAAT1, hEAAT2 and hEAAT3 in the presence of each of the test compounds (1 mM) is given as a percentage of the control influx with no inhibitor present in **Figure 4.1**. Compounds that demonstrated >40% inhibition were examined further in concentration dependence experiments (**Figures 4.2-4.15**). The test concentration of 1 mM used in **Figure 4.1** was at the limit of solubility of some compounds. For these compounds, the maximum concentration used in the remaining experiments described in this Chapter was 300 µM.

hEAAT Inhibition Curves

Effect of AF314 on hEAAT2 – A plot of mediated [³H]glutamate influx (10 μM) as a function of increasing AF314 concentration (0-300 μM) is shown in **Figure 4.2** giving an IC_{50} value of 116 ± 37 μM and a Hill coefficient of -2.82 ± 1.57 (**Table 4.2**).

Effect of AF327 on hEAAT2 – A plot of mediated [³H]glutamate influx (10 μM) as a function of increasing AF314 concentration (0-300 μM) is shown in **Figure 4.3**, giving an IC_{50} value of 0.8 ± 2.4 μM (**Table 4.2**). The Hill coefficient could not be determined. Inhibition plateaued at approximately 70% inhibition.

Effect of AF340 on hEAAT1 – A plot of mediated [³H]glutamate influx (10 μM) as a function of increasing AF314 concentration (0-300 μM) is shown in **Figure 4.4**. Due to solubility limits and weak inhibition, determination of an IC_{50} value was not possible.

Effect of AF340 on hEAAT2 – A plot of mediated [³H]glutamate influx (10 μM) as a function of increasing AF314 concentration (0-300 μM) is shown in **Figure 4.5**, giving an IC_{50} value of 0.6 ± 1.4 μM and a Hill coefficient of -0.73 ± 0.15 (**Table 4.2**).

Effect of AF375 on hEAAT2 – A plot of mediated [³H]glutamate influx (10 μM) as a function of increasing AF314 concentration (0-300 μM) is shown in **Figure 4.6**, giving an IC_{50} value of 33.3 ± 1.5 μM and a Hill coefficient of -0.61 ± 0.16 (**Table 4.2**).

Effect of AF380 on hEAAT2 – A plot of mediated [³H]glutamate influx (10 μM) as a function of increasing AF314 concentration (0-300 μM) is shown in **Figure 4.7**, giving an IC_{50} value of 23.1 ± 1.2 μM and a Hill coefficient of -0.85 ± 0.15 (**Table 4.2**).

Effect of AF403 on hEAAT1 – A plot of mediated [³H]glutamate influx (10 μM) as a function of increasing AF314 concentration (0-300 μM) is shown in **Figure 4.8**. Due to solubility limits and weak inhibition, determination of an IC_{50} value was not possible (**Table 4.2**).

Effect of AF403 on hEAAT2 – A plot of mediated [³H]glutamate influx (10 μM) as a function of increasing AF314 concentration (0-300 μM) is shown in **Figure 4.9**, giving an IC_{50} value of 61.2 ± 1.2 μM and a Hill coefficient of -2.05 ± 0.58 (**Table 4.2**).

Effect of AF451 on hEAAT1 – A plot of mediated [³H]glutamate influx (10 μM) as a function of increasing AF314 concentration (0-300 μM) is shown in **Figure 4.10**, giving an IC_{50} value of 10.6 ± 1.3 μM and a Hill coefficient of -1.07 ± 0.27 (**Table 4.2**).

Effect of AF451 on hEAAT2 – A plot of mediated [³H]glutamate influx (10 μM) as a function of increasing AF314 concentration (0-300 μM) is shown in **Figure 4.11**, giving an IC_{50} value of 2.2 ± 1.6 μM and a Hill coefficient of -0.90 ± 0.21 (**Table 4.2**).

Effect of AF451 on hEAAT3 – A plot of mediated [^{3}H]glutamate influx (10 μM) as a function of increasing AF314 concentration (0-300 μM) is shown in **Figure 4.12**, giving an IC$_{50}$ value of 6.3 $\pm$ 1.9 μM and a Hill coefficient of -0.94 $\pm$ 0.51 (**Table 4.2**). Inhibition plateaued at approximately 70% inhibition.

Effect of AF452 on hEAAT1 – A plot of mediated [^{3}H]glutamate influx (10 μM) as a function of increasing AF314 concentration (0-300 μM) is shown in **Figure 4.13**. Due to solubility limits and weak inhibition, determination of an IC$_{50}$ value was not possible (**Table 4.2**).

Effect of AF452 on hEAAT2 – A plot of mediated [^{3}H]glutamate influx (10 μM) as a function of increasing AF314 concentration (0-300 μM) is shown **Figure 4.14**, giving an IC$_{50}$ value of 2.5 $\pm$ 2.1 μM and a Hill coefficient of -0.69 $\pm$ 0.32 (**Table 4.2**). Inhibition plateaued at approximately 70% inhibition.

Effect of AF452 on hEAAT3 – A plot of mediated [^{3}H]glutamate influx (10 μM) as a function of increasing AF314 concentration (0-300 μM) is shown in **Figure 4.15**. Due to solubility limits and weak inhibition, determination of an IC$_{50}$ value was not possible (Table 4.2).

Discussion

The objective of the experiments described in this Chapter was to test each of the eight compounds provided by our University of Leeds collaborators as potential inhibitors of hEAAT1, hEAAT2, and hEAAT3 produced individually in *Xenopus laevis* oocytes.

The experiments revealed several novel inhibitors of glutamate transport. AF340, AF375, AF380, AF403, and AF452 all demonstrated strong and selective inhibition of hEAAT2. AF451 was found to be broadly inhibitory to all three isoforms. The goal to identify isoform-specific inhibitors of hEAATs has, at least for hEAAT2, been achieved. The compound with highest potency was AF340, with an IC_{50} value of 0.6 ± 1.4 μM, providing a potential new tool for studies of hEAAT2 physiology and therapeutics.

Calculated Hill coefficients (**Table 4.2**) indicate the potential for cooperativity effects between transporter protomers. While Hill coefficients of AF375 and AF452 for hEAAT2 suggest the possibility of negative cooperativity, the Hill coefficients for AF314 and AF403 for hEAAT2 suggest the possibility of positive cooperativity. No cooperativity was apparent for AF340 and AF380 for hEAAT2, or AF451 for all three transporters. In the cases of negative or positive cooperativity, the binding of inhibitor is likely exerting conformational changes to the multimeric structure of the transporter, resulting in affinity changes to inhibitor binding sites on other protomers. It may also be possible that the inhibitors are binding to an allosteric site, allosteric inhibition having been previously reported in hEAAT3 (Callender *et al.*, 2012). This, however, is unlikely because our compounds were designed from, and contain, the competitively inhibitory TBOA moiety.

Comparison between chemical structure and inhibitory potency can provide important structure/function insights into the mechanism of inhibition and variations of the inhibitor/permeant binding pocket of the different transporter isoforms. Displacement of the nosyl substituent from the 4' position in AF340 to the 3' position in AF314, for example, resulted in an approximately 200-fold reduction in inhibitor activity for hEAAT2. This is likely due to the positioning of the nosyl substituent relative to HP2, the rat hEAAT2 homology model *in silico* docking experiment by our Leeds collaborators shown in **Figure 4.16** suggesting a close interaction between HP2 and the nosyl phenyl group of AF340, an interaction that mirrors TBOA's phenyl group interaction with HP2 as seen with resolved crystal structures (Yernool *et al.*, 2004).

Benzene rings play important roles in non-covalent interactions with ligands and other residues (Du *et al.*, 2013). Due to its unique structure, the pi orbitals within the benzene ring can be involved in interactions with other pi orbital systems (aromatic stacking) or in stabilizing systems with localized electron deficiencies, such as in polar compounds. The unique replacement of a neutral non-polar glycine on HP2 with the polar amino acid serine (Yernool *et al.*, 2004), may therefore explain the hEAAT2 selectivity of our panel of compounds. The ability for TBOA and AF451 to broadly inhibit all examined transporters may stem from the presence of the polar amino acid glutamine located 2 residues downstream on the hairpin (Yernool *et al.*, 2004).

While TBOA is a competitive inhibitor of hEAATs (Shimamoto *et al.*, 1998) several of the compounds studied here (AF327 and AF452 on hEAAT2, and AF451 on hEAAT3) showed concentration-response inhibition curves that plateaued at approximately 70% inhibition, suggesting that more complex inhibition mechanisms may be at play.

References

Callender R, Gameiro A, Pinto A, DeMicheli C & Grewer C (2012). Mechanism of inhibition of the glutamate transporter EAAC1 by the conformationally-constrained glutamate analog (+)-HIP-B. *Biochemistry (Mosc)* **51,** 5486–5495.

Du Q-S, Wang Q-Y, Du L-Q, Chen D & Huang R-B (2013). Theoretical study on the polar hydrogen-π (Hp-π) interactions between protein side chains. *Chemistry Central Journal* **7,** 92.

Fowkes A (2010). *Synthesis and Evaluation of Skeletally Diverse Inhibitors of Excitatory Amino Acid Transporters* (thesis). University of Leeds, Leeds, England.

Shimamoto K, Lebrun B, Yasuda-Kamatani Y, Sakaitani M, Shigeri Y, Yumoto N & Nakajima T (1998). DL-threo-beta-benzyloxyaspartate, a potent blocker of excitatory amino acid transporters. *Mol Pharmacol* **53,** 195–201.

Yernool D, Boudker O, Jin Y & Gouaux E (2004). Structure of a glutamate transporter homologue from Pyrococcus horikoshii. *Nature* **431,** 811–818.
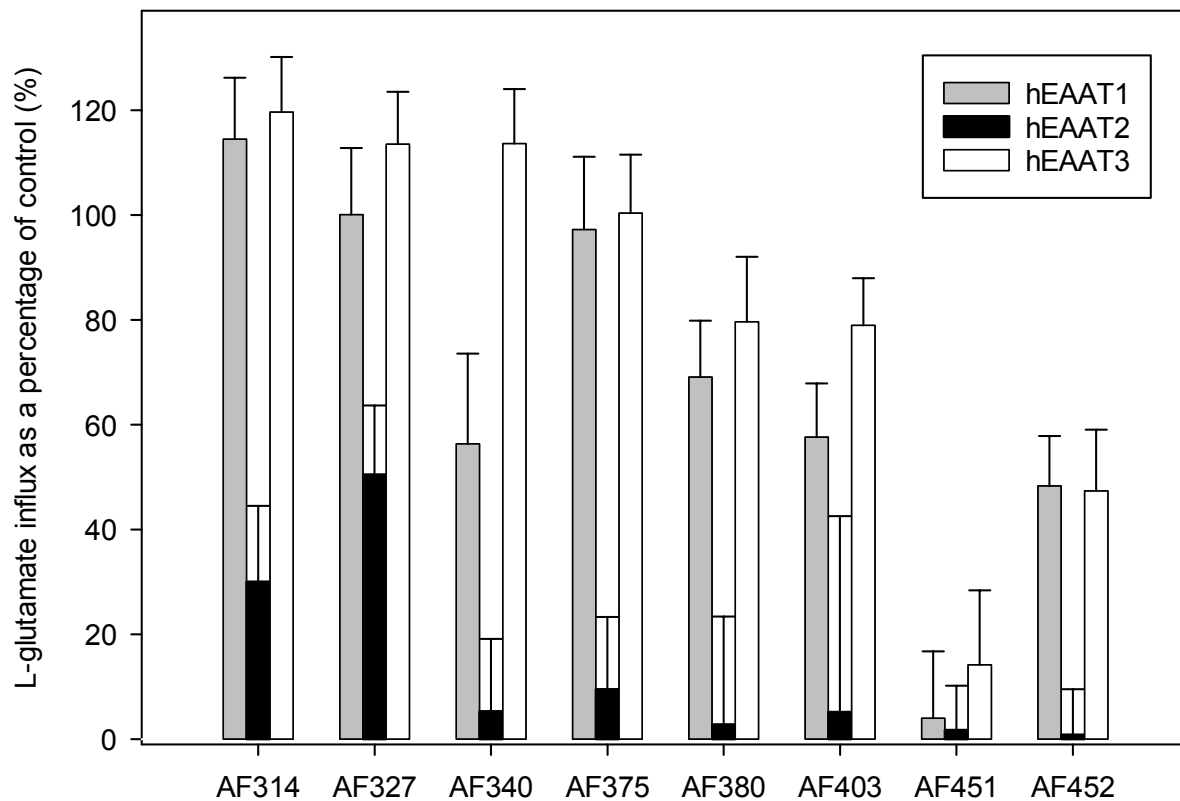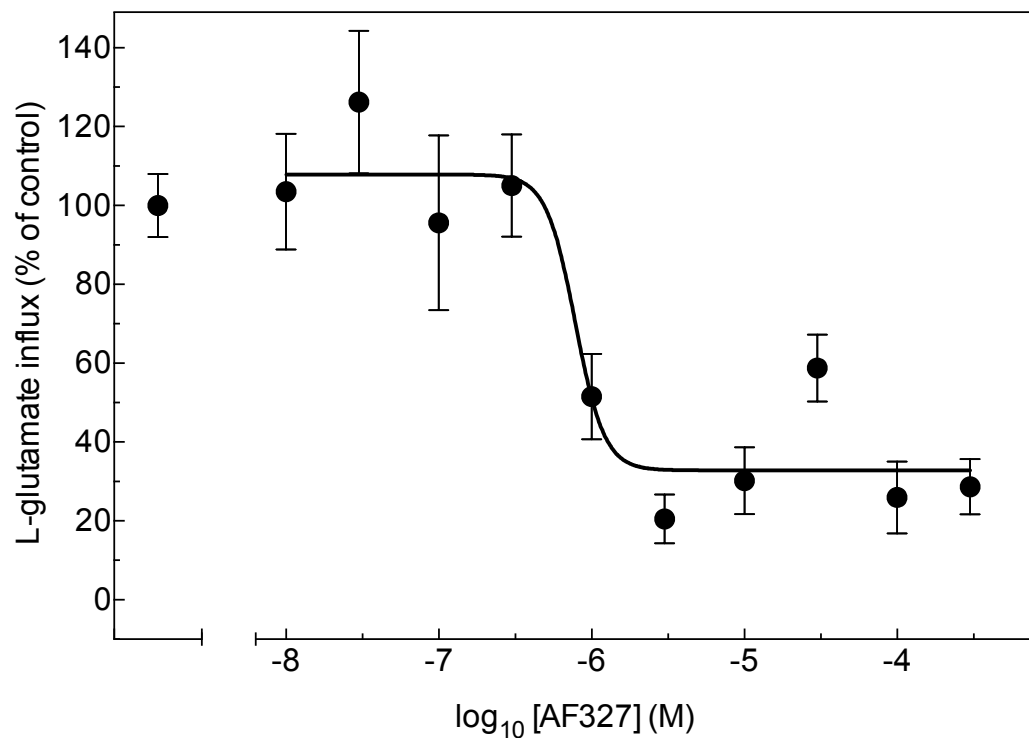
Figure 4.1 Initial 1 mM screen of glutamate mimetics as inhibitors on hEAAT-mediated glutamate influx. Values for [3H]glutamate influx (5-min uptake interval) are means ± SEM of 10-12 oocytes, are corrected for the low glutamate uptake in control water-injected oocytes, and are presented as a percentage of control uptake in the absence of inhibitor.
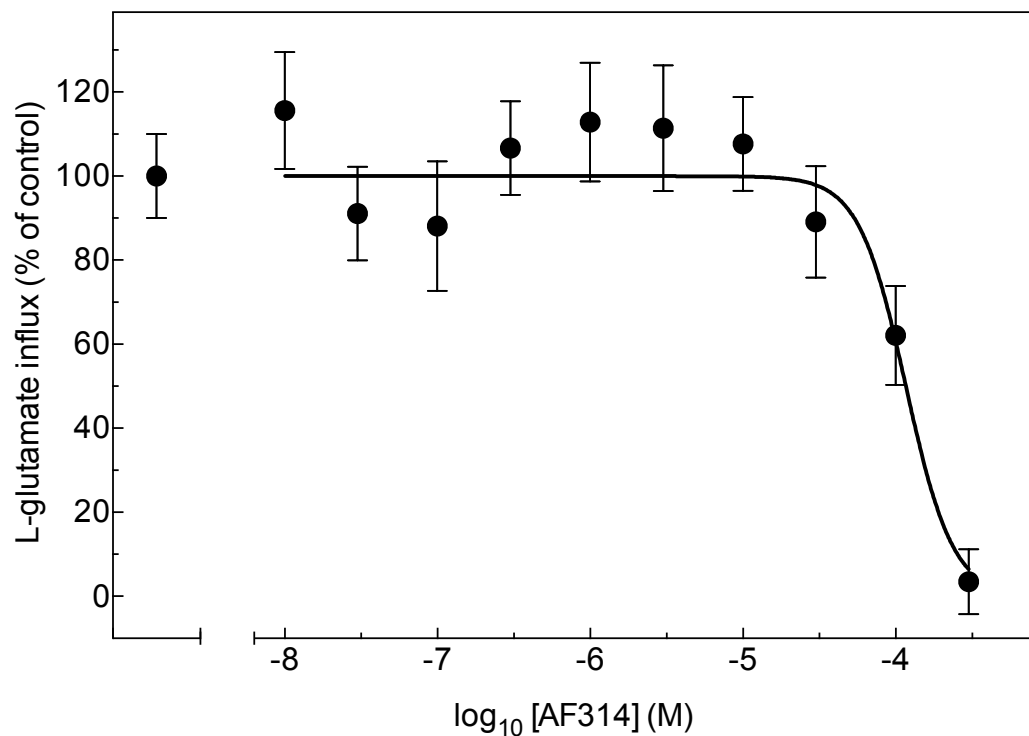
Figure 4.2: Concentration dependence of AF314 inhibition of hEAAT2-mediated glutamate influx. Values for [^{3}H]glutamate influx (5-min uptake interval) are means ± SEM of 10-12 oocytes, were corrected for the low glutamate uptake in control water-injected oocytes, and are presented as a percentage of control uptake in the absence of inhibitor. The IC_{50} value and Hill coefficient were determined by non-linear regression analysis (Prism, Graphpad Software Inc., USA) and are presented in **Table 4.1** and **4.2**, respectively.

Figure 4.3: Concentration dependence of AF327 inhibition of hEAAT2-mediated glutamate influx. Values for [³H]glutamate influx (5-min uptake interval) are means ± SEM of 10-12 oocytes, were corrected for the low glutamate uptake in control water-injected oocytes, and are presented as a 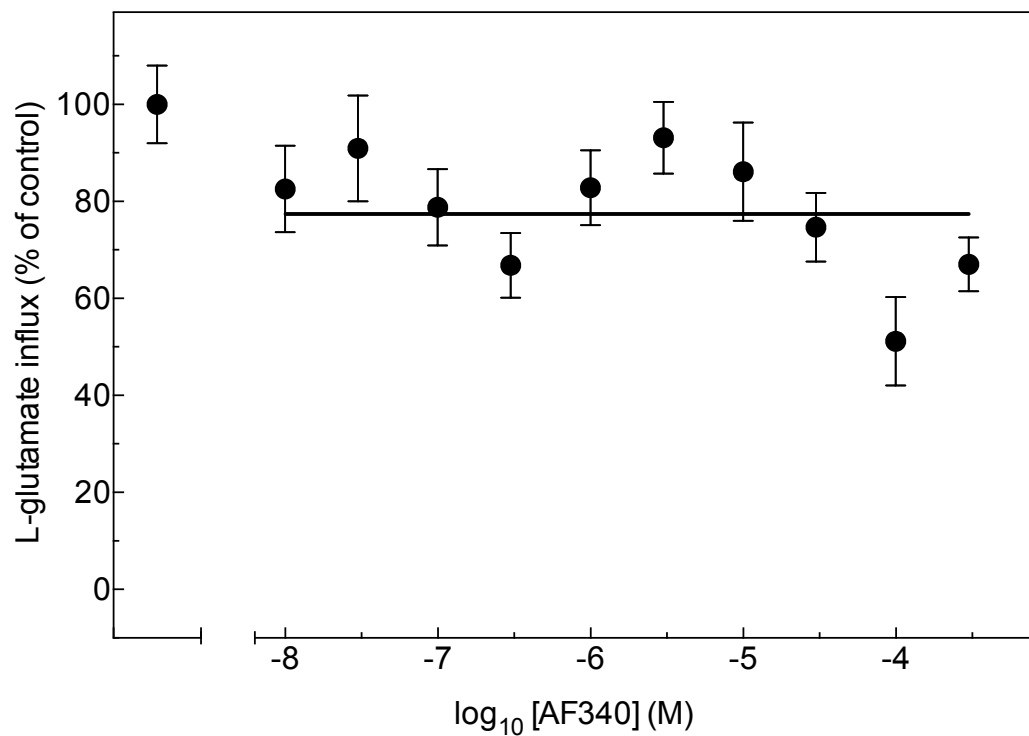percentage of control uptake in the absence of inhibitor. The IC_{50} value was determined by non-linear regression analysis (Prism, Graphpad Software Inc., USA) and is presented in **Table 4.1**. The Hill coefficient could not be determined (**Table 4.2**). Inhibition plateaued at approximately 70% inhibition.

Figure 4.4: Concentration dependence of AF340 inhibition of hEAAT1-mediated glutamate influx. Values for [³H]glutamate influx (5-min uptake interval) are means ± SEM of 10-12 oocytes, were corrected for the low glutamate uptake in control water-injected oocytes, and are presented as a percentage of control uptake in the absence of inhibitor. An IC_{50} value could not be determined (**Table 4.1**).

Figure 4.5: Concentration dependence of AF340 inhibition of hEAAT2-mediated glutamate influx. Values for [3H]glutamate influx (5-min uptake interval) are means ± SEM of 10-12 oocytes, were corrected for the low glutamate uptake in control water-injected oocytes, and are presented as a percentage of control uptake in the absence of inhibitor. The IC_{50} value and Hill coefficient were determined by non-linear regression analysis (Prism, Graphpad Software Inc., USA) and are presented in **Table 4.1** and **4.2**, respectively.
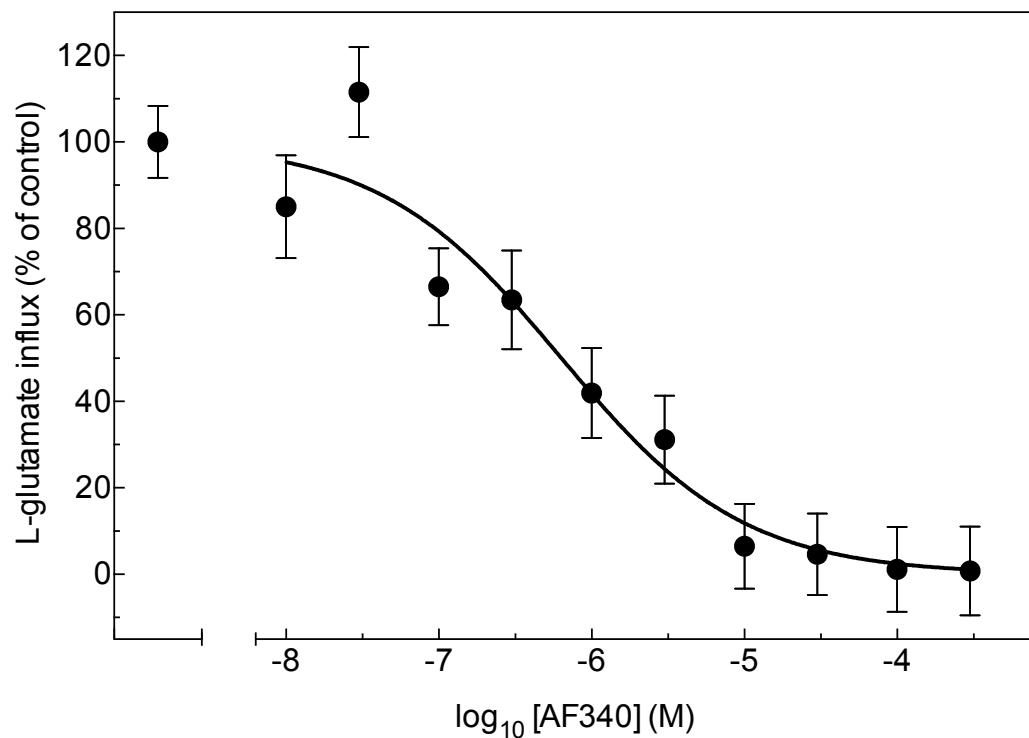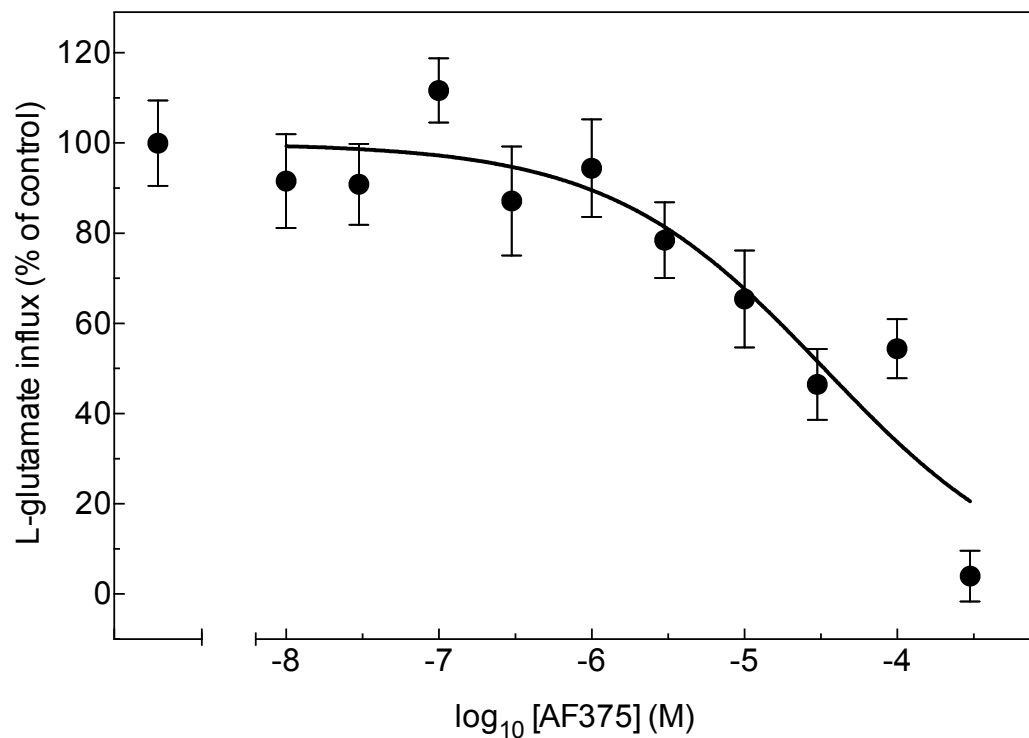
Figure 4.6: Concentration dependence of AF375 inhibition of hEAAT2-mediated glutamate influx. Values for [^{3}H]glutamate influx (5-min uptake interval) are means ± SEM of 10-12 oocytes, were corrected for the low glutamate uptake in control water-injected oocytes, and are presented as a percentage of control uptake in the absence of inhibitor. The IC_{50} value and Hill coefficient were determined by non-linear regression analysis (Prism, Graphpad Software Inc., USA) and are presented in **Table 4.1** and **4.2**, respectively.
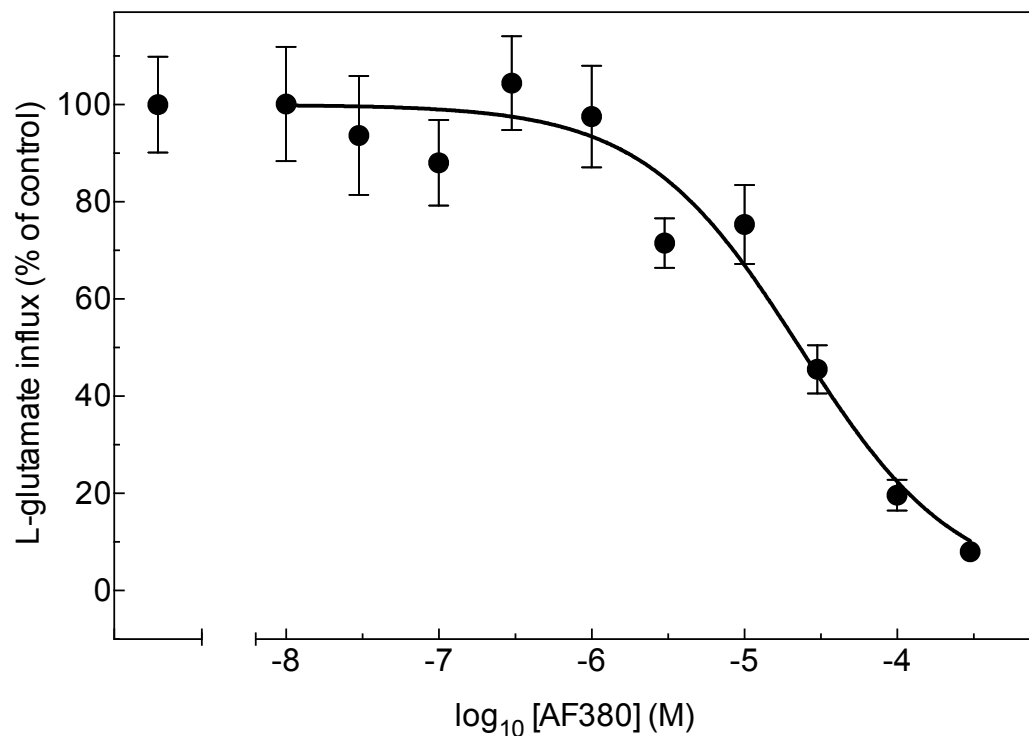
Figure 4.7: Concentration dependence of AF380 inhibition of hEAAT2-mediated glutamate influx. Values for [3H]glutamate influx (5-min uptake interval) are means ± SEM of 10-12 oocytes, were corrected for the low glutamate uptake in control water-injected oocytes, and are presented as a percentage of control uptake in the absence of inhibitor. The IC_{50} value and Hill coefficient were determined by non-linear regression analysis (Prism, Graphpad Software Inc., USA) and are presented in **Table 4.1** and **4.2**, respectively.

Figure 4.8: Concentration dependence of AF403 inhibition of hEAAT1-mediated glutamate influx. Values for [3H]glutamate influx (5-min uptake interval) are means ± SEM of 10-12 oocytes, were corrected for the low glutamate uptake in control water-injected oocytes, and are presented as a percentage of control uptake in the absence of inhibitor. An IC_{50} value could not be determined (**Table 4.1**).
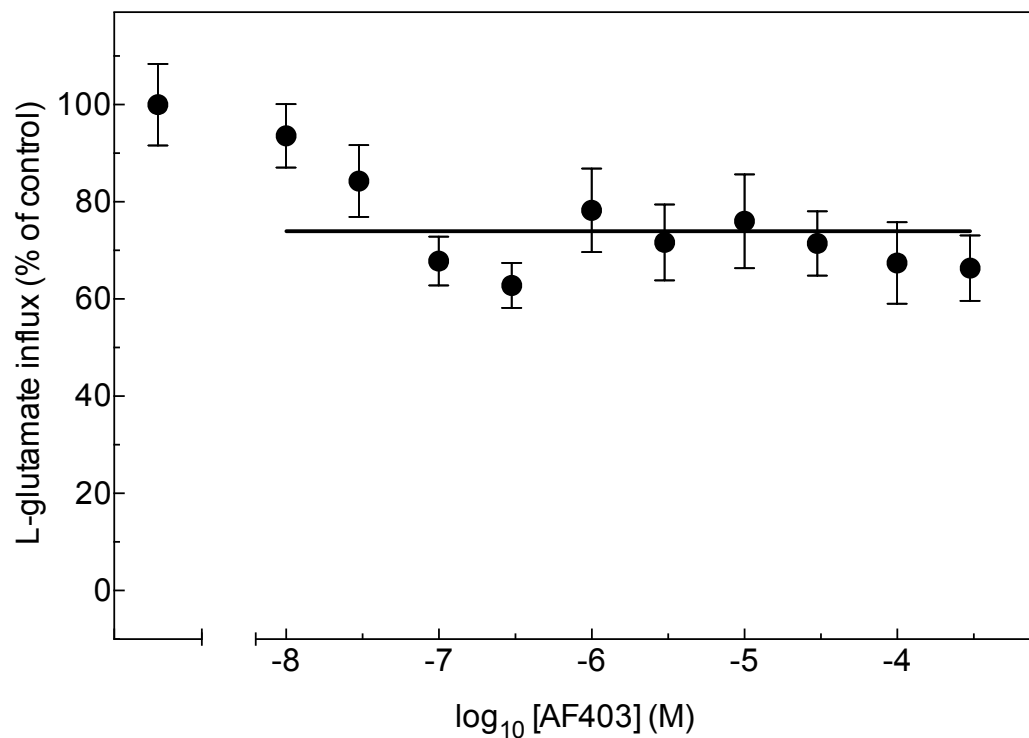
Figure 4.9: Concentration dependence of AF403 inhibition of hEAAT2-mediated glutamate influx. Values for [³H]glutamate influx (5-min uptake interval) are means ± SEM of 10-12 oocytes, were corrected for the low glutamate uptake in control water-injected oocytes, and are presented as a percentage of control uptake in the absence of inhibitor. The IC_{50} value and Hill coefficient were determined by non-linear regression analysis (Prism, Graphpad Software Inc., USA) and are presented in **Table 4.1** and **4.2**, respectively.
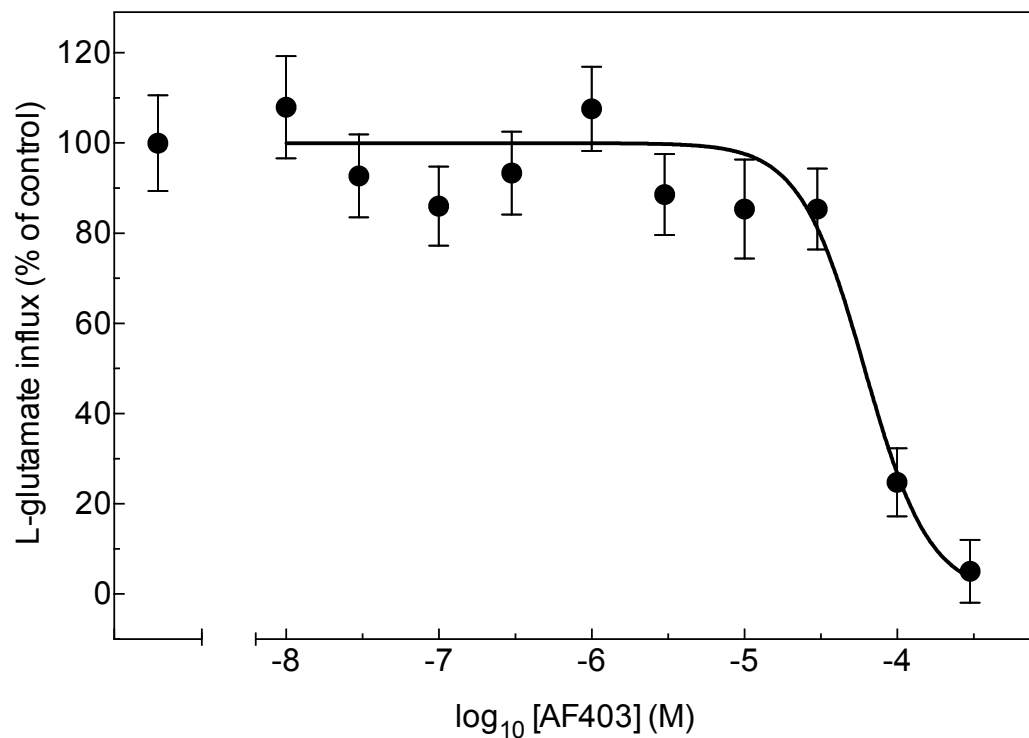
Figure 4.10: Concentration dependence of AF451 inhibition of hEAAT1-mediated glutamate influx. Values for [³H]glutamate influx (5-min uptake interval) are means ± SEM of 10-12 oocytes, were corrected for the low glutamate uptake in control water-injected oocytes, and are presented as a percentage of control uptake in the absence of inhibitor. The IC_{50} value and Hill coefficient were determined by non-linear regression analysis (Prism, Graphpad Software Inc., USA) and are presented in **Table 4.1** and **4.2**, respectively.
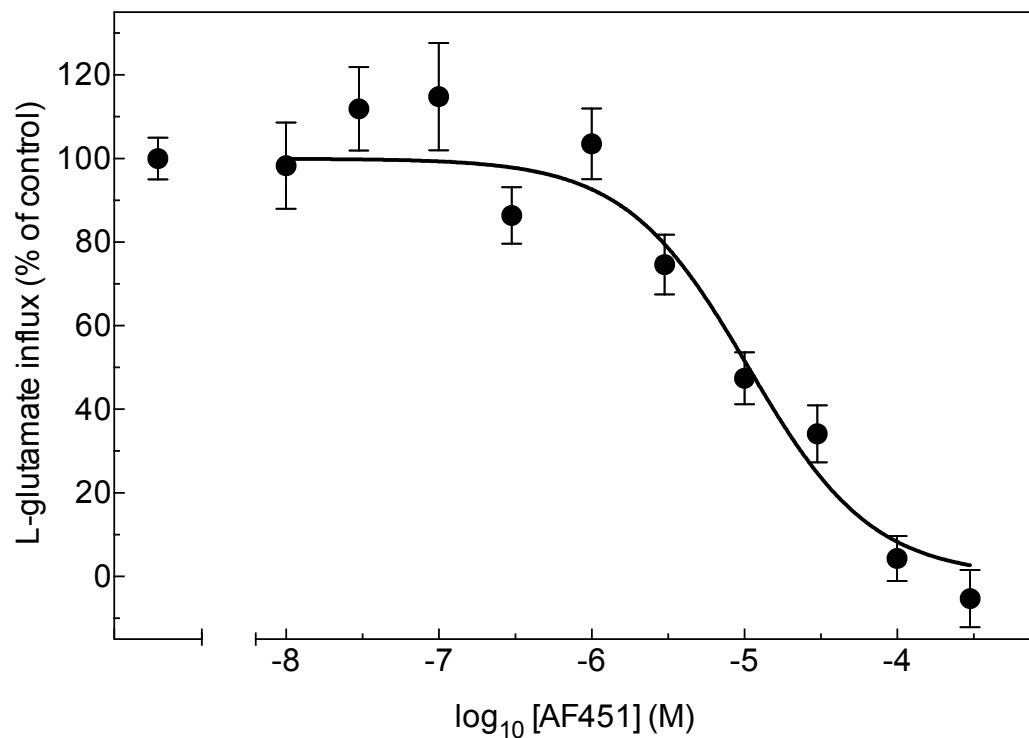
Figure 4.11: Concentration dependence of AF451 inhibition of hEAAT2-mediated glutamate influx. Values for [^{3}H]glutamate influx (5-min uptake interval) are means ± SEM of 10-12 oocytes, were corrected for the low glutamate uptake in control water-injected oocytes, and are presented as a percentage of control uptake in the absence of inhibitor. The IC$_{50}$ value and Hill coefficient were determined by non-linear regression analysis (Prism, Graphpad Software Inc., USA) and are presented in **Table 4.1** and **4.2**, respectively.

Figure 4.12: Concentration dependence of AF451 inhibition of hEAAT3-mediated glutamate influx. Values for [^{3}H]glutamate influx (5-min uptake interval) are means ± SEM of 10-12 oocytes, were corrected for the low glutamate uptake in control water-injected oocytes, and are presented as a percentage of control uptake in the absence of inhibitor. The IC_{50} value and Hill coefficient were determined by non-linear regression analysis (Prism, Graphpad Software Inc., USA) and are presented in **Table 4.1** and **4.2**, respectively. Inhibition plateaued at approximately 70% inhibition.

Figure 4.13: Concentration dependence of AF452 inhibition of hEAAT1-mediated glutamate influx. Values for [³H]glutamate influx (5-min uptake interval) are means ± SEM of 10-12 oocytes, were corrected for the low glutamate uptake in control water-injected oocytes, and are presented as a percentage of control uptake in the absence of inhibitor. An IC_{50} value could not be determined (**Table 4.1**).
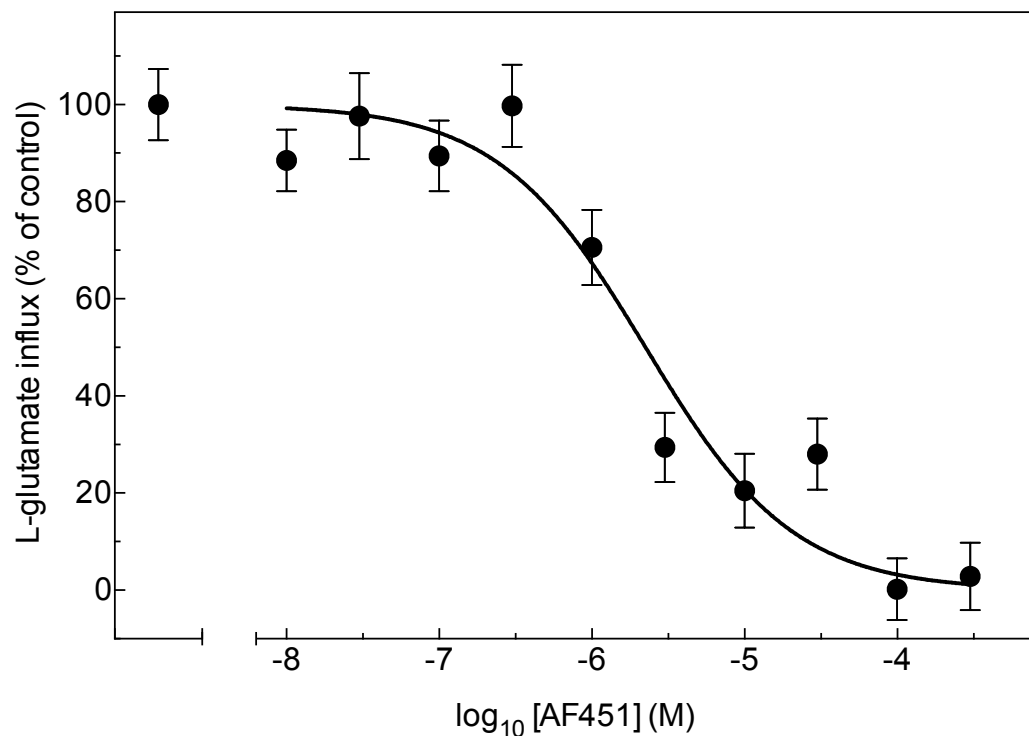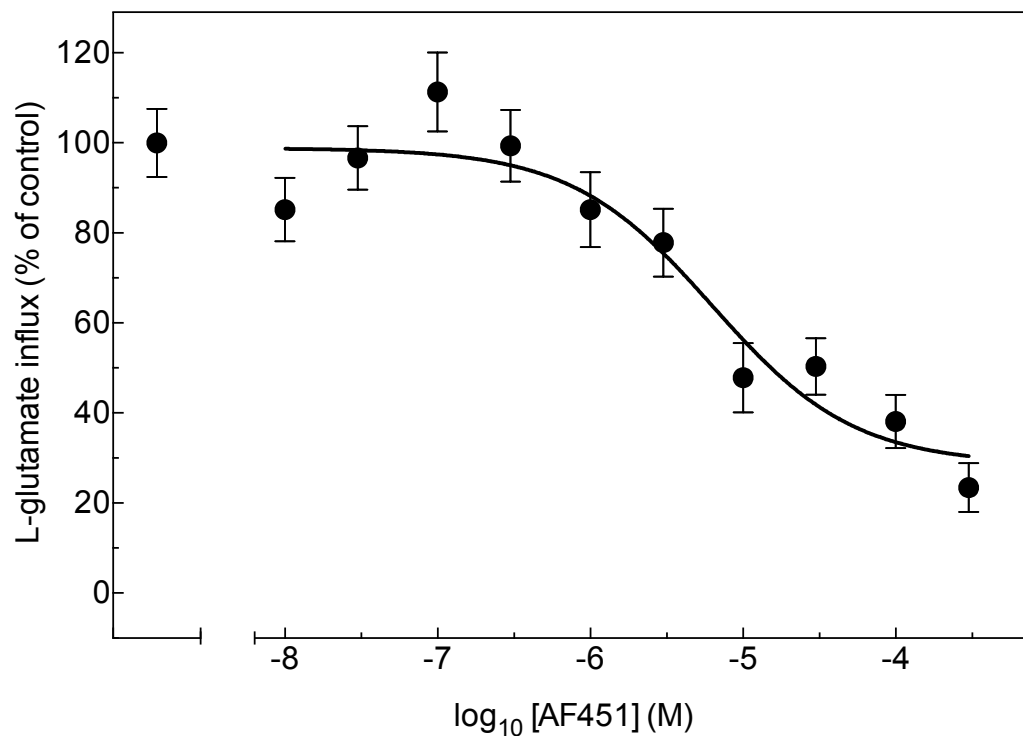
Figure 4.14: Concentration dependence of AF452 inhibition of hEAAT2-mediated glutamate influx. Values for [^{3}H]glutamate influx (5-min uptake interval) are means ± SEM of 10-12 oocytes, were corrected for the low glutamate uptake in control water-injected oocytes, and are presented as a percentage of control uptake in the absence of inhibitor. The IC$_{50}$ value and Hill coefficient were determined by non-linear regression analysis (Prism, Graphpad Software Inc., USA) and are presented in **Table 4.1** and **4.2**, respectively. Inhibition plateaued at approximately 70% inhibition.
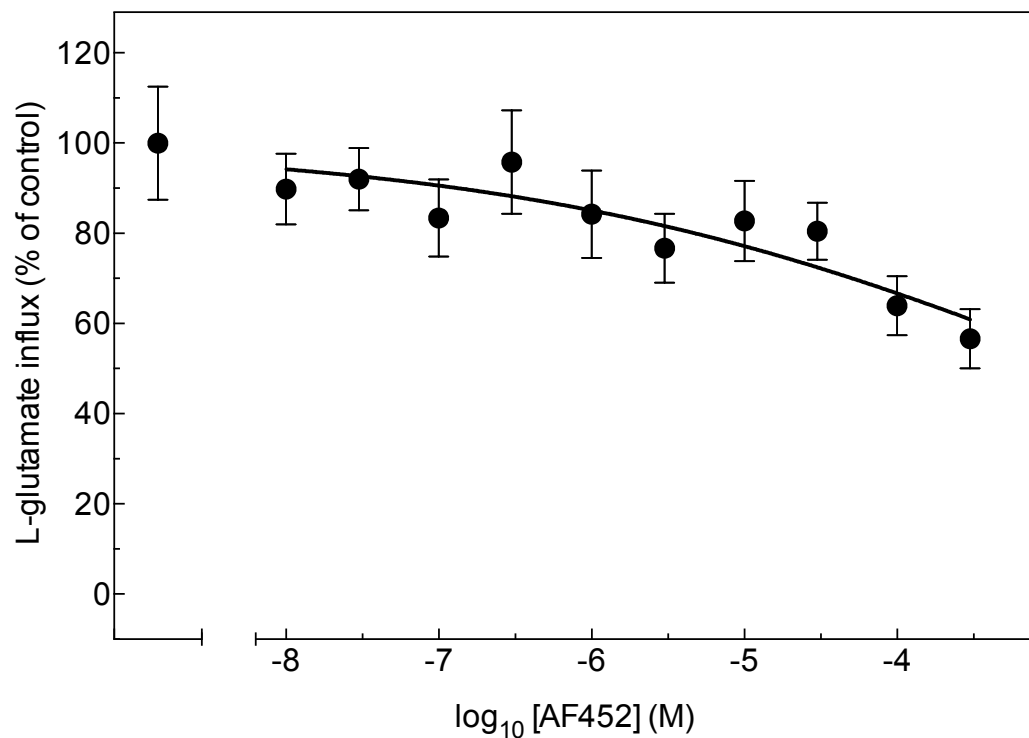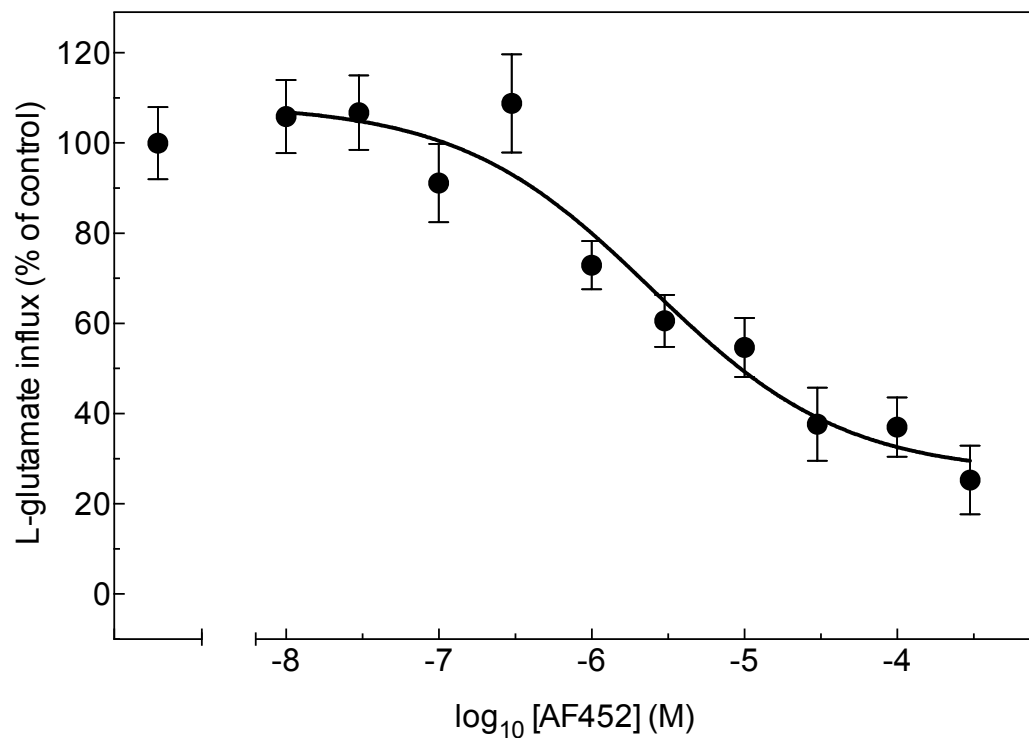
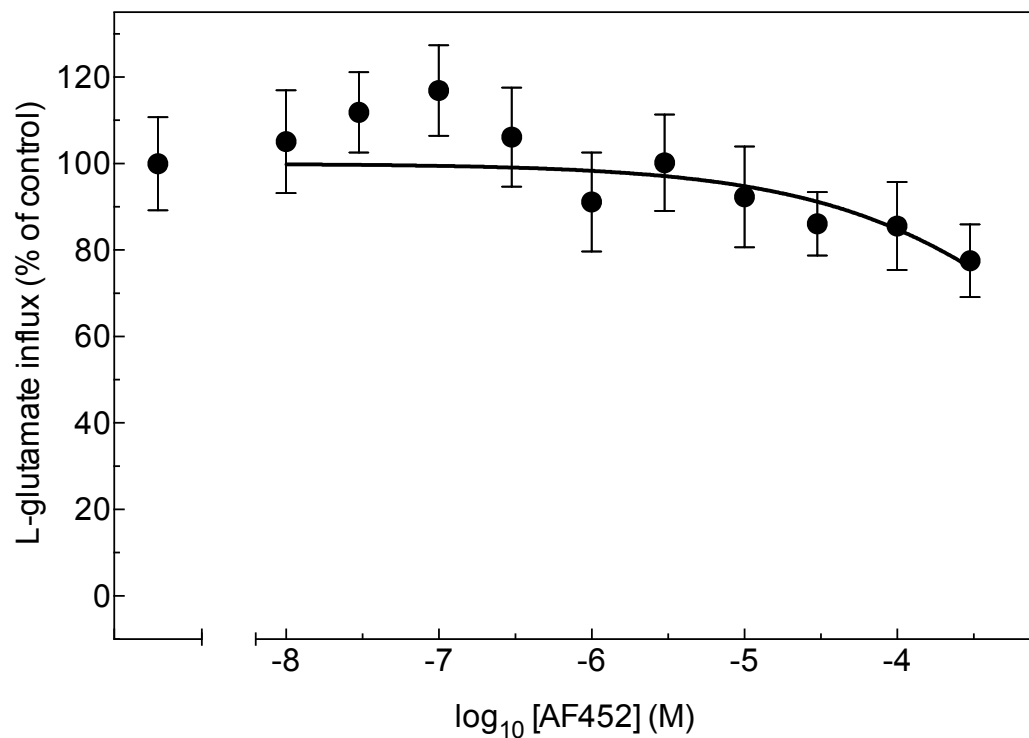**Figure 4.15: Concentration dependence of AF452 inhibition of hEAAT3-mediated glutamate influx.** Values for [³H]glutamate influx (5-min uptake interval) are means ± SEM of 10-12 oocytes, were corrected for the low glutamate uptake in control water-injected oocytes, and are presented as a percentage of control uptake in the absence of inhibitor. An IC_{50} value could not be determined (**Table 4.1**).
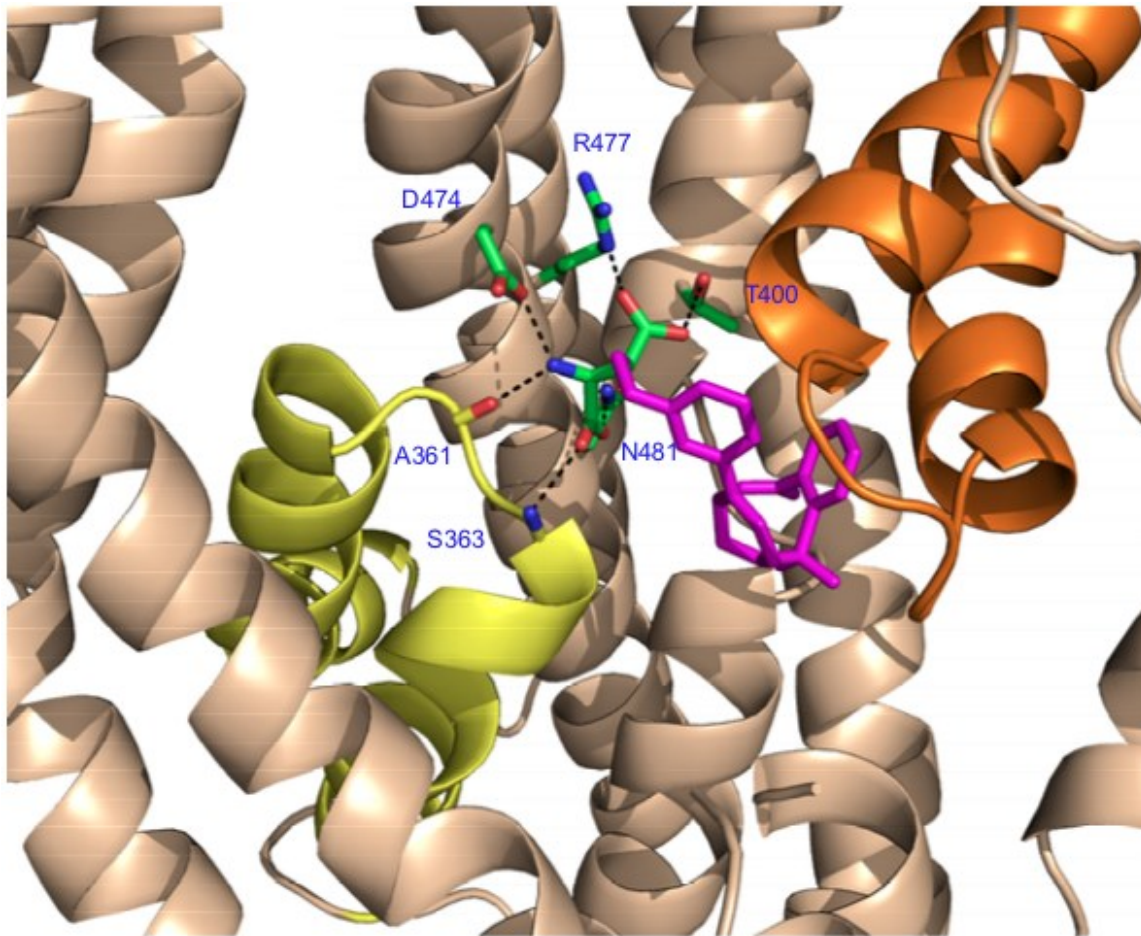
Figure 4.16: *In silico* **docking simulation.** Homology model of rat EAAT2 with AF340 bound in the putative permeant binding site. The model was generated by our collaborators using a CHARMM22 force field (CHARMM, Harvard University, USA) utilizing the GLT$_{Ph}$ crystal structure as the template. The **Figure** is reproduced with permission from the University of Leeds PhD thesis of Dr. Adrian Fowkes (Fowkes, 2010).

Table 4.1: IC$_{50}$ summary of hEAAT inhibition experiments (Figures 4.1-4.12). †

Compound Name	hEAAT1 (µM)	hEAAT2(µM)	hEAAT3 (µM)
AF314	>1000	116 ± 37	>1000
AF327	>1000	0.8 ± 2.4*	>1000
AF340	>300	0.6 ± 1.4	>300
AF375	>1000	33.3 ± 1.5	>1000
AF380	>1000	23.1 ± 1.2	>1000
AF403	>300	61.2 ± 1.2	>300
AF451	10.6 ± 1.3	2.2 ± 1.6	6.3 ± 1.9*
AF452	>300	2.5 ± 2.1*	>300

†IC$_{50}$ values were determined from dose-response curves (0-300 or 0-1000 µM inhibitor concentration range; 10 µM [^{3}H]glutamate) by non-linear regression analysis using Prism (Graphpad Software Inc., USA). Compounds with IC$_{50}$ values that extended beyond their solubility limits are noted either as > 300 or >1000 µM.

*For several inhibitors, concentration-effect curves plateaued at less than 100% inhibition and are presented as relative IC$_{50}$ values.

Table 4.2: Hill coefficient summary of hEAAT inhibition experiments.

Compound Name	hEAAT1	hEAAT2	hEAAT3
AF314	nd	-2.82 ± 1.57	nd
AF327	nd	nd*	nd
AF340	nd	-0.73 ± 0.15	nd
AF375	nd	-0.61 ± 0.16	nd
AF380	nd	-0.85 ± 0.15	nd
AF403	nd	-2.05 ± 0.58	nd
AF451	-1.07 ± 0.27	-0.90 ± 0.21	-0.94 ± 0.51*
AF452	nd	-0.69 ± 0.32*	nd

Hill coefficients ($\pm$ SE) were determined from concentration-effect curves by non-linear regression analysis using Prism (Graphpad Software Inc., USA).

nd, not determined, or could not be determined.

*For several inhibitors, concentration-effect curves plateaued at less than 100% inhibition.

Chapter 5:

Effects of MEK Inhibitors on Human Concentrative and

Equilibrative Nucleoside Transporters hCNT1-3 and hENT1-4

Introduction

Because the mitogen-activated protein kinase (MAPK) signaling pathway regulates cell growth and proliferation, aberrant signaling within this pathway comprises a significant portion of cancer etiologies. Consequently, the development of drugs targeting proteins within this pathway is a major focus for pharmaceutical companies and oncology researchers. Anticipated to be highly specific due to perceived binding site uniqueness, the development of MAPK kinase (MEK) inhibitors was initially a very promising development (Sebolt-Leopold & Bridges, 2009). Clinical trials, however, have demonstrated a clear set of adverse effects that are widespread throughout the drug class, including ocular (Urner-Bloch *et al.*, 2014; Duncan *et al.*, 2015; van Dijk *et al.*, 2015; Niro *et al.*, 2015), dermatological (Thomas *et al.*, 2015; Abdel-Rahman *et al.*, 2015), and gastrointestinal toxicities (Grimaldi *et al.*, 2015; Lugowska *et al.*, 2015), indicative of potential unintended spillover effects on other targets.

Due to the utilization of phosphorylation as a means of control and amplification within the MAPK signaling pathway, many of the designed inhibitors are structured to permit interaction with kinase ATP-binding pockets. This has resulted in the difficulty of creating compounds with sufficient similarity to ATP to allow for binding to the intended target, but also retaining sufficiently unique structures to mitigate widespread spillover effects on the binding pockets found on other ATP-binding and similar proteins. While it appears that this research has been moderately successful in discriminating between different ATP-binding proteins, with numerous new inhibitors entering drug pipelines and clinical trials, evidence has begun to show that design constraints may have unintentionally led to these compounds affecting another class of proteins: nucleoside transporters. While

the two human nucleoside transporter families (hCNTs and hENTs) do not transport nucleotides or undergo phosphorylation by nucleotide energy carriers, it appears that the purine mimicking portions of these compounds may be sufficient to allow for binding and inhibition. Evidence for this comes from the demonstration that p38 MAPK inhibitors have effects on nucleoside transporters, specifically hENT1 (Huang *et al.*, 2002). More recently, it has been shown that the tyrosine kinase inhibitor (TKI) sunitinib exhibits spillover inhibition of hCNTs (Damaraju *et al.*, 2015), suggesting that nucleoside transporters may be more susceptible to inhibition by these classes of compounds than previously thought.

Xu *et al.* (2013) determined that selumetinib efficacy *in vitro* in combination with the nucleoside analogue gemcitabine was heavily dependent on dosing schedule, since selumetinib given 48 hours after gemcitabine resulted in the highest efficacy as compared to concurrent dosing. This finding is consistent with our hypothesis that MEK inhibitors have inhibitory effects on nucleoside transporters, since concurrent dosing would result in selumetinib interfering with gemcitabine transport into the cell. The present Chapter tests this hypothesis by investigating the effects of three representative MEK inhibitors (binimetinib, trametinib and selumetinib) on hCNT1-3 and hENT1-4 produced individually in *Xenopus laevis* oocytes. While all of the compounds exhibited modest effects at high concentration on hCNT1-3 and hENT1/2, these compounds inhibited hENT3/hAA and hENT4 at pharmacologically relevant concentrations in the low micromolar range.

Results

Three compounds (binimetinib, trametinib, selumetinib), whose structures as shown in **Figure 1.1**, were initially screened for inhibition of the hCNTs (hCNT1, hCNT2, hCNT3) and the hENTs (hENT1, hENT2, hENT3/hAA, hENT4) at a concentration of 200 μM (**Figure 5.1**), a concentration representing the maximum solubility of trametinib (the least soluble of the three compounds) in NaCl transport medium. The uptake intervals used (2 min for hCNTs, 2 min for hENT1/2, and 5 min for hENT3/hAA and hENT4) approximated initial rates of transport (Kwong *et al.*, 1988; Huang *et al.*, 1994; Griffiths *et al.*, 1997; Ritzel *et al.*, 1998, 2001; Hyde *et al.*, 2001; Acimovic & Coe, 2002).

This screen identified hENT3/hAA as highly susceptible to inhibition by all three compounds, followed by hENT4 which was quite sensitive to inhibition by trametinib and selumetinib. In contrast, the other hCNTs and hENTs demonstrated only modest (20 – 60%) sensitivities to inhibition at this concentration. Subsequent dose response experiments focused on hENT3/hAA and hENT4.

MEK Inhibitor 200 μM Screen

Initial Screen – A plot of [^{3}H]uridine (20 μM) influx (5 minute flux) for hCNT1, hCNT2, hCNT3, hENT1, hENT2, hENT3/hAA and [^{14}C]adenosine (20 μM) influx for hENT4 in the presence of each of the three test compounds (200 μM) is presented as percentages of control uptake values with no inhibitor present in **Figure 5.1**. Influx values were corrected for the small non-mediated nucleoside uptake in control H_2O-injected oocytes. hENT3/hAA markedly inhibited by all three compounds, while hENT4 showed similar sensitivities to

trametinib and selumetinib. The inhibition of hENT3/hAA and hENT4 by these compounds was examined further in concentration dependence experiments (**Figures 5.2-5.13**)

hENT3/hAA and hENT4 Inhibition Curves

Effect of binimetinib on hENT3/hAA – Plots of mediated [³H]uridine influx (20 μM) as a function of increasing binimetinib concentration (0-500 μM; pH 5.5) in two different experiments are shown in **Figures 5.2** and **5.3**, giving an average IC_{50} value of 5.1 ± 2.6 μM (**Table 5.1**) and an average Hill coefficient of -0.65 ± 0.23 (**Table 5.2**).

Effect of trametinib on hENT3/hAA - Plots of mediated [³H]uridine influx (20 μM) as a function of increasing trametinib concentration (0-200 μM; pH 5.5) in two different experiments are shown in **Figures 5.4** and **5.5**, giving an average IC_{50} value of 22.3 ± 12.4 μM (**Table 5.1**) and an average Hill coefficient of -0.50 ± 0.15 (**Table 5.2**).

Effect of selumetinib on hENT3/hAA - Plots of mediated [³H]uridine influx (20 μM) as a function of increasing selumetinib concentration (0-300 μM; pH 5.5) in two different experiments are shown in **Figures 5.6** and **5.7**, giving an average IC_{50} value of 3.5 ± 3.1 μM (**Table 5.1**) and an average Hill coefficient of -0.45 ± 0.15 (**Table 5.2**).

Effect of binimetinib on hENT4 - Plots of mediated [¹⁴C]adenosine influx (20 μM) as a function of increasing binimetinib concentration (0-500 μM; pH 7.5) in two different

experiments are shown in **Figures 5.8** and **5.9**, giving an average IC_{50} value of 274 ± 2 μM (**Table 5.1**) and an average Hill coefficient of -0.86 ± 0.22 (**Table 5.2**).

Effect of trametinib on hENT4 - Plots of mediated [^{14}C]adenosine influx (20 μM) as a function of increasing trametinib concentration (0-200 μM; pH 7.5) in two different experiments are shown in **Figures 5.10** and **5.11**, giving an average IC_{50} value of 57.1 ± 1.9 μM (**Table 5.1**) and an average Hill coefficient of -0.84 ± 0.29 (**Table 5.2**).

Effect of selumetinib on hENT4 - Plots of mediated [^{14}C]adenosine influx (20 μM) as a function of increasing selumetinib concentration (0-300 μM; pH 7.5) in two different experiments are shown in **Figures 5.12** and **5.13**, giving an average IC_{50} value of 136 ± 10 μM (**Table 5.1**) and an average Hill coefficient of -0.90 ± 0.30 (**Table 5.2**).

Discussion

The objective of the experiments described in this Chapter was to examine the potential effects that the MEK inhibitors binimetinib, trametinib and selumetinib might have on nucleoside transport. An initial screen narrowed our focus to dose-response experiments with hENT3/hAA and hENT4, which displayed strong sensitivity to inhibition at an inhibitor concentration of 200 μM in comparison to controls.

Analysis of the dose-response experiments was consistent with initial findings in the preliminary screen (**Figure 5.1**). Specifically, hENT3/hAA is particularly susceptible to inhibition by the panel of selected MEK inhibitors, demonstrating complete inhibition of nucleoside transport in all cases at higher inhibitor concentrations. While hENT4 demonstrated high levels of inhibition by MEK inhibitors, the effects were not as marked, and greatest for trametinib and selumetinib. IC_{50} values and Hill coefficients are summarized in **Tables 5.1** and **5.2**.

In duplicate experiments there are discrepancies between the calculated IC_{50} values of trametinib for hENT3/hAA and selumetinib for hENT4. This is likely due to the use of different batches of oocytes from different animals in the two experiments, to low inhibitor solubility not allowing testing of inhibition at higher concentrations, and to the relatively low transport activity of these two transporters resulting in relatively low signal to noise ratios.

Calculated Hill coefficients indicate the potential for negative cooperativity between transporter protomers in the binding of MEK inhibitors to hENT3/hAA and no cooperativity between transporter protomers in the binding of MEK inhibitors to hENT4. If,

like hENT1 (Jarvis *et al.*, 1980; Cravetchi *et al.*, 2015), both transporters are homodimers, it is possible that binding of these MEK inhibitors to one protomer may induce conformational changes affecting inhibitor binding to the other protomer.

Below are discussed some MEK inhibitor-associated side effects that potentially involve spill-over effects on nucleoside transporters.

Retinopathy

With the increasing numbers of new MEK inhibitors entering clinical trials, more and more side effects of this compound class are being revealed. MEK inhibitor-associated retinopathy is one such adverse effect, and has been a major focus of recent research due to the frequency of symptom presentation (Duncan *et al.*, 2015). One review of clinical trial data found that approximately 10-20% of patients exhibited retinal toxicity, a symptom compounded upon by the severity of the effect (LoRusso *et al.*, 2010). In one trial, MEK inhibitor-associated retinal toxicity resulted in halting of further recruitment into the trial until a detailed examination of the effects could be completed (PD-0325901). Common ophthalmologic adverse effects include transient blurring of vision, retinal vein occlusion, cystoid macular edema (CME), and retinal detachment. Mild blurring and CME were typically self-limiting, but in cases that did not resolve, halting therapy or altering dosage reversed retinal damage.

Due to the severity of these side effects, MEK inhibitor clinical trials now exclude patients with a history of glaucoma and retinal diseases. In addition to this, clinicians

prescribing MEK inhibitors typically refer patients to an ophthalmologist for preemptive treatment and monitoring.

Current hypotheses for the mechanisms behind these retinopathies focus on oxidative stress. A recent discovery by Jiang *et al.* (2009) has also implicated altered trafficking and expression of aquaporin 1 (AQP1) in the retinal pigment epithelia (RPE). Regulation by the MAPK pathway reduces expression of AQP1 resulting in an increase in subretinal fluid accumulation.

Oxidative stress-mediated retinopathy may in turn be related to our discovery that hENT3 is potently inhibited by MEK inhibitors. Since hENT3 is a lysosomal transport protein responsible for export of nucleosides from nucleic acid breakdown, inhibition of hENT3 will potentially result in lysosomal nucleoside and nucleobase accumulation and, therefore, cell stress. Cells within the RPE rely heavily on the proper functioning of lysosomes due to rapid outer segment turnover from photo-oxidative damage (Khoh-Reiter *et al.*, 2015), which may possibly explain why the effects of hENT3 inhibition are more prominent in the RPE, despite hENT3 expression in other retinal tissues (Morgan *et al.*, 2010; Akanuma *et al.*, 2013). Intracellular accumulation of the products of nucleic acid degradation might additionally sequester water, thereby contributing to CME. An examination of a large panel of 20 proprietary compounds known to cause retinal lesions in animal models has revealed a correlation between retinal toxicity and lysosomal dysfunction (Khoh-Reiter *et al.*, 2015). Thus, retinal lesions are a common clinical presentation in MEK inhibitory therapy, and lysosomal transporter inhibition (hENT3) by MEK inhibitors may be responsible.

The self-resolving nature of some of these adverse effects may be due to cell stress compensatory pathways increasing Transcription Factor EB (TFEB), which induces autophagy and lysosome biogenesis (Raben & Puertollano, 2016).

Dermatological Adverse Effects

Non-functional or low-functioning hENT3 mutations result in a congenital lysosomal storage disease termed H-Syndrome, so named for its clinical presentations (hepatomegaly, hypogonadism, hyperpigmentation) (El-Khateeb, 2010; Morgan *et al.*, 2010). With around 100 diagnosed cases worldwide, very little is known about the specific etiology of H-Syndrome. Individuals with H-Syndrome present with several pathophysiological symptoms similar to individuals undergoing MEK inhibitor therapy, and which may be the result of hENT3 inhibition.

Cardiovascular Abnormalities

Reduced cardiac left-ventricular ejection volume is a common adverse effect in MEK inhibitor therapy (Templeton & Musib, 2015). This side effect is particularly significant in the evaluation of dosing due to the importance of maintaining healthy cardiac function in patients.

hENT4 is found in cardiovascular tissues with high expression in the plasma membrane of ventricular cardiomyocytes and associated T-tubules (Barnes *et al.*, 2006). While the pH dependence of this transporter results in essentially no transport of

nucleosides at physiological pH, its localization in the heart suggests potentially important roles under ischemic conditions, which are associated with low local pH. Since hENT4 transports adenosine, inhibition of hENT4 as a result of MEK inhibitor therapy may perturb local adenosine homeostasis within ventricular cardiomyocytes. Because adenosine efflux relies on nucleoside transporters (hENT1 and hENT4) to cross into the extracellular fluid, inhibitory effects of MEK inhibitors may contribute to reduced extracellular adenosine during ischemia, thereby reducing its cardioprotective inotropic effects.

Additionally, while adenosine transport by hENT4 is pH-dependent, it has been demonstrated that hENT4 transport of serotonin is not (Barnes *et al.*, 2006). The positive inotropic effects of serotonin, which acts via a cAMP-mediated mechanism, may therefore be inhibited by MEK inhibitor therapy, thereby compounding any potential effects potentiated by perturbed adenosine transport.

References

Abdel-Rahman O, ElHalawani H & Ahmed H (2015). Risk of selected dermatological toxicities in cancer patients treated with MEK inhibitors: a comparative systematic review and meta-analysis. *Future Oncol Lond Engl* **11,** 3307–3319.

Akanuma S, Soutome T, Hisada E, Tachikawa M, Kubo Y & Hosoya K (2013). Na+-independent nucleoside transporters regulate adenosine and hypoxanthine levels in Müller cells and the inner blood-retinal barrier. *Invest Ophthalmol Vis Sci* **54,** 1469–1477.

Baldwin SA, Yao SYM, Hyde RJ, Ng AML, Foppolo S, Barnes K, Ritzel MWL, Cass CE & Young JD (2005). Functional Characterization of Novel Human and Mouse Equilibrative Nucleoside Transporters (hENT3 and mENT3) Located in Intracellular Membranes. *J Biol Chem* **280,** 15880–15887.

Barnes K, Dobrzynski H, Foppolo S, Beal PR, Ismat F, Scullion ER, Sun L, Tellez J, Ritzel MWL, Claycomb WC, Cass CE, Young JD, Billeter-Clark R, Boyett MR & Baldwin SA (2006). Distribution and functional characterization of equilibrative nucleoside transporter-4, a novel cardiac adenosine transporter activated at acidic pH. *Circ Res* **99,** 510–519.

Cravetchi X, Vilas G & Hammond J (2015). Oligomerization of Equilibrative Nucleoside Transporter 1. *FASEB J* **29,** 939.8.

Damaraju VL, Kuzma M, Mowles D, Cass CE & Sawyer MB (2015). Interactions of multitargeted kinase inhibitors and nucleoside drugs: Achilles heel of combination therapy? *Mol Cancer Ther* **14,** 236–245.

van Dijk EHC, van Herpen CML, Marinkovic M, hENT3/hAAnen JBAG, Amundson D, Luyten GPM, Jager MJ, Kapiteijn EHW, Keunen JEE, Adamus G & Boon CJF (2015). Serous Retinopathy Associated with Mitogen-Activated Protein Kinase Kinase Inhibition (Binimetinib) for Metastatic Cutaneous and Uveal Melanoma. *Ophthalmology* **122,** 1907–1916.

Duncan KE, Chang LY & Patronas M (2015). MEK inhibitors: a new class of chemotherapeutic agents with ocular toxicity. *Eye*; DOI: 10.1038/eye.2015.82.

El-Khateeb EA (2010). The H Syndrome. *Pediatr Dermatol* **27,** 65–68.

Grimaldi AM, Simeone E, Festino L, Vanella V, Palla M & Ascierto PA (2015). Novel Mechanisms and Therapeutic Approaches in Melanoma: Targeting the MAPK Pathway. *Discov Med* **19,** 455–461.

Huang M, Wang Y, Collins M, Gu JJ, Mitchell BS & Graves LM (2002). Inhibition of Nucleoside Transport by p38 MAPK Inhibitors. *J Biol Chem* **277,** 28364–28367.

Jarvis SM, Young JD & Ellory JC (1980). Nucleoside transport in human erythrocytes. Apparent molecular weight of the nitrobenzylthioinosine-binding complex estimated by radiation-inactivation analysis. *Biochem J* **190,** 373–376.

Jiang Q, Cao C, Lu S, Kivlin R, Wallin B, Chu W, Bi Z, Wang X & Wan Y (2009). MEK/ERK pathway mediates UVB-induced AQP1 downregulation and water permeability impairment in human retinal pigment epithelial cells. *Int J Mol Med* **23,** 771–777.

Khoh-Reiter S, Sokolowski SA, Jessen B, Evans M, Dalvie D & Lu S (2015). Contribution of membrane trafficking perturbation to retinal toxicity. *Toxicol Sci Off J Soc Toxicol* **145,** 383–395.

LoRusso PM, Krishnamurthi SS, Rinehart JJ, Nabell LM, Malburg L, Chapman PB, DePrimo SE, Bentivegna S, Wilner KD, Tan W & Ricart AD (2010). Phase I pharmacokinetic and pharmacodynamic study of the oral MAPK/ERK kinase inhibitor PD-0325901 in patients with advanced cancers. *Clin Cancer Res Off J Am Assoc Cancer Res* **16,** 1924–1937.

Lugowska I, Koseła-Paterczyk H, Kozak K & Rutkowski P (2015). Trametinib: a MEK inhibitor for management of metastatic melanoma. *OncoTargets Ther* **8,** 2251–2259.

Morgan NV et al. (2010). Mutations in SLC29A3 , Encoding an Equilibrative Nucleoside Transporter ENT3, Cause a Familial Histiocytosis Syndrome (Faisalabad Histiocytosis) and Familial Rosai-Dorfman Disease. *PLOS Genet* **6,** e1000833.

Niro A, Strippoli S, Alessio G, Sborgia L, Recchimurzo N & Guida M (2015). Ocular Toxicity in Metastatic Melanoma Patients Treated With Mitogen-Activated Protein Kinase Kinase Inhibitors: A Case Series. *Am J Ophthalmol* **160,** 959–967.e1.

Raben N & Puertollano R (2016). TFEB and TFE3: Linking Lysosomes to Cellular Adaptation to Stress. *Annu Rev Cell Dev Biol*; DOI: 10.1146/annurev-cellbio-111315-125407.

Sebolt-Leopold JS & Bridges AJ (2009). Road to PD0325901 and beyond: The MEK Inhibitor Quest. In *Kinase Inhibitor Drugs*, ed. Li R & Stafford JA, pp. 203–227. John Wiley & Sons, Inc. Available at: http://onlinelibrary.wiley.com/doi/10.1002/9780470524961.ch8/summary.

Templeton I & Musib L (2015). MEK inhibitors beyond monotherapy: current and future development. *Curr Opin Pharmacol* **23,** 61–67.

Thomas CL, Mortimer PS, Larkin JM, Basu TN, Gore ME & Fearfield L (2015). A mitogen-activated protein kinase kinase inhibitor induced compound skin toxicity with

oedema in metastatic malignant melanoma. *Clin Exp Dermatol*; DOI: 10.1111/ced.12722.

Urner-Bloch U, Urner M, Stieger P, Galliker N, Winterton N, Zubel A, Moutouh-de Parseval L, Dummer R & Goldinger SM (2014). Transient MEK inhibitor-associated retinopathy in metastatic melanoma. *Ann Oncol Off J Eur Soc Med Oncol ESMO* **25,** 1437–1441.

Xu J, Knox JJ, Ibrahimov E, Chen E, Serra S, Tsao M, Cao P, Vines D, Green DE, Metran-Nascente C, McNamara MG & Hedley DW (2013). Sequence Dependence of MEK Inhibitor AZD6244 Combined with Gemcitabine for the Treatment of Biliary Cancer. *Am Assoc Cancer Res* **19,** 118–127.
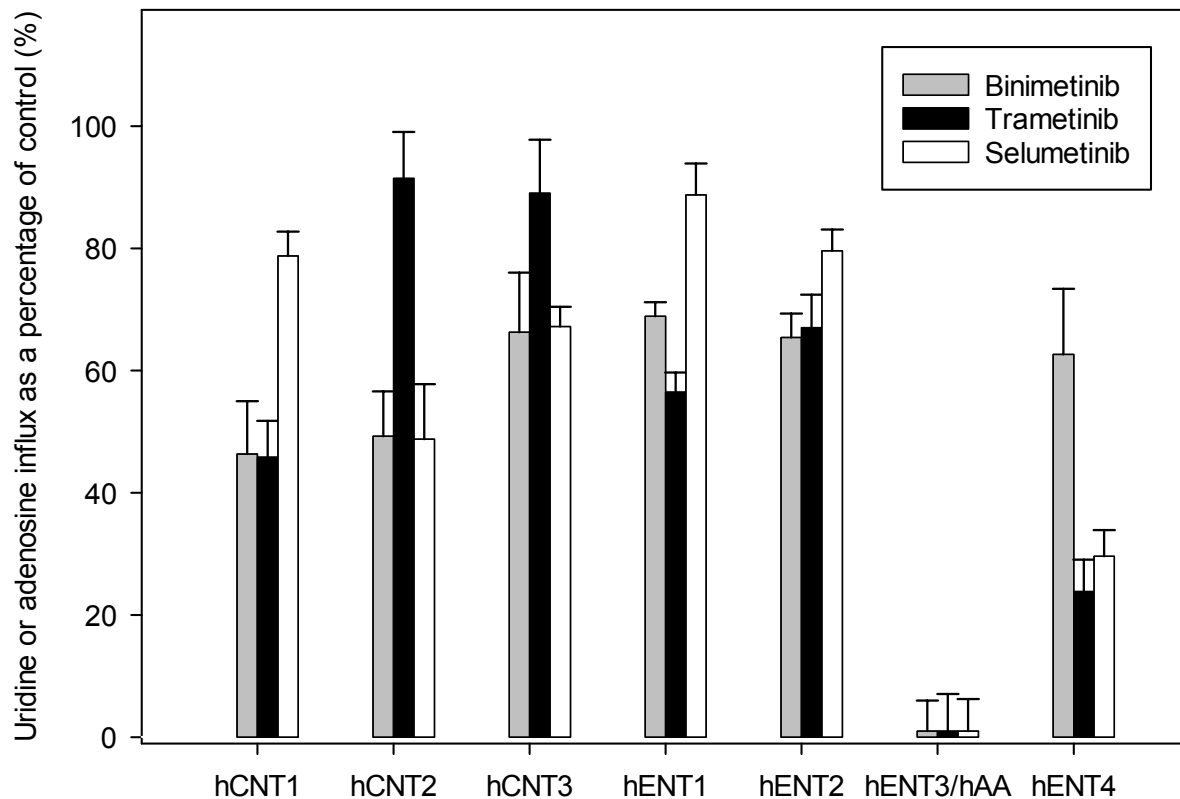
Figure 5.1: Initial 200 μM screen of binimetinib, trametinib, and selumetinib inhibition of hCNT1-3- and hENT1-3-mediated uridine and hENT4-mediated adenosine influx. Values for 20 μM [^{3}H]uridine and [^{14}C]adenosine influx (5-min uptake interval) are means of 10-12 oocytes, were corrected for the low uridine/adenosine uptake in control water-injected oocytes, and are presented as a percentage of control uptake in the absence of inhibitor. Oocytes were preincubated with 200 μM of inhibitor for 1 hour prior to addition of permeant.
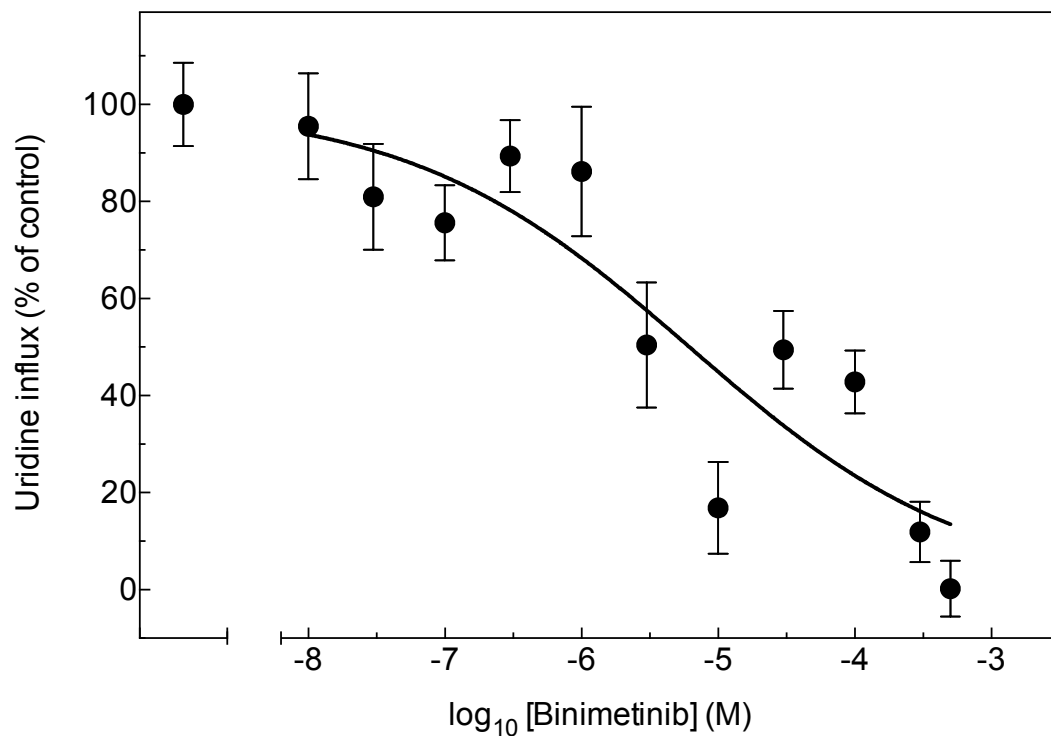
Figure 5.2: Concentration dependence of binimetinib inhibition of hENT3/hAA-mediated uridine influx (1). Values for [^{3}H]uridine influx are means ± SEM of 10-12 oocytes and were corrected for the low uridine uptake in control water-injected oocytes. The IC_{50} value and Hill coefficient were determined by non-linear regression analysis (Prism, Graphpad Software Inc., USA) and are presented in **Table 5.1** and **5.2**, respectively.
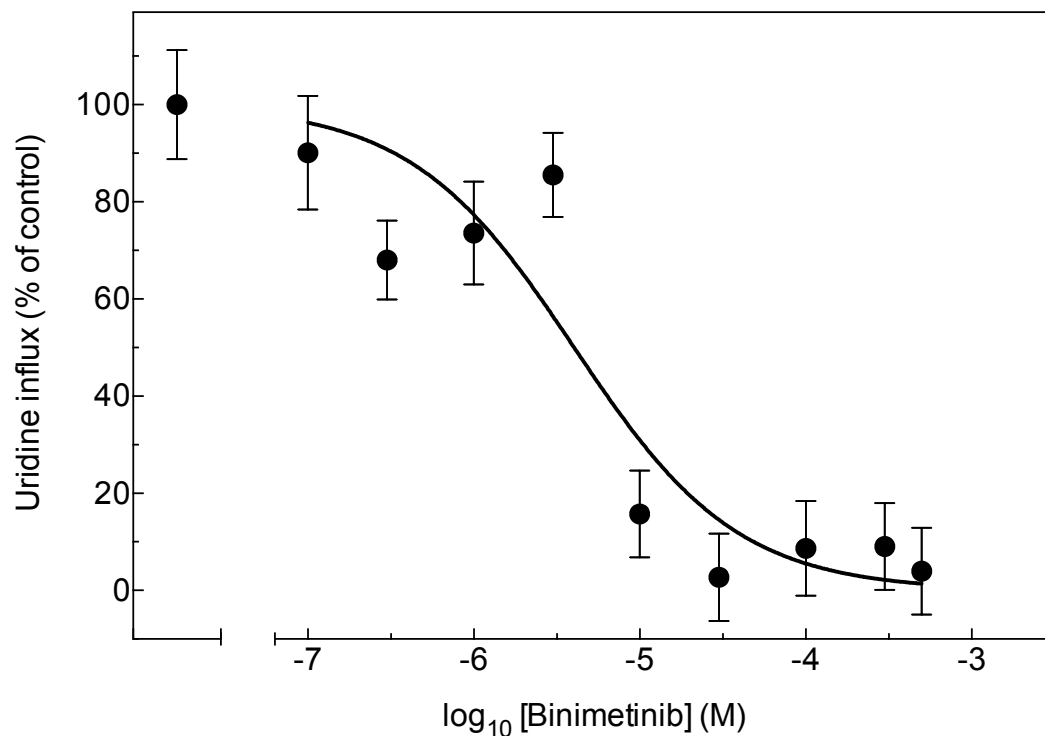
Figure 5.3: Concentration dependence of binimetinib inhibition of hENT3/hAA-mediated uridine influx (2). Values for [³H]uridine influx are means ± SEM of 10-12 oocytes and were corrected for the low uridine uptake in control water-injected oocytes. The IC$_{50}$ value and Hill coefficient were determined by non-linear regression analysis (Prism, Graphpad Software Inc., USA) and are presented in **Table 5.1** and **5.2**, respectively.
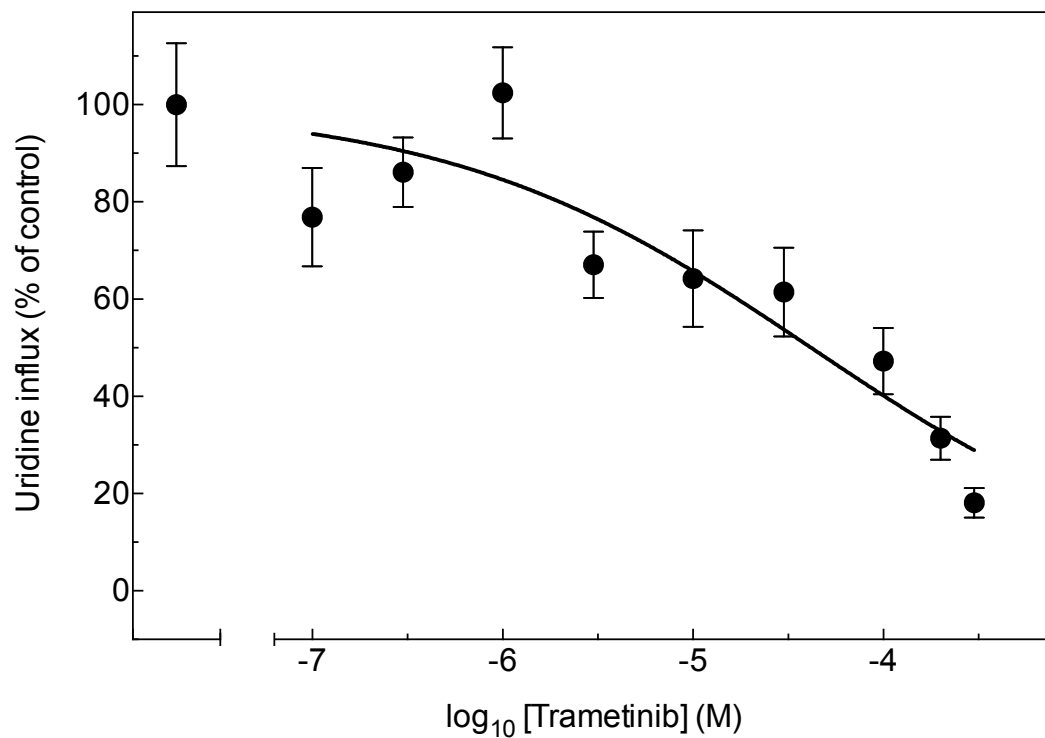
Figure 5.4: Concentration dependence of trametinib inhibition of hENT3/hAA-mediated uridine influx (1). Values for [³H]uridine influx are means ± SEM of 10-12 oocytes and were corrected for the low uridine uptake in control water-injected oocytes. The IC_{50} value and Hill coefficient were determined by non-linear regression analysis (Prism, Graphpad Software Inc., USA) and are presented in **Table 5.1** and **5.2**, respectively.

Figure 5.5: Concentration dependence of trametinib inhibition of hENT3/hAA-mediated uridine influx (2). Values for [^{3}H]uridine influx are means ± SEM of 10-12 oocytes and were corrected for the low uridine uptake in control water-injected oocytes. The IC_{50} value and Hill coefficient were determined by non-linear regression analysis (Prism, Graphpad Software Inc., USA) and are presented in **Table 5.1** and **5.2**, respectively.
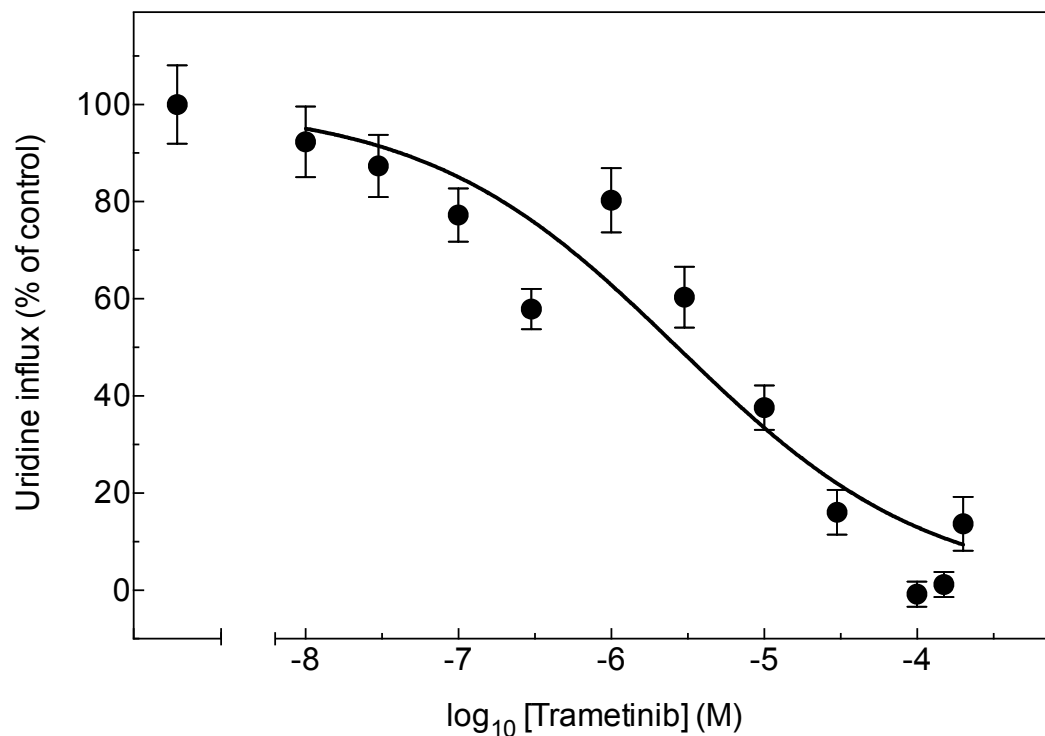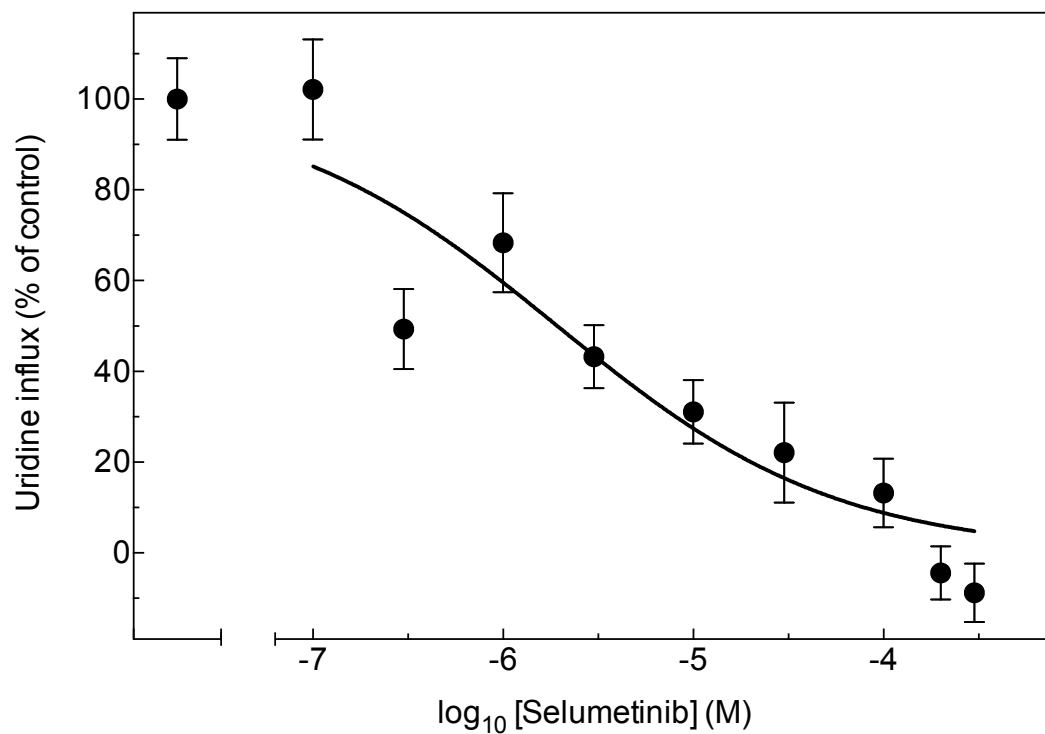
Figure 5.6: Concentration dependence of selumetinib inhibition of hENT3/hAA-mediated uridine influx (1). Values for [^{3}H]uridine influx are means ± SEM of 10-12 oocytes and were corrected for the low uridine uptake in control water-injected oocytes. The IC_{50} value and Hill coefficient were determined by non-linear regression analysis (Prism, Graphpad Software Inc., USA) and are presented in **Table 5.1** and **5.2**, respectively.

Figure 5.7: Concentration dependence of selumetinib inhibition of hENT3/hAA-mediated uridine influx (2). Values for [³H]uridine influx are means ± SEM of 10-12 oocytes and were corrected for the low uridine uptake in control water-injected oocytes. The IC_{50} value and Hill coefficient were determined by non-linear regression analysis (Prism, Graphpad Software Inc., USA) and are presented in **Table 5.1** and **5.2**, respectively.
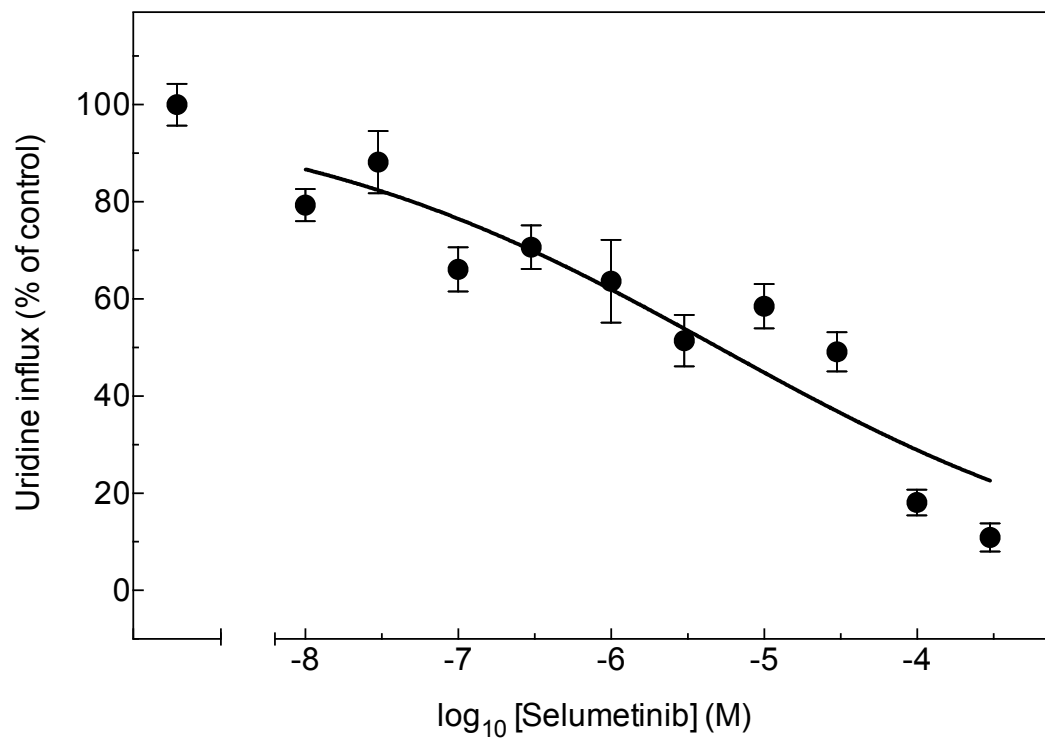
Figure 5.8: Concentration dependence of binimetinib inhibition of hENT4-mediated adenosine influx (1). Values for [^{14}C]adenosine influx are means $\pm$ SEM of 10-12 oocytes and were corrected for the low adenosine uptake in control water-injected oocytes. The IC$_{50}$ value and Hill coefficient were determined by non-linear regression analysis (Prism, Graphpad Software Inc., USA) and are presented in **Table 5.1** and **5.2**, respectively.
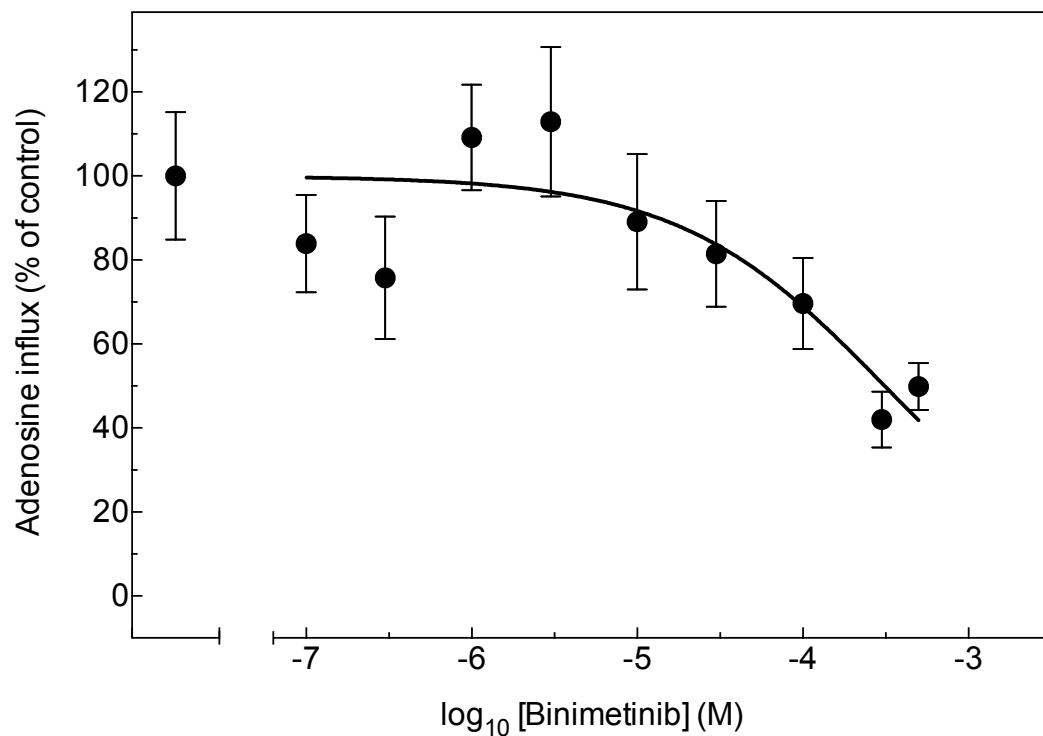
Figure 5.9: Concentration dependence of binimetinib inhibition of hENT4-mediated adenosine influx (2). Values for [^{14}C]adenosine influx are means ± SEM of 10-12 oocytes and were corrected for the low adenosine uptake in control water-injected oocytes. The IC$_{50}$ value and Hill coefficient were determined by non-linear regression analysis (Prism, Graphpad Software Inc., USA) and are presented in **Table 5.1** and **5.2**, respectively.
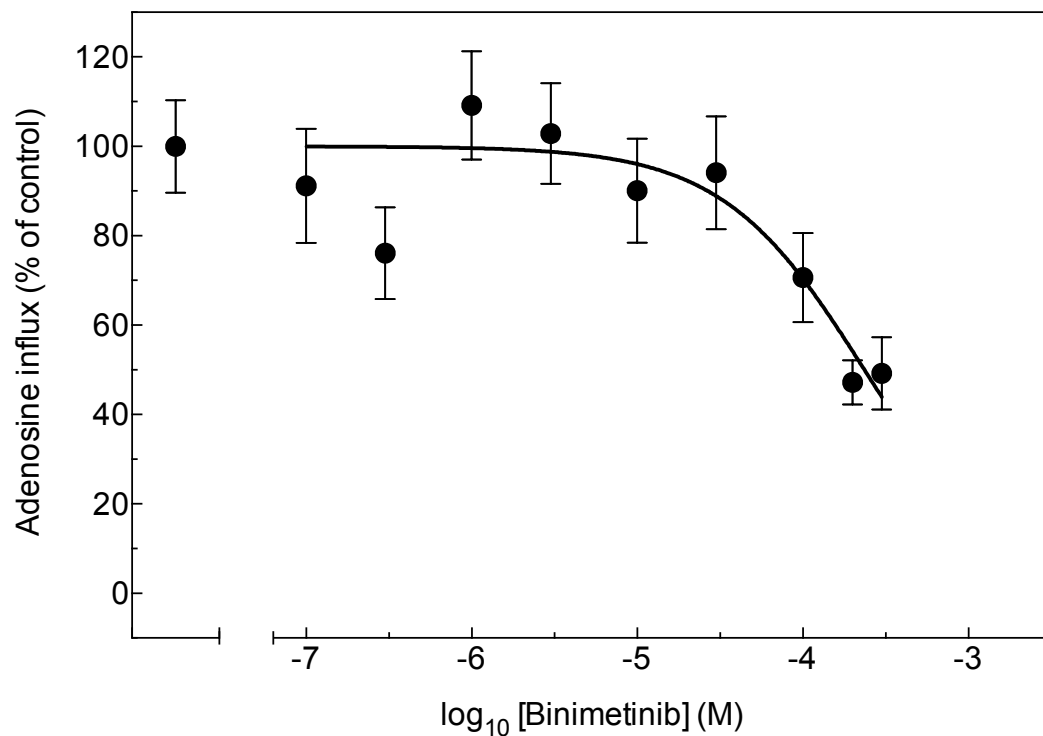
Figure 5.10: Concentration dependence of trametinib inhibition of hENT4-mediated adenosine influx (1). Values for $[^{14}C]$adenosine influx are means $\pm$ SEM of 10-12 oocytes and were corrected for the low adenosine uptake in control water-injected oocytes. The IC_{50} value and Hill coefficient were determined by non-linear regression analysis (Prism, Graphpad Software Inc., USA) and are presented in **Table 5.1** and **5.2**, respectively.
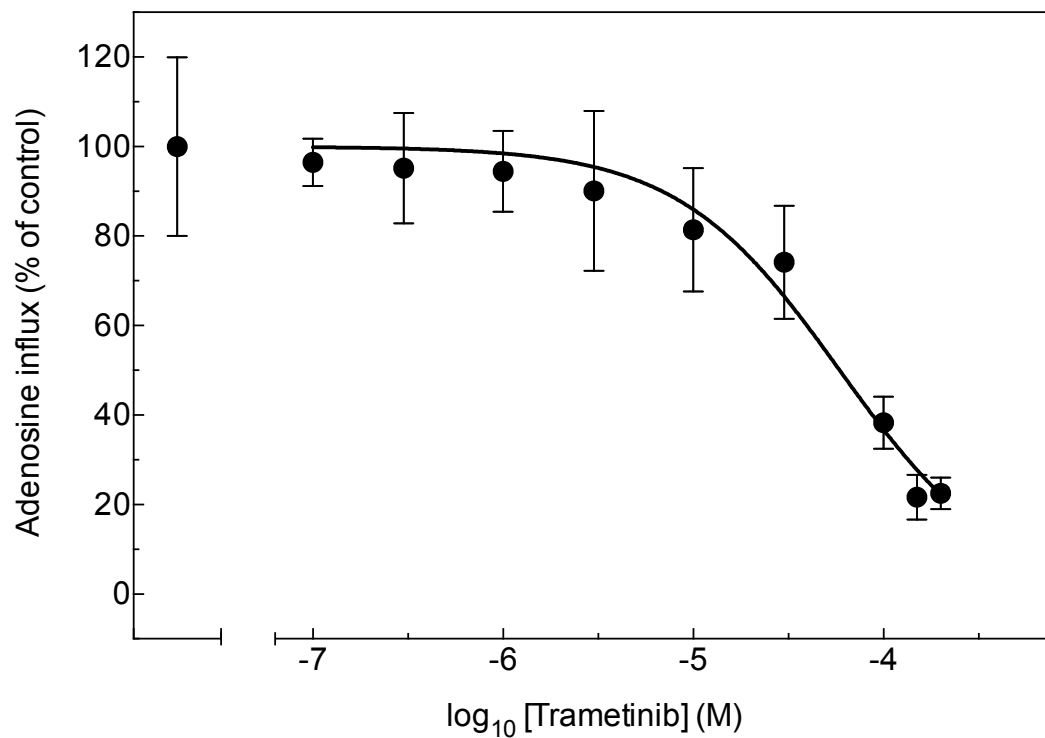
Figure 5.11: Concentration dependence of trametinib inhibition of hENT4-mediated adenosine influx (2). Values for [^{14}C]adenosine influx are means $\pm$ SEM of 10-12 oocytes and were corrected for the low adenosine uptake in control water-injected oocytes. The IC$_{50}$ value and Hill coefficient were determined by non-linear regression analysis (Prism, Graphpad Software Inc., USA) and are presented in **Table 5.1** and **5.2**, respectively.
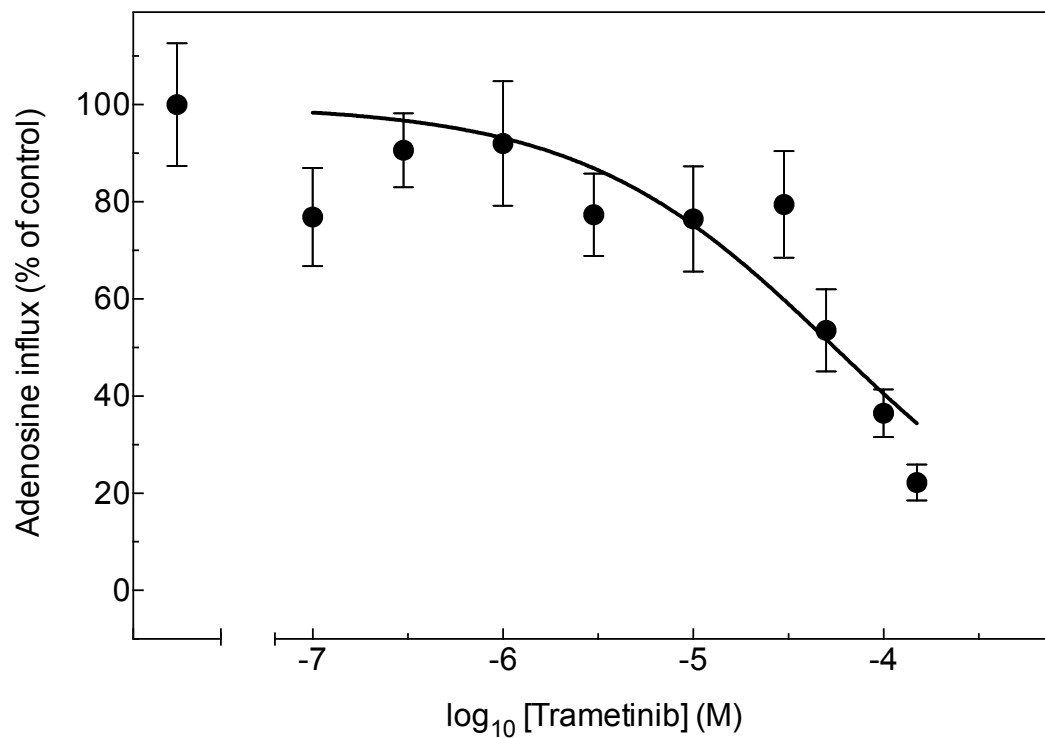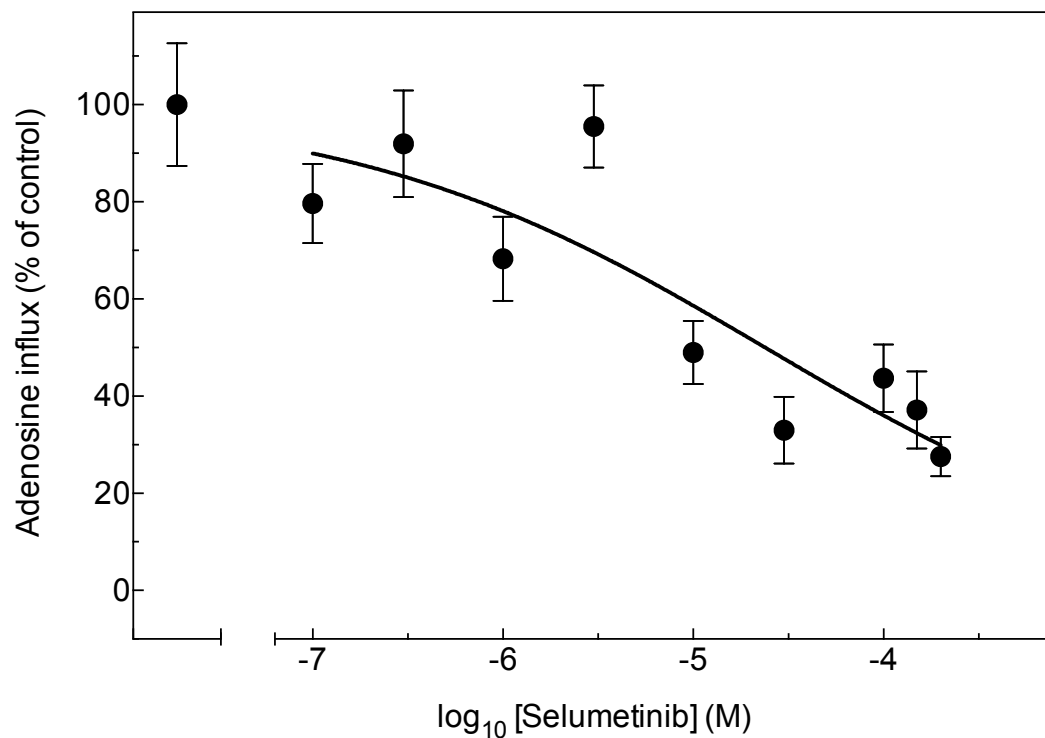
Figure 5.12: Concentration dependence of selumetinib inhibition of hENT4-mediated adenosine influx (1). Values for $[^{14}C]$adenosine influx are means $\pm$ SEM of 10-12 oocytes and were corrected for the low adenosine uptake in control water-injected oocytes. The IC_{50} value and Hill coefficient were determined by non-linear regression analysis (Prism, Graphpad Software Inc., USA) and are presented in **Table 5.1** and **5.2**, respectively.

Figure 5.13: Concentration dependence of selumetinib inhibition of hENT4-mediated adenosine influx (2). Values for [^{14}C]adenosine influx are means ± SEM of 10-12 oocytes and were corrected for the low adenosine uptake in control water-injected oocytes. The IC$_{50}$ value and Hill coefficient were determined by non-linear regression analysis (Prism, Graphpad Software Inc., USA) and are presented in **Table 5.1** and **5.2**, respectively.
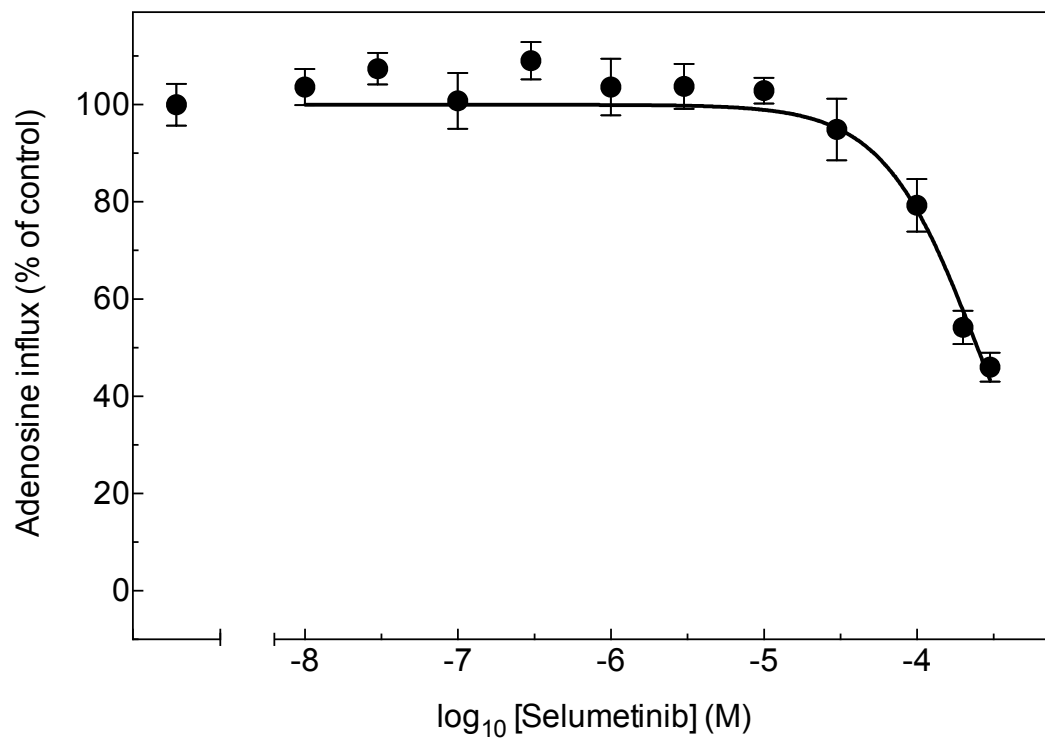
Table 5.1: IC$_{50}$ summary of hENT3/hAA and hENT4 inhibition experiments (Figures 5.2-5.13).

	hENT3/hAA (μM)	hENT4 (μM)
Binimetinib (1)	6.2 ± 1.9	312 ± 2
Binimetinib (2)	4.0 ± 1.6	235 ± 1
Mean	5.1 ± 2.6	274 ± 2
Trametinib (1)	41.8 ± 1.6	55.4 ± 1.5
Trametinib (2)	2.7 ± 1.5	58.8 ± 1.1
Mean	22.3 ± 12.4	57.1 ± 1.9
Selumetinib (1)	1.9 ± 1.6	23.4 ± 1.8
Selumetinib (2)	5.0 ± 1.7	249 ± 1
Mean	3.5 ± 3.1	136 ± 10

IC$_{50}$ values ($\pm$ SE) were determined from concentration-effect curves (0-500, 0-200, or 0-300 μM inhibitor concentration range for binimetinib, trametinib, and selumetinib, respectively, and 20 μM [^{3}H]uridine and [^{14}C]adenosine for hENT3/hAA and hENT4 respectively) by non-linear regression analysis with a variable Hill slope using Prism (Graphpad Software Inc., USA). Each experiment was repeated twice.

Table 5.2: Hill coefficient summary of hENT3/hAA and hENT4 inhibition experiments.

	hENT3/hAA	hENT4
Binimetinib (1)	-0.42 ± 0.11	-0.70 ± 0.22
Binimetinib (2)	-0.88 ± 0.20	-1.01 ± 0.41
Mean	-0.65 ± 0.23	-0.86 ± 0.44
Trametinib (1)	-0.46 ± 0.11	-0.65 ± 0.21
Trametinib (2)	-0.53 ± 0.10	-1.02 ± 0.12
Mean	-0.50 ± 0.15	-0.84 ± 0.29
Selumetinib (1)	-0.59 ± 0.16	-0.40 ± 0.11
Selumetinib (2)	-0.30 ± 0.06	-1.40 ± 0.27
Mean	-0.45 ± 0.15	-0.90 ± 0.30

Hill coefficient values ($\pm$ SE) were determined from concentration-effect curves (0-500, 0-200, or 0-300 μM inhibitor concentration range for binimetinib, trametinib, and selumetinib, respectively, and 20 μM [^{3}H]uridine and [^{14}C]adenosine for hENT3/hAA and hENT4 respectively) by non-linear regression analysis using Prism (Graphpad Software Inc., USA). Each experiment was repeated twice.

Chapter 6:

General Discussion

Glutamate Transport Inhibitors

The excitatory neurotransmitter glutamate necessitates a high-affinity removal mechanism within the synaptic cleft to prevent excitotoxic neuronal death. The excitatory amino acid transporter family that fulfills this function consists of five distinct members (hEAAT1-5), each with varying membrane localizations and affinities for glutamate and, therefore, varying roles within the nervous system. The central role that these transporters play within the CNS inevitably implicates them in a variety of disease states. Additionally, since the concentration of glutamate within the synapse is very tightly controlled by hEAATs, these transporters are very attractive targets for pharmacologic intervention (Dunlop, 2006). The current lack of high-affinity, isoform-specific glutamate transport inhibitors, however, has both impeded functional and physiological characterization of this important transporter family, as well as restricted the therapeutic applications of hEAAT-modulating drugs (Dunlop, 2006).

To approach the issue of lack of isoform-specific inhibitors, our collaborators at the University of Leeds utilized diversity orientated synthesis (DOS) to generate novel glutamate-mimetics that had varying functional groups systematically placed at different positions on the molecule, therefore allowing for the examination of potential differences within the permeant-binding pockets of different hEAAT family members (Fowkes, 2010). It was hypothesized that different glutamate mimetics might interact uniquely with different hEAATs, resulting in potential isoform-specific inhibition.

Synthesis of these compounds utilized a TBOA backbone, TBOA being the archetype β-hydroxy-substituted aspartate hEAAT inhibitor. TBOA inhibition of different

118

recombinant EAATs has been widely studied in the literature, but there is incomplete information on its inhibitory profile against hEAATs produced in *Xenopus laevis* oocytes. Specifically, the IC$_{50}$ value for TBOA inhibition of hEAAT3 in oocytes has not been reported. The published TBOA IC$_{50}$ values in *Xenopus laevis* oocytes of 67 µM for hEAAT1 and 5.5 µM hEAAT2 (Shimamoto, 2008) are higher than for a number of our TBOA-derived inhibitor compounds. Our broadly inhibitory compound AF451, for example, had IC$_{50}$ values of 16.4 µM for hEAAT1 and 2.91 µM for hEAAT2. It is important to note, however, that the literature reports additional compounds such as (2S,3S)-3-[3-[4-(trifluoromethyl)benzoylamino]benzyloxy]aspartate (TFB-TBOA) with nanomolar IC$_{50}$ values for hEAATs (22, 17, and 300 nM for hEAAT1, hEAAT2, and hEAAT3, respectively) (Shimamoto *et al.*, 2004). These studies, however, used the COS-1 cell line to characterize the compounds, and it is known for example in studies of nucleoside transport inhibitors that inhibitor potencies are often higher in such systems when compared to *Xenopus laevis* oocytes. Further examination of our compounds in other model systems (or of those compounds in our system) to better define relative inhibitor potencies.

Analysis of the bacterial GLT$_{Ph}$ structures in the presence of glutamate versus TBOA suggests the importance of the phenyl substituent in the inhibitory mechanism. Not only does the bulky phenyl group reduce transportability due to size (Shigeri *et al.*, 2004), but *in silico* docking experiments and molecular dynamics (MD) simulations suggest that the phenyl group's interaction with the extracellular gate (HP2) plays a key role in the stabilization of the outward facing conformation of the transporter, preventing permeant translocation (Boudker *et al.*, 2007). This electron coordination and positioning is also observed here with a docking simulation undertaken on a hEAAT2 homology model by our

collaborators with the hEAAT2 specific-inhibitor AF340 (Fowkes, 2010), an observation supported by the displacement of the phenyl ring on the nosyl substituent in the regioisomer AF314, resulting in a ~ 100-fold reduction in inhibition of hEAAT2. This is likely because changing the location of the nosyl substituent results in displacing the nosyl phenyl away from HP2, and thus physically restricting interaction and stabilization. The continued, but reduced, ability to inhibit hEAAT2 may stem from remaining interactions involving the phenyl group in the TBOA backbone of the molecule.

While we were able to identify several novel and specific inhibitors of hEAATs, the isoform-specificity was limited to hEAAT2. This is advantageous because of the functional importance of hEAAT2 at the synapse, but also raises questions as to why our isoform-specific inhibitors were limited to this particular isoform. Since HP2 is likely a region of critical importance in the inhibitory mechanism of our compounds, it stands to reason that any amino acid substitutions on this hairpin between hEAAT2 and other isoforms may be contributing factors. There are two key residues on HP2 that are involved in permeant and inhibitor interaction (Boudker *et al.*, 2007), both of which are uniquely present as serine residues in hEAAT2 compared to glutamine in hEAAT1 and hEAAT3 (Yernool *et al.*, 2004). Due to the highly conserved nature of the flanking residues, the non-polar to polar substitution in hEAAT2 is the likely reason for increased selectivity, since this may serve to strengthen pi-polar interactions between the hairpin and the inhibitor's phenyl group. It is also possible that additional minor differences in the binding and positioning of our compounds to the various transporters may impede access to HP2 or make it more difficult for HP2 to be stabilized. If this is the case, our compounds appear to be uniquely suited to exploit these differences in hEAAT2, potentially due to the structure of the shared initial

anchoring blocks compounds used in their synthesis. Further experimentation and 3D modelling is required to determine this.

The identification of novel glutamate transport inhibitors also has other implications. Our success adds to the body of literature that validates the use of DOS in the generation of novel drug libraries with diverse structures. Also, our successful compounds can be further modified and improved upon through additional rounds of DOS, which eliminates the lengthy process of screening large combinatory libraries for chance hits.

Our characterization of the current inhibitory compounds was limited to dose-dependent testing using radioisotope uptake assays. This, while providing important information, does not provide the complete picture with regard to mechanisms of action. There are several important future directions that could be undertaken to further explore and characterize these compounds.

Since glutamate plays such a pivotal role within the CNS, it is no surprise that a large number of proteins bind glutamate, most of which are similarly localized to the synapse (Shigeri *et al.*, 2004). While it is perhaps unlikely that our new compounds would interact with these due to their bulk, screening of our compounds against the most common glutamate binding proteins would be an important first step in evaluating the therapeutic potential of these compounds.

Additionally, experiments should also be undertaken to characterize mechanism(s) of inhibition, such as using radioisotope uptake assays to perform experiments to kinetically investigate if inhibition was competitive or non-competitive. Although radioisotope uptake assays are simple and powerful tools to characterize membrane transporters, there are aspects of transporter function that are difficult to explore using

this technique alone. Electrophysiological techniques such as the two microelectrode voltage clamp (TEVC), for example, can more easily be employed to determine properties such as transportability of an inhibitor.

In silico docking experiments performed by our collaborators in Leeds helped elucidate a potential mechanism for inhibition (Fowkes, 2010). These experiments, however, are incomplete, and further modelling studies may help explain why the isoform-specific compounds within our panel displayed only hEAAT2-specific inhibition. Continued *in silico* work on glutamate transporters will not only serve to clarify interactions with existing compounds, but increase our capacity to rationally design new drugs that target specific glutamate transporter isoforms. Ultimately, however, the accuracy of the insights gained from examining homology models is limited, and high resolution crystal structures of each human isoform is ultimately required.

In summary, the aim of this project was the examination of novel hEAAT inhibitors generated by our collaborators at the University of Leeds through dose-dependent radioisotope uptake assays. The experiments were successful in having identified several isoform-specific inhibitors of hEAAT2. Additionally, the identification of potentially important molecular interactions, such as that between HP2 residues and the inhibitor's nosyl phenyl ring, may prove useful in future research into the hEAAT inhibitor pharmacophore.

MEK Nucleoside Transport Inhibitors

The evolution of transporters involved in the nucleoside salvage and repurposing pathways was likely spurred by the energy- and resource-intensive nature of nucleotide biosynthesis (Young *et al.*, 2008). As such, hNTs have central physiological roles in cellular energy and nucleotide, RNA and DNA metabolism. Modulation of extracellular adenosine concentrations further involves hNTs in purinoreceptor activation and, therefore, modulation of the diverse downstream cellular processes that such receptors regulate (Young, 2016). Additionally, the ability of hNTs to also transport nucleoside analogue drugs used in anticancer and antiviral therapies has been of immense clinical importance (Zhang *et al.*, 2007). Given their metabolic, physiological and clinical significance, it is therefore, important to examine whether or not the two human nucleoside transporter families are potential spillover targets for chemotherapeutic compounds designed for other drug targets. Historically, this has not been common practice. MEK inhibitors are one such class of compounds that are now being revealed as having unintended inhibitory effects on nucleoside transporters. The three such compounds examined in this thesis, binimetinib, trametinib and selumetinib, add to this list.

This collaborative project stemmed from observations of unexpected low clinical efficacy of the nucleoside analogue drug gemcitabine when used in cancer treatment trials in combination with the MEK inhibitor trametinib (Infante *et al.*, 2014). Since nucleoside analogues are a drug class frequently used in the treatment of cancer, the potential implications of such findings are large. Mechanistically, the structural similarities between MEK inhibitors and nucleosides are sufficient to hypothesize competition for binding to hNT permeant binding pockets. In addition, potential interference with adenosine transport has the potential to explain the frequently documented adverse diarrhea effects

of orally-dosed MEK inhibitors. The disruptive nature of this symptom in day-to-day life means that it often becomes the dose-limiting symptom for prescribing oncologists. That is to say, the dosing of the drug in question is no longer dependent on the ideal concentration for its anticancer properties, but on the concentration that makes this side effect tolerable for the patient. As such, addressing the molecular mechanism behind this symptom is crucial for the long term therapeutic potential of these compounds.

Our experiments revealed modest inhibition of hCNTs, hENT1, and hENT2 by binimetinib, trametinib and selumetinib, and more substantial inhibition of hENT3/hAA and hENT4. Mechanistically, structural similarities between these MEK inhibitor molecules and nucleosides may allow for their binding to hNT permeant-binding pockets. This structural similarity formed the basis for our original hypothesis.

Alternatively, a second potential mechanism of inhibition mirrors the way in which these MEK inhibitors exert their effects on their intended targets, MEK 1/2: allosteric inhibition though substrate/permeant coordination. MEK inhibitors fall under two categories, competitive and allosteric inhibitors of MEK. Competitive inhibitors interfere directly with ATP binding. The overwhelming majority of MEK inhibitors, however, are designed to be allosteric inhibitors that, while retaining structural similarities with ATP, interact with a unique binding pocket present in MEK 1/2 adjacent to that for ATP. This second, non-ATP, binding site confers the potential for higher specificity of inhibition and, therefore, reduced likelihood of spillover interactions as compared to competitive ATP-mimicking MEK inhibitors. The uniqueness of this binding pocket may be a contributing factor to the perhaps unrealistic expectations that such compounds will have high specificity for their intended drug targets.

Crystal structures of MEK 1 co-crystallized in the presence of the non-competitive MEK inhibitor TAK-733 and Mg-ATP demonstrate the structural basis of this allosteric inhibition in which coordination of the phosphates of ATP by the MEK inhibitor stabilizes conformational changes that prevent active site activity (Dong *et al.*, 2011). Allosteric inhibition of hNTs by MEK inhibitors is therefore also possible, although nucleosides lack the negatively charged phosphate groups present within ATP. To address the mode of inhibition further, competition studies need to be undertaken. A complicating factor is that these inhibitors are lipophilic, such that their entrance into the cell is typically not dependent on protein-facilitated transport. Interactions with both the inward-facing as well as outward-facing permeant binding sites are therefore possible.

Lipophilicity also dictates the relative concentrations of the inhibitors in different tissues. Tissue sequestration is a common characteristic of small-molecule kinase inhibitors, with certain tyrosine kinase inhibitors, for example, demonstrating concentrations of up to 300 times that of plasma in certain tissues, including regions of the gastrointestinal tract, particularly the large intestine where fluid movement is important (Di Gion *et al.*, 2011; Speed *et al.*, 2012). Since local tissue concentrations likely determine spillover inhibition effects *in vivo* more so than plasma concentrations, additional information in individuals undergoing therapy with MEK inhibitors would be an important next step.

If the compounds studied are indeed hNT competitive inhibitors as we hypothesize, then determination of transportability by hNTs, and in particular hENT3/hAA and hENT4, is the logical next step of investigation. hENT3/hAA and hENT4 are potentially electrogenic (proton-coupled) (Young *et al.*, 2008), such that electrophysiological techniques may have

use in transportability studies, which would otherwise require the availability of radiolabelled compounds.

The observed isoform selectivity of binimetinib, trametinib and selumetinib for hENT3 and hENT4 likely reflects similarities in the nucleoside binding pockets of the two transporters, hENT4 being more closely related phylogenetically to hENT3 than to hENT1 or hENT2 (Young *et al.*, 2008). hENT3 and hENT4, unlike hENT1 and hENT2, also share the potential for proton dependence in the transport of nucleosides (Baldwin *et al.*, 2005; Barnes *et al.*, 2006)

The surprise in our findings was that the hNTs more typically implicated in gastrointestinal adenosine homeostasis and function (hCNTs, hENT1/2) were less sensitive to MEK inhibitors than hENT3 and hENT4. In particular, it was anticipated that hENT1 and/or hENT2 would be the primary site(s) of inhibition, causing activation of cell surface purinergic receptors (Colgan *et al.*, 2013). In a mechanism similar to that of cholera toxin poisoning, activation of these receptors would be anticipated to induce cystic fibrosis transmembrane conductance regulator (CFTR) chloride efflux, pulling water into the GI compartment, and resulting in the documented symptom of diarrhea.

Additional studies of binimetinib, trametinib, and selumetinib interactions with hCNTs, hENT1, and hENT2 were not possible because of limitations of drug solubility, but it should be noted that, as with glutamate transport inhibitors, efficacy in mammalian cell expression systems may be greater than in *Xenopus laevis* oocytes. Also, these compounds are dosed orally, their lipophilic nature potentially resulting in gastrointestinal sequestration at high concentration, and thus amplifying their inhibitory effects on nucleoside transport.

Of the other common adverse effects seen in MEK inhibitor administration, several stand out as potentially involving nucleoside transporter inhibition. As described in Chapter 5, these include dermatological toxicities and cardiovascular abnormalities.

In summary, the aim of this project was examination of the effects of MEK inhibitors on hNTs. The experiments were successful, identifying binimetinib, trametinib and selumetinib as potent inhibitors of hENT3/hAA, and trametinib and selumetinib as inhibitors of hENT4. With the growing body of clinical and experimental reports documenting spillover inhibition of nucleoside transporters by small-molecule kinase inhibitors, the screening of newly developed drugs against the hENT and hCNT protein family is required. Re-evaluation of past failed clinical trials may also yield valuable information on previously dismissed or overlooked compounds.

References

Baldwin SA, Yao SYM, Hyde RJ, Ng AML, Foppolo S, Barnes K, Ritzel MWL, Cass CE & Young JD (2005). Functional Characterization of Novel Human and Mouse Equilibrative Nucleoside Transporters (hENT3 and mENT3) Located in Intracellular Membranes. *J Biol Chem* **280,** 15880–15887.

Barnes K, Dobrzynski H, Foppolo S, Beal PR, Ismat F, Scullion ER, Sun L, Tellez J, Ritzel MWL, Claycomb WC, Cass CE, Young JD, Billeter-Clark R, Boyett MR & Baldwin SA (2006). Distribution and Functional Characterization of Equilibrative Nucleoside Transporter-4, a Novel Cardiac Adenosine Transporter Activated at Acidic pH. *Circ Res* **99,** 510–519.

Boudker O, Ryan RM, Yernool D, Shimamoto K & Gouaux E (2007). Coupling substrate and ion binding to extracellular gate of a sodium-dependent aspartate transporter. *Nature* **445,** 387–393.

Colgan SP, Fennimore B & Ehrentraut SF (2013). Adenosine and gastrointestinal inflammation. *J Mol Med* **91,** 157–164.

Di Gion P, Kanefendt F, Lindauer A, Scheffler M, Doroshyenko O, Fuhr U, Wolf J & Jaehde U (2011). Clinical pharmacokinetics of tyrosine kinase inhibitors: focus on pyrimidines, pyridines and pyrroles. *Clin Pharmacokinet* **50,** 551–603.

Dong Q, Dougan DR, Gong X, Halkowycz P, Jin B, Kanouni T, O'Connell SM, Scorah N, Shi L, Wallace MB & Zhou F (2011). Discovery of TAK-733, a potent and selective MEK allosteric site inhibitor for the treatment of cancer. *Bioorganic & Medicinal Chemistry Letters* **21,** 1315–1319.

Dunlop J (2006). Glutamate-based therapeutic approaches: targeting the glutamate transport system. *Curr Opin Pharmacol* **6,** 103–107.

Fowkes A (2010). *Synthesis and Evaluation of Skeletally Diverse Inhibitors of Excitatory Amino Acid Transporters* (thesis). University of Leeds, Leeds, England.

Infante JR, Somer BG, Park JO, Li C-P, Scheulen ME, Kasubhai SM, Oh D-Y, Liu Y, Redhu S, Steplewski K & Le N (2014). A randomised, double-blind, placebo-controlled trial of trametinib, an oral MEK inhibitor, in combination with gemcitabine for patients with untreated metastatic adenocarcinoma of the pancreas. *European Journal of Cancer* **50,** 2072–2081.

Shigeri Y, Seal RP & Shimamoto K (2004). Molecular pharmacology of glutamate transporters, EAATs and VGLUTs. *Brain Res Brain Res Rev* **45,** 250–265.

Shimamoto K (2008). Glutamate transporter blockers for elucidation of the function of excitatory neurotransmission systems. *Chem Record* **8,** 182–199.

Shimamoto K, Sakai R, Takaoka K, Yumoto N, Nakajima T, Amara SG & Shigeri Y (2004). Characterization of novel L-threo-beta-benzyloxyaspartate derivatives, potent blockers of the glutamate transporters. *Mol Pharmacol* **65,** 1008–1015.

Speed B, Bu H-Z, Pool WF, Peng GW, Wu EY, Patyna S, Bello C & Kang P (2012). Pharmacokinetics, distribution, and metabolism of [14C]sunitinib in rats, monkeys, and humans. *Drug Metab Dispos* **40,** 539–555.

Yernool D, Boudker O, Jin Y & Gouaux E (2004). Structure of a glutamate transporter homologue from Pyrococcus horikoshii. *Nature* **431,** 811–818.

Young JD (2016). The SLC28 (CNT) and SLC29 (ENT) nucleoside transporter families: a 30-year collaborative odyssey. *Biochem Soc Trans* **44,** 869–876.

Young JD, Yao SYM, Sun L, Cass CE & Baldwin SA (2008). Human equilibrative nucleoside transporter (ENT) family of nucleoside and nucleobase transporter proteins. *Xenobiotica* **38,** 995–1021.

Zhang J, Visser F, King KM, Baldwin SA, Young JD & Cass CE (2007). The role of nucleoside transporters in cancer chemotherapy with nucleoside drugs. *Cancer Metastasis Rev* **26,** 85–110.